SOME IONOSPHERIC EFFECTS OBSERVED AT SUNRISE.

A thesis submitted for the
Degree of Master of Science
of Rhodes University.

by

D. C. BAKER.

April, 1964.

Except where it is clear from the text that I am describing the work of others, or where it is obvious that I am making a survey of existing knowledge of the ionosphere, the work described in this thesis is my own.

TO

LYNNE

AND

RORY.

thesis.

Lastly I wish to thank my wife for her forbearance and encouragement over the many months of writing up and her unfailing optimism.

ACKNOWLEDGEMENTS.

I would like to thank Professor J. A. Gledhill, my research director, for his constant encouragement and unfailing interest in this project. The many discussions, which I had with him, and his vast fund of ideas never failed to stimulate me when what seemed to be a promising line of enquiry ended in a cul-de-sac.

My friends in the Rhodes University Physics Department have been extremely helpful. Of these I must single out Mr. A.D.M. Walker and Miss L.V. Pound with whom I had many useful discussions and who were responsible for calculating some of the Titheridge coefficients while working on related projects. My thanks are also due to the late Mr. J.W. Smallberger who was responsible for running the ionosonde on the 10th August, 1960, Mr. A. Ross Scanlen who modified the V.F.O.-sweep and programme unit to enable ionograms to be taken at approximately one minute intervals and Mr. A.L. Eichstadt who frequently assisted in maintaining the ionosonde in good working condition.

The time and care devoted to the photography by Mr. G. Walters is much appreciated.

I am also indebted to my friends of SANAE 3, especially Messrs. D.C. Neethling, D. Moller and Dr. E.E.G. Lautenbach, who kept my interest in ionosphere research work alive during 1962 and the other residents of SANAE who shared all our problems, real and imagined, during the winter nights.

INTRODUCTION.

The study of the ionosphere over the sunrise period is necessary for an understanding of the variations in layer structure with time and has been a topic of research of many workers.

On the whole these investigations have been restricted to a study of critical frequency variations with relatively short intervals of a few minutes between successive records, of N-h curves deduced from ionograms with long intervals (15 minutes or so) between successive N-h curves or of continuously monitored single frequency reflections.

Not one of the three techniques is entirely satisfactory for a detailed study of ionospheric behaviour over sunrise. The first two do not give a sufficiently clear indication of what happens in the initial stages of layer development, while from the third incomplete data is obtained as to what is happening at a specific electron-density level.

For this reason a preliminary investigation of the ionosphere over sunrise was made at Rhodes University during August, 1959. The records were obtained at four-and-a-half minute intervals and scaled by the method of KELSO (1952). Many of the results were inconclusive but it appeared that records would have to be taken at approximately one minute intervals and reduced to N-h curves by a scaling technique which made full allowance for low-level ionization if useful results were to be obtained.

An attempt has been made in this thesis to investigate the behaviour of the ionosphere over sunrise more fully than can be done by the three techniques referred to. A number of observed phenomena are also examined.

Part I deals with the theoretical background to ionosphere physics in general and describes the equipment, equipment modifications and experimental procedure.

Part II presents the results obtained. The records for a large-scale travelling disturbance are analysed. Various observed phenomena are described and discussed. A simple method of obtaining production rates from experimental data is described. The implications of the observed variations of production rates with height and time are discussed. Suggestions for further research and improvement of the methods used are made in Chapter 9.

Notes concerning numbering.

Sections, equations and diagrams are numbered independently in each Chapter. Thus, for instance, section 3.2 is the second section of Chapter 3, equation 5.22 will be equation 22 of Chapter 5 while Figure 4.2 will refer to the second diagram of Chapter 4, and so on. Diagrams are also labelled with their figure number on the back to facilitate reference to them. A list of page references for Tables and diagrams is included at the end of the Table of Contents.

CONTENTS.

Page references for diagrams.

PART 1

BACKGROUND.

CHAPTER 1

THE IONOSPHERE.

1.1 Historical

KAISER (1962) points out that C. F. GAUSS (1839) in his General Theory of Terrestrial Magnetism made the earliest known suggestion of an electrically conducting region in the upper atmosphere. Gauss maintained that the existence of such a region could not be excluded as an explanation for the "regular and irregular changes which are hourly taking place in this (terrestrial magnetic) force".

The existence of a conducting region was again postulated in 1860 by W. THOMSON (later LORD KELVIN) in a discussion of atmospheric electricity and he estimated that this region would start at a height of 100 km. (CHALMERS, 1962).

The idea of a conducting region was again introduced in 1878 by BALFOUR-STEWART in connection with variations in the terrestrial magnetic field. In 1902 KENNELLY and HEAVISIDE independently postulated the existence of this region in order to account for the success of the radio communications link established by Marconi in 1901 across the Atlantic.

The first direct evidence of this region came in 1925 when APPLETON and BARNETT (1925) proved the existence of "skywaves" coming down after reflection from the Kennelly-Heaviside layer.

The most striking evidence, however, was that furnished by BREIT and TUVE (1926) who showed that a pulsed radio frequency transmission produced two or more impulses in a receiver placed a few kilometres

from the transmitter. The first pulse was concluded to be from the direct wave travelling along the ground and the other pulses were due to the reflected or skywave.

This method of Breit and Tuve has been greatly refined and is at present the most powerful method for studying the ionosphere (so called by WATSON-WATT) despite the recent advances made in rocket and satellite methods.

1.2. Radio exploration of the ionosphere.

The radio-sounding technique used for obtaining information about the ionosphere is essentially an extension of Breit and Tuve's method.

The pulse used to fire off the transmitter circuits is also used to initiate a sweep on a cathode ray oscilloscope. Pulses received from the ionosphere are rectified and applied to the cathode or one of the grids (depending on the pulse polarity after amplification) of the oscilloscope. This produces a blanking in the trace. If the oscilloscope sweep can be calibrated the time delay between the ground and indirect pulses can be measured. This time delay, when measured in terms of the distance covered by an electromagnetic wave at the velocity of light in vacuo, is referred to as the virtual height and is related to the travel time of the indirect or reflected wave by the following expression:-

$$2h' = ct \qquad (1.1)$$

where h' is the apparent or virtual height, c the velocity of light

Fig 1.1

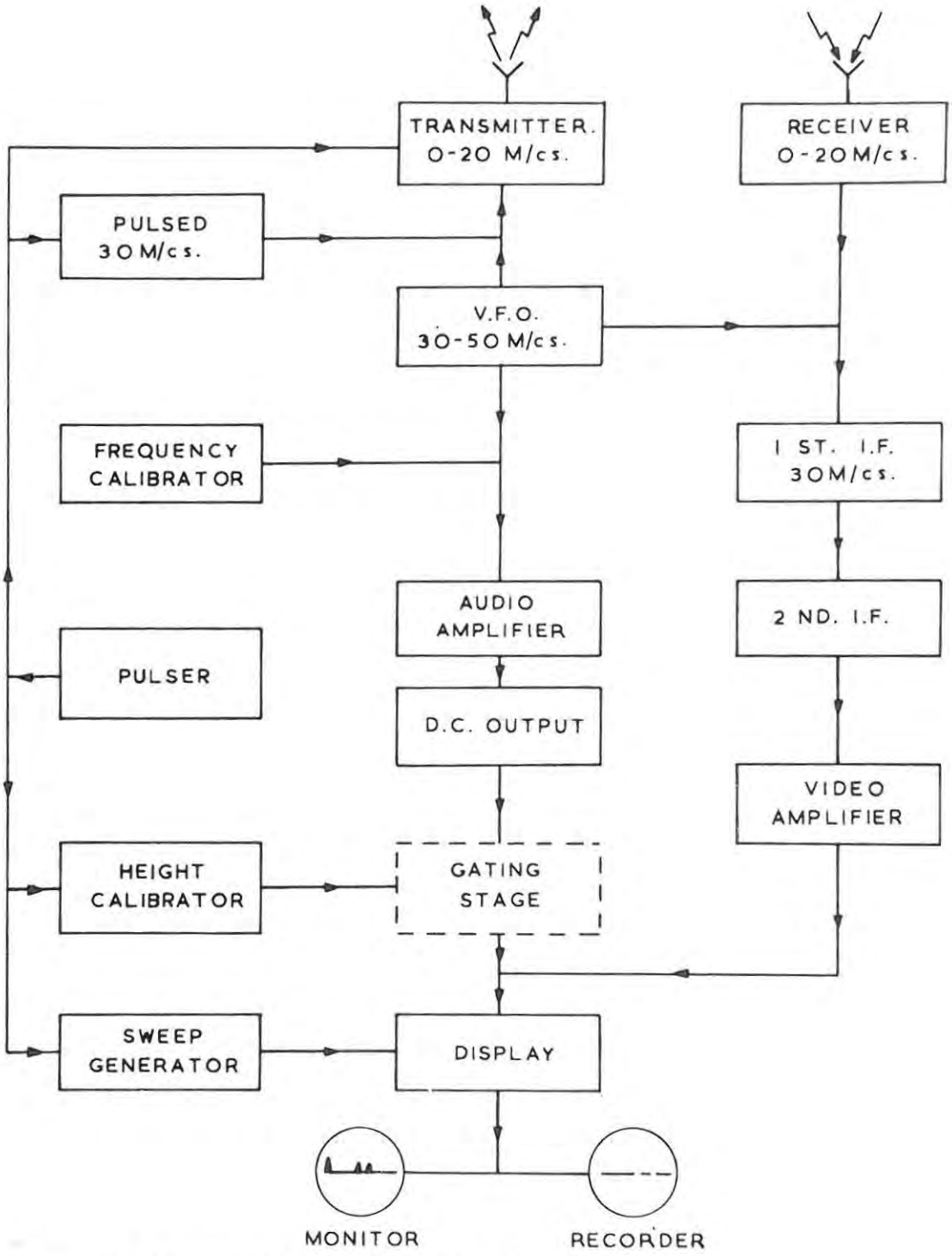

FIG.1.1 BLOCK DIAGRAM OF A TYPICAL IONOSONDE.

and t the time taken for the pulse to travel to the point of reflection and return, a distance of 2h'.

The next step is to change the frequency of the radio wave which is being transmitted. Virtual heights for a range of frequencies will thus be obtained.

Figure 1.1 shows the block diagram of a typical ionosonde. The superheterodyne circuit on which this is based is due to WADLEY (1949). The ionosonde operates as follows:-

A variable frequency oscillator (V.F.O.) is programmed in such a way that it sweeps through the frequency range 30-50 Mc/s. This V.F.O. output is mixed with a pulsed 30 Mc/s signal and the resultant difference frequency (0-20 Mc/s) is amplified and transmitted. The pulses received after reflection are in turn mixed with the V.F.O. signal and this results in an intermediate frequency of 30 Mc/s. If for example the V.F.O. is oscillating at 31.5 Mc/s, the transmitted and received signal will be 1.5 Mc/s and in this way the transmitter and receiver are always tuned to each other. The 30 Mc/s I.F. is converted to a lower frequency by being mixed with the output of a crystal oscillator. The signal is detected and is applied to the grid or cathode of an oscilloscope after video-amplification to produce a blanking of the trace.

The time base of the oscilloscope is triggered off at the same time as the pulsed 30 Mc/s oscillator.

In order to calibrate the time base a ringing circuit with a basic frequency of 1500 c/s or 3000 c/s (for 100 and 50 km. marker

Fig 1.2

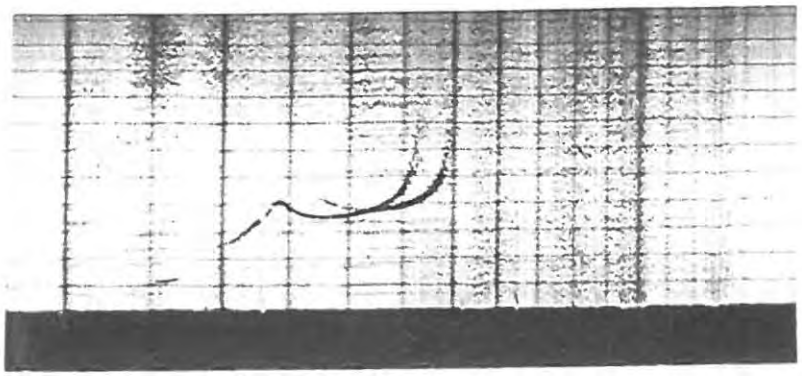

a.

Sanae 24/10/62 0815 U.T.

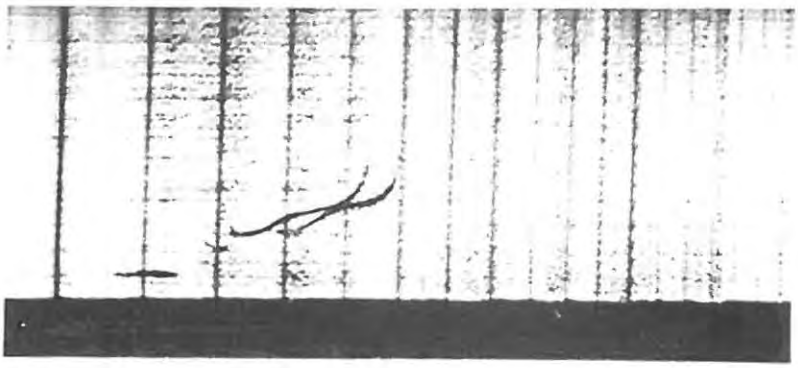

b

Sanae 14/11/62 1615 U.T.

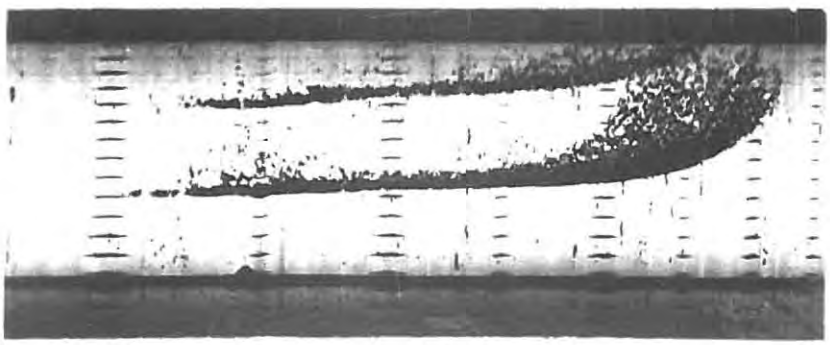

C.

Grahamstown 2/10/60 0354·8 SAST.

Fig. 1.2 Typical ionograms obtained with swept-frequency ionosondes. First frequency mark 1 Mc/s.

a and b Height marks represent 100 km intervals. Frequency marks every 1 Mc/s.

c Height marks represent 50 km intervals. Frequency marks every 0.5 Mc/s.

Fig 1.3

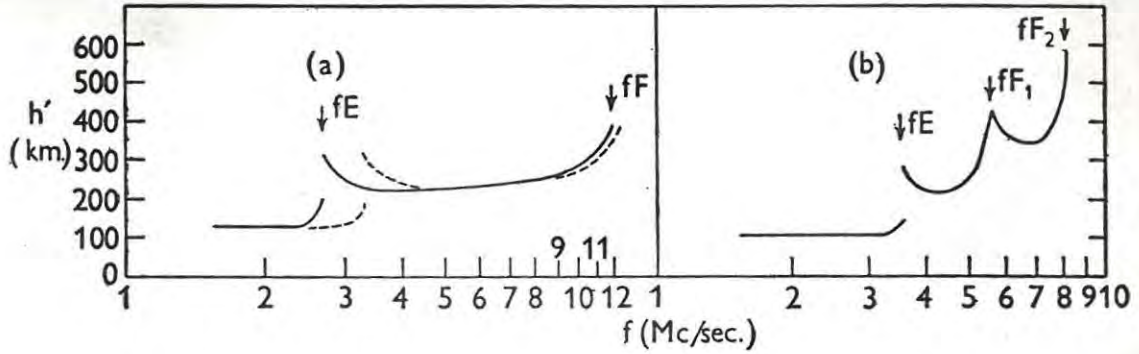

FIG. 1.3 Examples of "ionograms" or $h'(f)$ curves, in which the equivalent height (h') of reflection of a radio wave is plotted against the frequency (f). The dashed line refers to the Extraordinary wave and is shown only in (a).

pips respectively) is brought into oscillation at the start of the oscilloscope sweep. These low-frequency signals are squared, differentiated and applied to the oscilloscope. The trace thus appears to be regularly blanked at 50 or 100 km. "intervals".

The transmitted frequency is calibrated by mixing the V.F.O. output with the highly distorted output of a crystal oscillator (100, 500 or 1000 kc/s). This crystal output will therefore be rich in harmonics and audio beats are produced whenever the V.F.O. is operating near one of these harmonics. This audio output is detected and the d.c.-potential thus developed is also applied to the oscilloscope to produce blanking of the trace.

If the oscilloscope trace is photographed by continuously moving film, ionograms such as those shown in figure 1.2 a and b will be obtained.

The above is also the principle of the Rhodes ionosonde, which is based on the original circuit by Wadley, except that the audio-beats between the V.F.O. and the crystal oscillator are used to operate a gating tube through which the height markers are applied to the oscilloscope. The ionograms therefore have a series of heightmarkers which also serve as frequency calibrations. (See figure 1.2.c)

1.3 The ionospheric regions.

From ionograms obtained with swept frequency ionosondes it has become apparent that several distinct regions exist in the ionosphere. Figure 1.3 shows some typical h'f distributions.

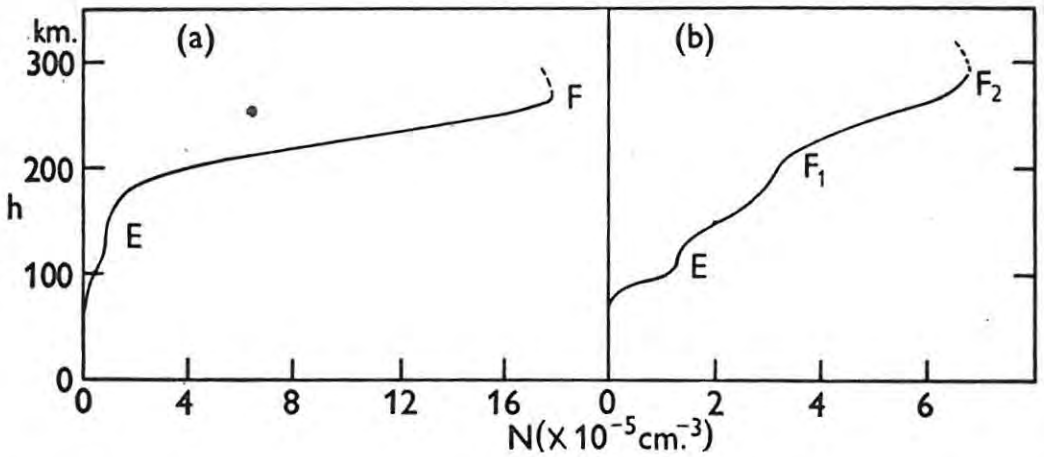

FIG. 1.4 Electron density (N) plotted against height (h) for the ionospheres which gave rise to the $h'(f)$ curves of Fig. 1.3

When ionograms are reduced to N-h curves by a method such as that discussed in section 3.3 the actual distribution of the electrons in the ionospheric regions will be obtained. Figure 1.4 gives the N-h curves corresponding to the h'-f curves of figure 1.3. The regions which give rise to the different curves in Fig. 1.3 are labelled.

The lowest of the ionospheric regions is the so-called D region. The existence of this region and information about its electron content are deduced more readily by inference than by direct observation. It is this region, with a high collision frequency between electrons and heavy particles, which is largely responsible for the attenuation of shortwave radio signals. Its height has been determined by BEST et al (1936) as varying between 70 and 90 km.

Above the D region is the E layer, the maximum ionization density of which is controlled by the amount of solar radiation reaching it. The peak electron density thus depends on the solar zenith angle, which determines the thickness of the atmosphere through which the radiation must pass, and solar activity. At night the ionization density of this layer becomes relatively insignificant.

Closer investigation reveals that ledges of ionization may occur within the E region (see for example WHALE, 1951). These ledges are designated E_1, E_2 etc.

The F region extends from about 150 to 400 km. This region is very often stratified into two layers, the F_1 and F_2 layers, although at night the F_1 layer disappears.

The bifurcation of this region is not always very marked but

appears with sufficient regularity to warrant the nomenclature F_1 and F_2 layers.

The maximum ionization density of the F_1 layer at any one place behaves in a regular manner. It is never observed at night, not always by day, it is most pronounced in summer at the minimum of solar activity and is not observed during winter at sunspot maximum. The height of peak electron density is in the neighbourhood of 170 km.

If the F_1 layer corresponded to an α Chapman layer in quasi-equilibrium, (see SECTION 2.4) the critical frequency should be proportional to $(\mathrm{Cos}\chi)^n$, where χ = solar zenith distance and n = 0.25. n, however, is found to vary from place to place.

The behaviour of the F_2 layer is more complicated. The critical frequency displays a number of departures from the behaviour of a hypothetical Chapman layer, although RATCLIFFE (1951) has shown that the total electron content of the F_2 layer behaves in a regular manner with respect to the sun.

The critical frequency displays a "geographic" or "equatorial" anomaly (APPLETON, 1954) which suggests movements of ionization associated with the geomagnetic field.

When f_oF_2 is plotted as a function of local mean time it is often found that the peak occurs well after noon ie. not when the electron production rate is at a maximum.

In addition to these there are the "December anomaly" and the "seasonal anomaly". The former is the occurrence of a noon value of f_oF_2 which is very large, during the Northern hemisphere winter months,

Fig 1.5

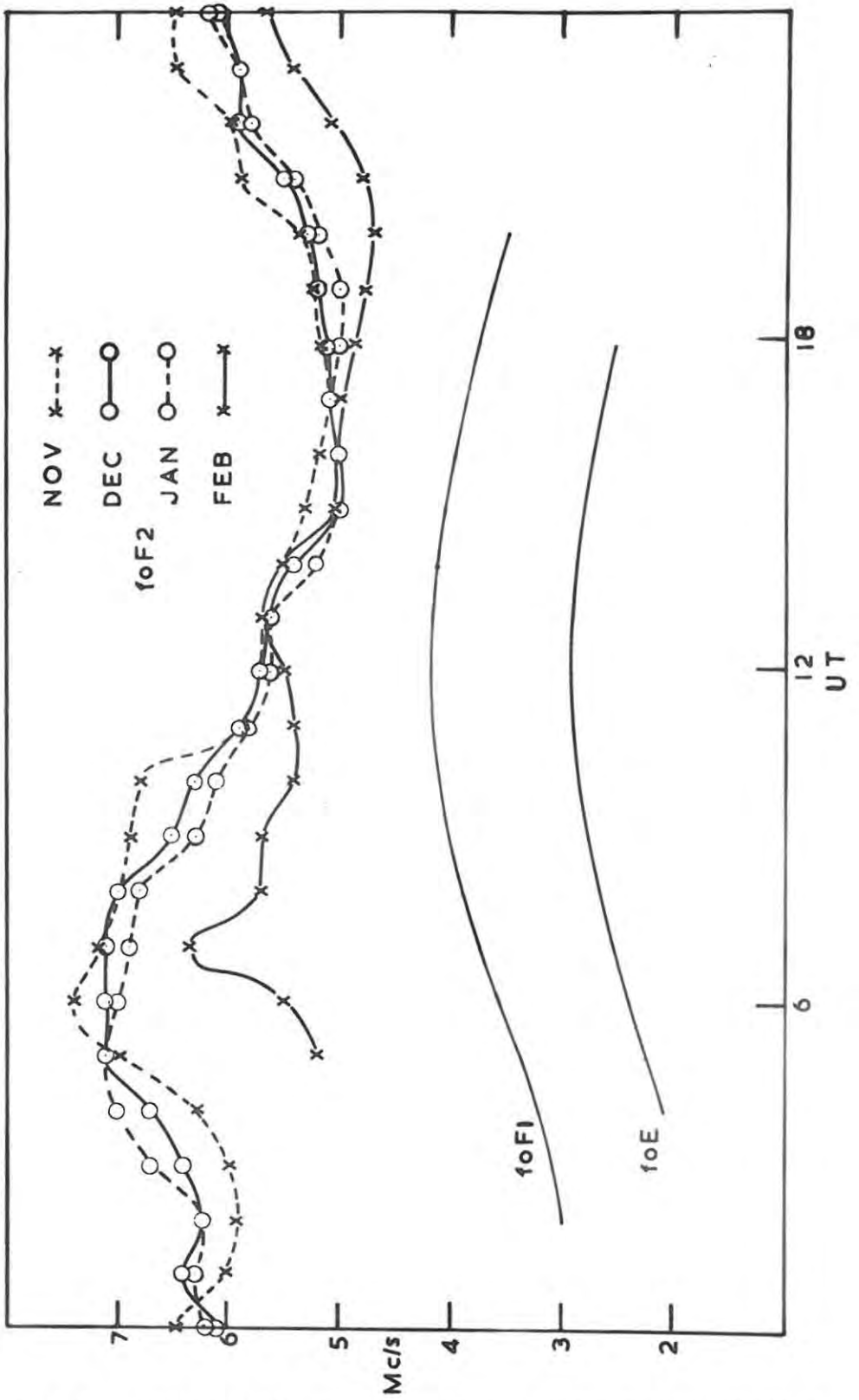

Fig. 1.5 Median plots of f_0F_2 values for magnetically quiet days and average of medians of f_0F_1 and f_0E values during 1962/3 summer season at SANAE, Antarctica.

between 50°N and 35°S and the latter the occurrence of abnormally high values of f_oF_2 during local winter. There is also a region in west Antarctica (between 0° and 60°W longitude) where f_oF_2 shows a distinct maximum shortly after local midnight during the summer months (BELLCHAMBERS and PIGGOTT, 1958). As an example of this see figure 1.5 which shows the f_oF_2 plots for the summer months 1962/63 at Sanae base, Antarctica (70° 18'S, 2° 21' W).

Also shown are the average values of f_oF_1 and f_oE for the same months. As can be seen these two layers have a regular diurnal variation.

The data used to draw Figure 1.5 was obtained by the author and D. G. Torr while attached to SANAE 3 and 4, respectively, as ionospherics. (Physics Department, Rhodes University 1962/63).

CHAPTER 2

IONIZED LAYER FORMATION.

2.1 Chapman Theory.

Experimental evidence has shown that electromagnetic radiation in the ultraviolet and X-ray region, originating from the sun, is mainly responsible for the production of ionized layers.

CHAPMAN (1931 a and b) considered the effect of ionizing radiation incident on an atmosphere consisting of a single gas over a flat earth.

As the ionizing radiation penetrates more deeply into this hypothetical atmosphere it encounters a greater density of gas and produces more electrons per unit volume. The radiation is, however, being absorbed in the process and below a certain height the rate at which its intensity decreases as it travels downwards is greater than the rate at which the gas density increases. The result of this is that a maximum electron production rate occurs at a certain level. The height of this level is also determined by the solar zenith angle since this determines the thickness of the atmosphere through which the ionizing radiation has to pass.

Chapman thus deduced that the electron production rate, q, at any height, h, would be given by

$$q = q_m \exp(1 - z - e^{-z} \operatorname{Sec}\chi) \qquad (2.1)$$

where $q_m = B\, I_\infty \operatorname{Cos}\chi\, H \exp(1)$ (2.2)

B = no. electrons produced when unit energy is absorbed.

I = photon flux per unit area incident from above at a solar zenith angle, χ.

z = normalised height.

$= (h - h_m) / H$

h_m = height where production rate is a maximum.

$H = KT/Mg$.

K = Boltzmann constant.

T = the absolute temperature.

M = molecular weight of the gas.

g = acceleration due to gravity.

It is convenient to use the height of the maximum of the layer when $\chi = 0$ as a reference level.

In this case in 2.1 q_m is replaced by q_o, the peak production rate when $\chi = 0$ and $Z = h - h_o/H$ where h_o is the height of the peak production rate, q_o.

From 2.2

$$q_o = BI_\infty / H \exp(1)$$

and $q_m = q_o \cos\chi$. This simple theory has been extended (CHAPMAN, 1931, b) to allow for the curvature of the earth. In this case, in 2.1, $\sec\chi$ is replaced by the Chapman function $Ch(\chi)$ which can be got from tables given by WILKES (1954). For $\chi < 75^\circ$ $Ch(\chi)$ approximates $\sec\chi$. A further extension has been to allow for change in scale height with temperature (GLEDHILL and SZENDREI, 1950; NICOLET, 1951).

RISHBETH and SETTY (1961) considered a mixed atmosphere of two

ionizable constituents with different scale heights and ionizing cross-section and absorbing the same radiation. In this case the resulting production function is the sum for the functions of the separate processes and it can be shown that q_m is still proportional to Cos χ as for a single gas.

2.2 Loss Processes.

2.2.1 Recombination.

An electron can combine with a positive ion to produce a neutral molecule or atom or a neutral atom or molecule to produce a negative ion. The rate of electron loss for the first process will then be given by

$$\frac{dN}{dt} = - \alpha N \, n(A^+)$$

where N = dlectron density

nA^+ = positive ion density and

α = the recombination coefficient.

If th number of negative ions is small and there is only one ion A^+ N will be approximately equal to $n(A^+)$ and we may write

$$\frac{dN}{dt} = - \alpha N^2 \qquad (2.3)$$

2.2.2 Attachment.

It will be seen from Chapter 3 that the effect of free charges on the propagation of radio waves is inversely proportional to their mass, thus electrons become relatively ineffective when attached to

an atom to form a heavy ion. The rate of this process is given by

$$\frac{dN}{dt} = b \,.N.n(A)$$

where b is the rate constant for the process and n(A) the number of neutral atoms. If n(A) is assumed to be so great that it is relatively unaffected by ionization processes we may write

$$\frac{dN}{dt} = -\beta N \qquad (2.4)$$

where β is the attachment coefficient.

2.2.3 Charge transfer and ion-atom interchange.

In addition to the above simple picture there are two more processes:

$A^+ + e \rightarrow A' + h\nu$ Radiative recombination, and

$A^+ + e \rightarrow A''$

$A'' \rightarrow A' + h\nu$ dielectronic recombination

where A is an atom or molecule, e an electron and $h\nu$ a photon.

(BATES, 1956) which are considered under recombination. The loss coefficient for both these processes is of the order of 10^{-12} $cm^3 sec^{-1}$. It has been found from eclipse measurements that recombination is the predominant process in the E and F_1 layers and that the loss coefficient is of the order of $10^{-8} cm^3 sec^{-1}$. The simple recombination processes do not yield a value of α as high as 10^{-8} cm^3/sec and BATES and MASSEY (1946, 1947) proposed the following recombination scheme to resolve this difficulty.

$$A + h\nu \longrightarrow A^+ + e \qquad \text{Production}$$

$$A^+ + XY \longrightarrow XY^+ + A$$

$$XY^+ + e \longrightarrow X' + Y' \qquad \text{Loss.}$$

where XY is a molecule composed of atoms X and Y.

The rates for the two loss processes are given by

$$\frac{dn}{dt}(A^+) = - k_1 \, n(A^+) \, n(XY) \tag{2.5}$$

$$\frac{dN}{dt} = - k_2 \, n(XY^+) \, N \tag{2.6}$$

where k_1 and k_2 are the loss coefficients for the processes.

It can be shown (HIRSH, 1959) that under equilibrium conditions the electron production rate q is given by

$$q = \frac{k_1 \, k_2 \, n(XY) \, N^2}{k_1 \, n(XY) + k_2 \, N} \tag{2.7}$$

If $k_1 \, n(XY) \gg k_2 \, N$

$$q = k_2 N^2 \tag{2.8}$$

which is the recombination equation

and if $k_1 \, n(XY) \ll k_2 N$

$$q = k_1 n(XY) \, N \tag{2.9}$$

which reduces to the attachment equation

$$q = \beta N.$$

This scheme also suggested the mode of formation of the F_2 layer.

From 2.8 we see that β is proportional to the atmospheric density, and that it decreases with height.

BRADBURY (1938) considered the electron distribution of a layer in which the loss coefficient is a function of height. RATCLIFFE

(1959 a) showed that, under practical conditions, the electron density of a so-called "Bradbury layer" would increase indefinitely. The process which is believed to produce the F_2 maximum will be discussed in the next section.

It was at first thought that the above charge transfer scheme was operative in the ionosphere but the following ion-atom interchange process (BATES and NICOLET, 1960) seems more likely.

$$A^+ + XY \longrightarrow AY^+ + X$$

$$AY^+ + e \longrightarrow A' + Y'.$$

and equations 2.5 and 2.6 will represent these two reactions provided the rate constants are taken to apply to them.

2.3 Movement of ionization.

If the mean drift velocity (V) of the free electrons is considered it can be shown that the rate of change of the electron density, as given by MARTYN (1947), is

$$\frac{dN}{dt} = q - L - \mathrm{div}(NV) \qquad (2.10)$$

where L is the loss term. This can be shown to reduce to

$$\frac{dN}{dt} = q - L - N\frac{dw}{dh} - w\frac{dN}{dh} \qquad (2.11)$$

where w is the upward component of the drift velocity, since there is good reason to believe that the vertical component is the most important (ie. the drift velocity and N change more rapidly with height than horizontal distance). This vertical drift could be due to (1) changes of temperature, (2) diffusion, or (3) electromagnetic

forces.

For the present we need only to consider the effects of diffusion. This has been discussed by various workers (DUNGEY, 1956; FERRARO, 1946; FERRARO and ÖZDOĞAN, 1958; GLIDDON and KENDALL, 1960 and MARTYN, 1955) and it is now believed that the F_2 maximum is caused by "ambi-polar" diffusion in which positive and negative ions diffuse together at the same rate due to electro-static interaction.

It can be shown that the diffusion term increases exponentially upwards as the neutral gas density decreases and it is believed that β decreases exponentially. The result of this is that at heights greater than 300 km diffusion is more important than attachment, and at lower heights the reverse is true. It is this fact which has led YONEZAWA (1956) to suggest that diffusion may be important in the formation of the F_2 peak.

We can therefore conclude that the electron loss process in the E and F_1 layers is recombination-like and that in the F_2 region is attachment-like.

It should, however, be noted that there is a transition region somewhere in the F layer where there is a changeover from a quadratic (αN^2) to a linear (βN) loss law.

This problem has been analysed by MARIANI, 1959; HIRSH, 1959 and YONEZAWA et al., 1959.

2.4 Layers in Quasi-Equilibrium.

If the effect of movement of ionization can be neglected, the electron density, N, at a fixed height will be determined by

$$\frac{dN}{dt} = q - L \qquad (2.12)$$

where q is the rate of electron production and L the rate of electron loss by recombination or attachment.

If ionospheric conditions are such that

$$\frac{dN}{dt} \ll q \text{ or } L$$

then we can write

$$q = L \qquad (2.13)$$

and the electron density is said to be in quasi-equilibrium. This equation is exact at a turning point of the function N(t), e.g. such as often occurs at midday, in the early morning and during eclipses.

If the electron density happens to be in quasi-equilibrium throughout the whole layer, we may write, at each level

$$q = \alpha N^2 \qquad (2.14)$$

or

$$q = \beta N \qquad (2.15)$$

depending on whether recombination or attachment is the loss process operative in the layer.

If α and β are independent of height we can substitute for q from equations 2.1 and 2.2 getting

$$N = \left\{(q_o\ \alpha)\ \mathrm{Cos}\chi\right\}^{\frac{1}{2}} \exp\left\{\tfrac{1}{2}\left[1-z-\exp(-z)\right]\right\} \qquad (2.16)$$

or

$$N = (q_o\ \beta)\ \mathrm{Cos}\chi\ \exp\left[1-z-\exp(-z)\right] \qquad (2.17)$$

In each case the peaks of the functions $N(z)$ and $q(z)$ will be at the same height.

The electron distribution given by (2.16) is called an equilibrium α-Chapman layer and that given by (2.17) an equilibrium β-Chapman layer (CHAPMAN, 1931b).

If N_m is the peak electron density the equations reduce to

$$N_m = \left[(q_o/\alpha) \operatorname{Cos}\chi \right]^{\frac{1}{2}} \quad \text{for } \alpha \text{ Chapman} \qquad (2.18)$$

and

$$N_m = (q_o/\beta) \operatorname{Cos}\chi \quad \text{for } \beta \text{ Chapman} \qquad (2.19)$$

If the loss coefficient (α or β) decreases as the height of the layer increases we can deduce from 2.16 and 2.17 that the peak of N is at a greater height than the peak of q.

BRADBURY (1938) considered an equilibrium layer in which the loss coefficient decreases with increasing height sufficiently rapidly to produce a peak of electron density at a height very much greater than the height of peak electron production. Such a layer is often referred to as a "Bradbury layer".

CHAPTER 3.

BEHAVIOUR OF RADIO WAVES IN IONIZED MEDIA.

3.1 Neglecting the magnetic field.

ECCLES (1912), neglecting the effect of collisions between electrons and heavy particles, derived the following expression for the refractive index of the ionosphere:-

$$\mu = \sqrt{1 - \frac{N e^2}{\pi m f^2}} \qquad (3.1)$$

where f = frequency of radio wave

N = electron density (electrons cm^{-3})

e = electronic charge (esu)

m = electron mass (gm)

The phase velocity

$$V = \frac{c}{\mu} \qquad (3.2)$$

where c = velocity of light.

and the group velocity

$$U = c\mu \qquad (3.3)$$

From this one can deduce that the group velocity is dependent on N/f^2 and that reflection occurs when

$$N = \frac{\pi m f^2}{e^2} = (1.24 \times 10^4)\, f^2 \text{ electrons } cm^{-3}. \qquad (3.4)$$

The expression for μ is sometimes written

$$\mu = \sqrt{1 - \frac{f_N^2}{f^2}} \qquad (3.5)$$

where f_N is the plasma frequency corresponding to the electron density N and

$$f_N = \sqrt{\frac{N e^2}{\pi m}} \qquad (3.6)$$

at reflection then $f = f_N$ (3.7)

It has been seen that the group velocity of a radio pulse depends on the electron density and that the pulse is more retarded when f is very nearly equal to f_N. If we assume a constant group velocity equal to the velocity of light we find that the effective height at which the wave is reflected is greater than the actual height of f_N. This height is the "virtual" or "apparent" height and in fact depends on the probing frequency, the geomagnetic field and the N-h distribution up to the point of reflection.

3.2 The effect of the geomagnetic field.

3.2.1 Introduction.

The effect of the geomagnetic field is to render the ionosphere birefringent. Thus, in general, any plane polarized wave incident on the ionosphere is split into two characteristic waves with opposite polarizations. These are referred to as the Ordinary (O-) and Extraordinary (E-) Waves. (See figures 1.2 and 1.3). The ordinary wave critical frequency of a layer is under ordinary circumstances the peak plasma frequency of the layer, just as it would be if the geomagnetic field were absent.

3.2.2 Magneto-Ionic Theory.

The basic difficulty is that the geomagnetic field and electron density in the ionosphere are not constant. However, these do not

change appreciably over short distances and one can assume that the wave at each level behaves as though it were in a large homogeneous medium, consisting of electrons, positive and negative ions and neutral atoms and molecules, to which a constant magnetic field is applied.

APPLETON (1927, 1932) and HARTREE (1931) independently derived an expression for the refractive index of a radio wave in terms of wave frequency, electron density, magnetic field and frequency of collisions between electrons and heavy particle. The full Appleton-Hartree equation (as it is now called) is given by various authors (RATCLIFFE, 1959 b and BUDDEN, 1961) and for practical purposes (ignoring collisions) reduces to

$$n^2 = 1 - \frac{X}{1 - \frac{Y_T^2}{2(1-X)} \pm \left\{ \frac{Y_T^4}{4(1-X)^2} + Y_L^2 \right\}^{\frac{1}{2}}} \qquad (3.8)$$

$n = \mu - i\chi$, the complex refractive index.

μ = phase refractive index = C/V

χ = attenuation factor.

c = velocity of electromagnetic radiation in vacuo.

V = velocity of electromagnetic radiation in medium.

$X = f_o^2/f^2$

$Y_T = Y \sin\Theta$, $Y_L = Y \cos\Theta$ $\qquad Y = f_H/f$.

f = wave frequency.

f_o = plasma frequency = $(\frac{1}{2}\pi)\ (Ne^2/\epsilon_o m)^{\frac{1}{2}}$

f_H = gyro frequency = $Be/2\pi m$.

e = electron charge.

m = electron mass.

ϵ_o = electric permittivity of free space.

μ_o = magnetic permittivity of free space.

B = magnitude of magnetic inductions in medium = $\mu_o H$ if relative permeability of the medium is unity.

Θ = angle made by the magnetic field with the direction of radiation. (Rationalised units are used.)

For $f > fH$ there will be three values of f_N, the plasma frequency, at which an electromagnetic wave will be reflected i.e. three conditions for which n = 0.

These are given by:-

$$f_{N_1}^2 = f^2 - f\, f_H \text{ or } X = 1 - Y \qquad (3.9)$$

$$f_{N_2}^2 = f^2 \qquad \text{or } X = 1 \qquad (3.10)$$

$$f_{N_3}^2 = f^2 + f\, f_H \text{ or } X = 1 + Y \qquad (3.11)$$

The one reflection level $f_N = f$ is independent of the geomagnetic field and is in fact the same reflection condition as equation 3.7.

The extraordinary ray is given by equation 3.9.

X = 1 + Y also gives n = 0, but in the ionosphere the wave cannot penetrate to this level since it is reflected lower down at the level X = 1 - Y.

From this one can also see that the frequency of the extraordinary ray is greater than the plasma frequency at its point of reflection.

3.2.3 The group refractive index.

From 3.8 it is possible to calculate μ for any values of X and Y.

The theory of wave-propagation in a dispersive medium, such as the ionosphere, shows that the electromagnetic wave is propagated at a group velocity U which is related to the phase velocity, V, and the frequency, f, by

$$\frac{1}{U} = \frac{d}{df}\left[\frac{f}{V}\right]. \qquad (3.12)$$

If we now define the group refractive index $\mu' = \frac{c}{U}$ (by analogy with equation 3.2) and differentiate 3.12 after substitution for V and u, then

$$\mu' = \mu + f\frac{d\mu}{df} \qquad (3.13)$$

Note that in the absence of a magnetic field

$$\mu^2 = 1 - X = 1 - f_o^2/f^2$$

$$\text{and} \quad \mu' = \frac{1}{\mu} \qquad (3.14)$$

Differentiation of equation 3.8 with respect to f leads to the expression

$$\mu' = \frac{1}{\mu\left[1-X\right]\left[1-Y_T^2/1-X\right] \pm \left[Y_T^4/4(1-X)^2 + Y_L^2\right]^{\frac{1}{2}}} \times \left\{1 - \mu^2 - {}^2 \pm \frac{(1-\mu^2)(1+X)\,Y_L^2}{2\left[Y_T^4/4\,(1-X)^2 + Y_L^2\right]^{\frac{1}{2}}}\right\} + \mu \qquad (3.15)$$

WALKER (1962) using the method of SHINN and WHALE (1952) calculated values of μ' for a range of values of X and Y for Grahamstown.

3.2.4 Lateral deviation.

One further effect of the geomagnetic field is that a radio wave follows a curved path from the bottom of the layer or layers to

the point of reflection. This problem is discussed by BOOKER (1936, 1938) and results from the fact that the ray direction (which defines the group path) and the direction of the wave normal do not necessarily coincide.

The Ordinary (O-) and Extraordinary (E-) rays are deflected in opposite directions and may be reflected from points 30 - 100 km. apart.

Thus horizontal differences in the ionospheric structure can lead to differently shaped O- and E- h'f curves.

Accurate measurements of the geomagnetic field by means of penetration frequencies can also not be made because of horizontal gradients of magnetic intensities although a useful indication of the field strength can be obtained.

3.3 Reduction of ionograms.

3.3.1 Introduction

The virtual height of reflection of a radio wave vertically incident on the ionosphere is given by

$$h' = \int_0^h \mu' \, dh \qquad (3.16)$$

where μ' is a complicated function of N, the wave frequency f, and the magnetic dip as shown in section 3.2.2.

A complete survey of existing methods of ionogram reduction is given by THOMAS (1959), and an extensive list of references is included in the survey.

Thomas gives a set of tables of Kelso-coefficients (KELSO, 1952)

for different conditions of magnetic intensity and magnetic dip angle.

A table of values for these coefficients were derived from this set for the magnetic parameters of Grahamstown.

These coefficients were at first used but were discarded in favour of the method developed by TITHERIDGE (1959 a). This method is discussed somewhat more fully in the next section. The ionograms obtained were scaled by the methods of 3.3.2, 4 and 5.

3.3.2 Titheridge method of ionogram reduction.

The N-h curve is divided into a series of heights, h_r, corresponding to a set of virtual heights, h'r, at a given series of frequencies f_n.

If $\overline{\mu'}_{r,n}$ is the mean value of μ' over the lamina h_{r-1} to h_r for a probing frequency f_n then from 3.16

$$\overline{\mu'}_{r,n} = \frac{1}{h_r - h_{r-1}} \int_{h_{r-1}}^{h_r} \mu' dh \qquad (3.17)$$

At any frequency the virtual height is given by the height at the bottom of the ionosphere, h_o, plus the sum of the virtual path lengths in each lamination up to the n th.

Let $\Delta h_r = h_r - h_{r-1}$.

We thus get the following set of equations for the virtual heights corresponding to r = 1, r = 2 ... r,

$$\begin{aligned} h'_o &= h_o \\ h'_1 &= h_o + \overline{\mu'}_{1,2}\, \Delta h_1 \\ h'_2 &= h_o + \overline{\mu'}_{1,2}\, \Delta h_1 + \overline{\mu'}_{2,2}\, \Delta h_2 \\ &\cdots\cdots\cdots\cdots\cdots \\ h'_r &= h_o + \overline{\mu'}_{1,r}\, \Delta h_1 + \overline{\mu'}_{2,r}\, \Delta h_2 + \ldots\ \overline{\mu'}_{r,r}\, \Delta h_r. \end{aligned} \qquad (3.18)$$

By subtraction

$$h'_o = h_o$$

$$\Delta h'_1 = \overline{\mu'}_{1,1}\, \Delta h_1$$

$$\Delta h'_2 = \overline{\mu'}_{2,2}\, \Delta h_2 - (\overline{\mu'}_{1,1} - \overline{\mu'}_{2,2})\, \Delta h_1$$

.....

$$\Delta h'_n = \overline{\mu'}_{n,n}\, \Delta h_n - (\overline{\mu'}_{n-1,n-1} - \overline{\mu'}_{n-1,n})\, \Delta h_{n-1} -$$
$$\ldots - (\overline{\mu'}_{r,n-1} - \overline{\mu'}_{r,n})\, \Delta h_r - \ldots$$
$$\ldots - (\overline{\mu'}_{1,n-1} - \overline{\mu'}_{1,n})\, \Delta h_n \qquad (3.19)$$

Let $\beta_{r,n} = \overline{\mu'}_{r,n-1} - \overline{\mu'}_{r,n}$ $\qquad r < n$

and $\beta_{n,n} = \overline{\mu'}_{n,n}$ $\qquad r = n \qquad (3.20)$

Equations 3.19 now reduces to

$$h'_o = h_o$$

$$\Delta h'_1 = \beta_{1,1}\, \Delta h_1$$

$$\Delta h'_2 = \beta_{2,2}\, \Delta h_2 - \beta_{1,2}\, \Delta h_1$$

.....

$$\Delta h'_n = \beta_{nn}\, \Delta h_n - \beta_{n-1,n}\, \Delta h_{n-1} - \ldots$$
$$- \beta_{r,n}\, \Delta h_r - \ldots - \beta_{1,n}\, \Delta h_1 \qquad (3.21)$$

Solving these successively

$$h_o = h_o'$$

$$\Delta h_1 = \frac{1}{\beta_{1,1}}\, \Delta h'_1$$

$$\Delta h_2 = \frac{1}{\beta_{2,2}} \left\{ \Delta h'_2 + \beta_{1,2}\, \Delta h_1 \right\}$$

.....

$$\Delta h_n = \frac{1}{\beta_{n,n}} \left\{ \Delta h'_n + \sum_{r=1}^{n-1} \beta_{r,n}\, \Delta h_r \right\} \qquad (3.22)$$

where $\beta_{n,n}$ is the mean value of μ' in the lamina n, for the wave to be reflected at the top of the lamina n, and

$$\beta_{r,n} = \overline{\mu'}_{r\ n-1} - \overline{\mu'}_{r,n} \qquad r = 1,2 \ldots n-1.$$

where the nomenclature $\overline{\mu'}_{r,n}$ indicates the mean group refractive index in the lamina r for a wave to be reflected at the top of the nth lamina.

β can be calculated from values of the mean refractive index and the heights of the laminas Δh_1, Δh_2 etc. can be calculated from equation (3.22)

Titheridge shows how the coefficients $\beta_{r,n}$ rapidly become negligible in comparison with $\beta_{n,n}$ as r decreases. For this reason only the larger β coefficients need be considered. To improve accuracy the larger β coefficients in the table obtained after applying equation 3.20 to tables of μ' may be increased to compensate for the neglected coefficients so that $\sum_{r=1}^{n} \beta_{r,n}$ remains unchanged.

These modified coefficients are sufficiently accurate for most purposes.

The application of the modified β-coefficients are exactly the same as that of the unmodified coefficients, except that in equation 3.22 only the last two or three of the Δh values already obtained need be considered in the summation

$$\sum \beta_{r,n}\ \Delta h_r.$$

r will in this case go from n - 3 or n - 2 to n - 1.

WALKER (1962) calculated a set of modified β coefficients for both ordinary and extraordinary rays for a range of frequencies up to 6 Mc/s. The frequency distribution for these coefficients was

Fig 3.1

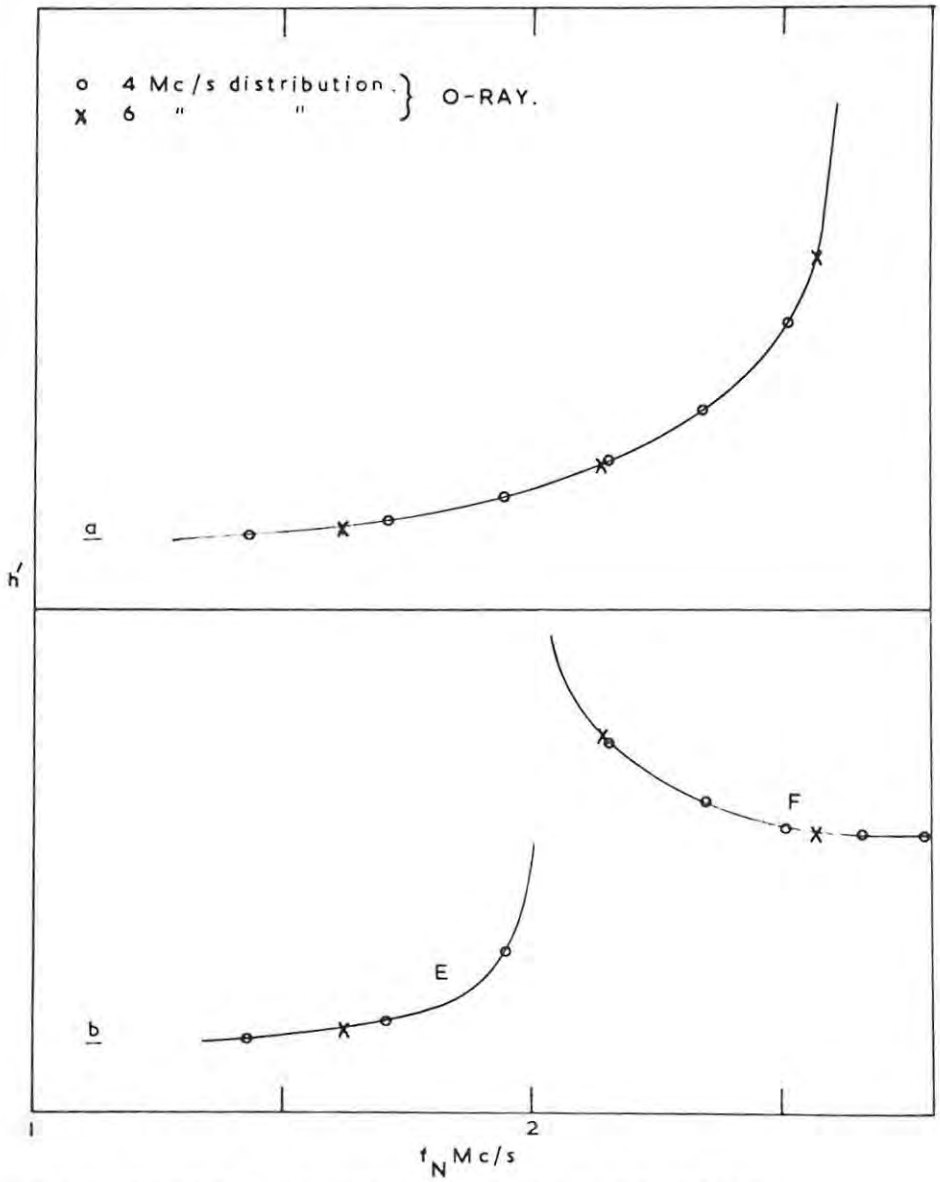

FIG.3.1. DISTRIBUTION TITHERIDGE SCALING POINTS.
a f_{crit} F LOW.
b E LAYER NEWLY FORMED.

obtained from

$$f_n = A \log \left(1 + \frac{n}{2}\right) \qquad (3.23)$$

where n goes from 1 to 25 and A is a constant chosen so that $f_{25} = 6$ Mc/s.

Equation 3.23 is obtained from Titheridge. The equation should have read

$$f_n = A \sqrt{\log \left(1 + \frac{n}{2}\right)} \qquad (3.24)$$

(TITHERIDGE private communication)

The reason for this distribution is to provide nearly equal real height intervals over the complete N-h curve.

Titheridge points out that the actual frequency distribution does not affect the validity of the β-coefficients for ionogram reduction, provided a sufficient number of points are scaled on the h'-f curve.

The author found it necessary to calculate a set of β-coefficients for O- and E- rays with a smaller interval between successive sampling frequencies than those used by WALKER (1962). The reason for this was the fact that very few sampling points are otherwise obtained when the critical frequency of the F-layer is low and that only one or two sampling points may lie on the cusp at an E layer critical frequency (see figure 3.1 a and b). If a greater number of sampling points are used under these conditions a more accurate N-h curve will be obtained and large values of Δh (which should nominally only be a few km) will be avoided.

The frequency distribution for these coefficients was also obtained from equation 3.23. n in this case is equal to 24 and A is chosen so that $f_{24} = 4$ Mc/s.

Tables 1 and 2 give the values of μ' for Grahamstown calculated by the author for the O- and E- rays for a frequency distribution up to 4 Mc/s. The modified β-coefficients obtained for the O-ray from the tables of μ' are given in table 3 and the modified WALKER 6 Mc/s β-coefficients are given in table 4.

These modified coefficients for the O- ray for 4 and 6 Mc/s (WALKER) frequency distribution were used for scaling the ionograms.

The 4 Mc/s distribution O-ray β-coefficients were used up to the layer maximum for records where the F layer critical frequency was less than about 3.3 Mc/s and to well beyond the cusp formed at the E layer critical frequency whenever the E layer was present. Large values of Δh and any possible errors caused by a lack of sampling points on the steeply sloping parts of the h'-f curves were thus avoided.

In general it was found convenient to use the 4 Mc/s distribution coefficients up to 2.92 Mc/s and then to switch to the WALKER 6 Mc/s β-coefficients starting at 2.93 Mc/s for the rest of the ionogram.

The necessary Δh's for multiplication with the first WALKER β-coefficients can be obtained by interpolation for h (2.14 Mc/s) and h (2.57 Mc/s) and subtracting h (2.57) - h (2.14). No interpolation is necessary for h (2.93 Mc/s) since the possible error in the Δh thus obtained by using h (2.92 Mc/s) is only about $1/40^{th}$ of the actual Δh. When the summation of equation 3.22 is performed for the next Δh it will be found that the total error introduced is negligible.

In order to check the accuracy of the modified 4 Mc/s and 6 Mc/s distribution O-rays β-coefficients an O-ray h'-f curve was

calculated for a known parabolic curve and scaled by the method already described.

The shape of the N-h curve was determined by the expression

$$f_N^2 = A\ h\ (a - h) \qquad (3.25)$$

where h is the height from the bottom of the layer, $A = 3.6 \times 10^{-3}$ $Mc/s^2\ km^{-2}$ and a = 200 km. The height of the layer maximum at f_N = 6.00 Mc/s is 100 km. from the bottom of the layer.

The values of μ' for the O-ray of this layer were calculated for the plasma frequencies, $f_N = f_o$ at the top of 25 laminae of equal thickness, Δh = 4 km. The virtual height for f_N at the top of the n^{th} lamina is thus given by

$$h' = \Delta h \sum_{n=1}^{n} \overline{\mu'_n}$$

where $\overline{\mu'_n}$ is the mean group refractive index in the laminae n = 1 to n for the wave reflected at the top of the n^{th} lamina.

This O-ray h' - f curve was scaled by using the 4 Mc/s and 6 Mc/s β coefficients and by using a combination of the 4 and 6 Mc/s - β-coefficients.

When the curve was scaled using only the 6 Mc/s-distribution coefficients it was found that the value of the deduced height, h, at 5.91 Mc/s was 82.4 km as compared with the real height of 82.7 km. This error (0.5%) is satisfactorily explained by a possible scaling error of 5 km on the h'f curve at this frequency point. It should be noted that in this case 5 km corresponds to an error of 0.005 Mc/s made in the Titheridge scaling frequency because of the steepness of the h'-f curve at this point which is near the critical frequency of 6.00 Mc/s, and to 0.25 km in real height since $\beta_{n,n}$ = 20.45 at 5.91 Mc/s.

The Titheridge method of ionogram reduction is thus limited only by the accuracy with which frequencies and virtual heights can be scaled.

When the h'-f curve for the parabolic layer was scaled by using a combination of the 4 and 6 Mc/s β-coefficients, with a switchover point at 2.92 Mc/s, it was found that agreement between the actual N-h curve and that deduced by scaling the h'-f curve was as good as that obtained by using only the 6 Mc/s β-coefficients.

Since the values of $\overline{\mu'}$ obtained in calculating the O-ray h'-f curve for the parabolic layer given by equation 3.25 may prove useful at some future date, they are given in table 5. The modified β-coefficients deduced from them by the application of 3.20 are given in table 6.

The frequencies in the frequency-distribution correspond to the plasma frequencies at the top of laminae of equal thickness for a parabolic N-h distribution. μ' is only given up to $f_N = 5.923$ Mc/s, which is the plasma frequency at the top of the twenty-first lamina, because of the very small differences between the remaining successive value of f_N and the subsequent difficulty of calculating $\mu'_{n,n}$ accurately for these frequency intervals.

3.3.3 h'f curves from N-h distributions.

The virtual height at any frequency (O- and E-waves) can be calculated for any known N-h distribution by the straightforward application of equation 3.17, since the values of Δh and the $\overline{\mu'}$ corresponding to each Δh are known. The advantage of this method over the reverse application of 3.13 lies in the fact that Δh is accurately known and

errors in the calculation of h' are not cumulative. These methods of ionogram reduction to N-h curves and production of ionograms from N-h curves lend themselves readily to use on a desk calculator.

3.3.4 The effect of lower layers.

It is possible for a monotonically increasing N-h curve to give the same h'-f curve as an N-h curve with a valley between two layers. If a valley is present and the h'-f curve is scaled, using only the O-ray and assuming a monotonic increase of N with h, the derived N-h profile would be lower than the actual profile above the valley by approximately the depth of the valley.

This effect is discussed fully by GLEDHILL and WALKER (1960), MANNING (1949) and TITHERIDGE (1959 b). Titheridge gives a method of calculating the valley ionization and depth which makes use of the O- and E-rays. The necessary coefficients to be used have been calculated by WALKER (1962).

The valley ambiguity is not discussed in detail since it does not have an immediate bearing on the ionosphere at sunrise, although the situation could well arise between the E and F layers.

A factor of greater importance to the sunrise ionosphere is that of ionization below the night-time F layer. This effect is discussed by TITHERIDGE (1959 c) and the method of TITHERIDGE (1961), which makes use of the O- and E-rays, was applied wherever possible.

This method, however, breaks down when ionospheric conditions are such that the E-ray cannot be separated from the O-ray and also when the h'-f curve is very steep and the O- and E-rays cannot be scaled with sufficient accuracy. This is in fact the case just before

Fig 3.2

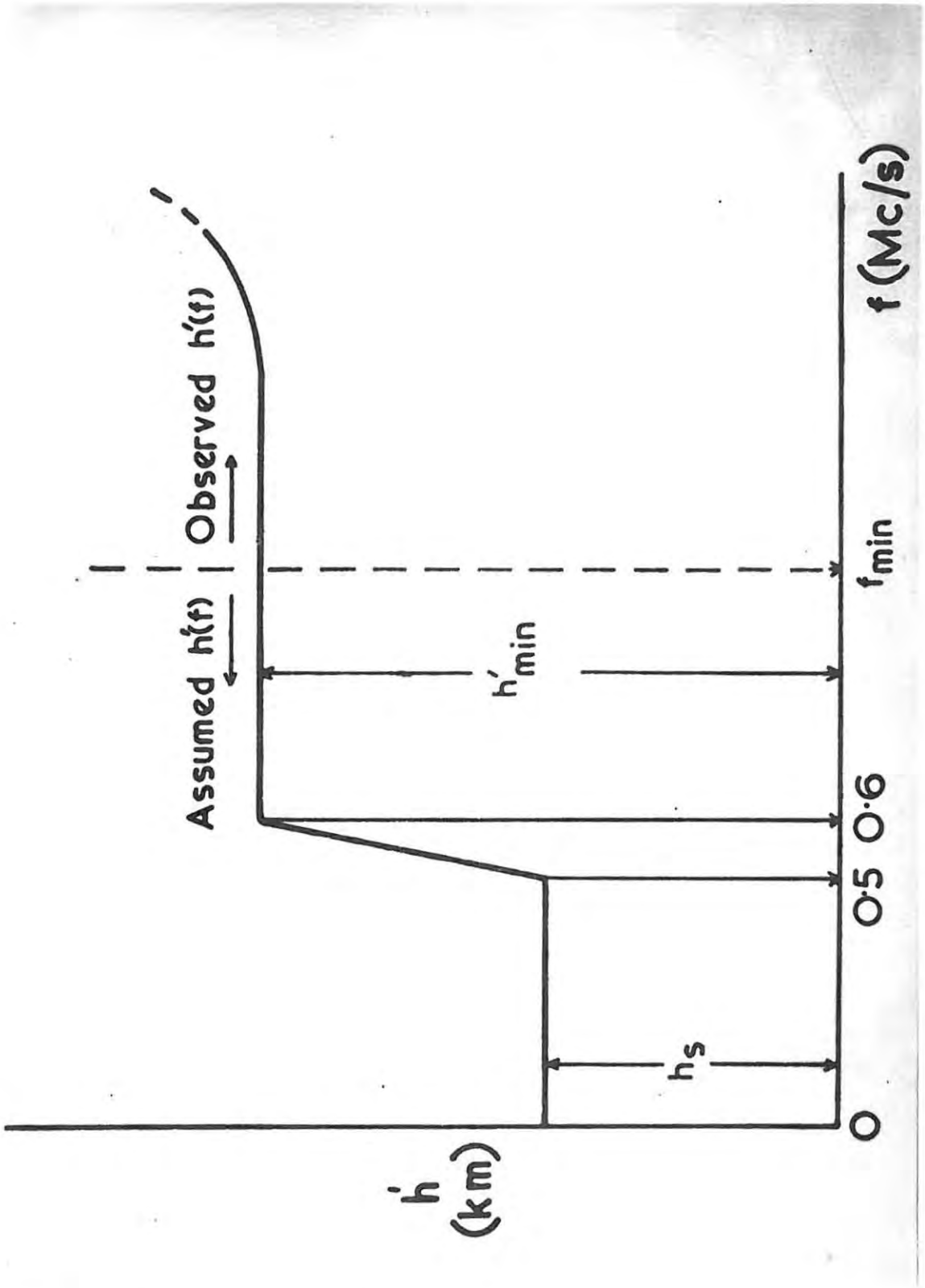

Fig. 3.2 The assumed h'(f) curve below f_{min}.

a lower layer, such as E, is formed.

A description of the method used to correct for the low-lying ionization follows.

Assume the virtual height to be equal to h'_{min} from f_{min} down to a frequency just greater than 0.5 Mc/s (say 0.6 Mc/s) and that it is equal to a value h_s from 0 - 0.5 Mc/s. The h'f curve now takes the form shown in figure 3.2.

The height h_s is chosen so that $h'_{min} - h_s$ is proportional to the amount of low-lying ionization. The amount of this ionization is approximately proportional to $h'_x - h'_{min}$, where h'_x is the virtual height corresponding to an E-ray frequency f_x which is obtained from $f^2_{min} = f^2_x - f_x f_H$.

f_{min} is the minimum observable O-ray frequency.

If the calculation is started at 0.5 Mc/s the value of h_s can be calculated from the equation given by Titheridge viz

$$h'_{min} - h_s = 0.74\ (5.98 - \text{Sin I})(f_x - f_H)^2\ \left[\overline{h'_x\ (f_x)} - h'_o\ (f_o)\right] \qquad (3.26)$$

where I = magnetic dip angle

$h'_x\ (f_x)$ is the virtual height at an E-ray frequency corresponding to a plasma frequency, $f_o = f_N$.

$h'_o\ (f_o)$ is the virtual height of the O-ray at a frequency f_o.

f_H = gyro-frequency (taken to be 0.82 Mc/s for Grahamstown).

If the calculation starts at a point where f_N = 1 Mc/s instead of 0.5 Mc/s the equation (given by Titheridge) is

$$h'_{min} - h_s = 0.36\ (5.48 - \text{Sin I})\ (f_x - f_H)^2\ \left[\overline{h'_x\ (f_x)} - h'_o\ (f_o)\right] \qquad (3.27)$$

In practice h'_x is measured at the lowest frequency at which the

Fig 3.3

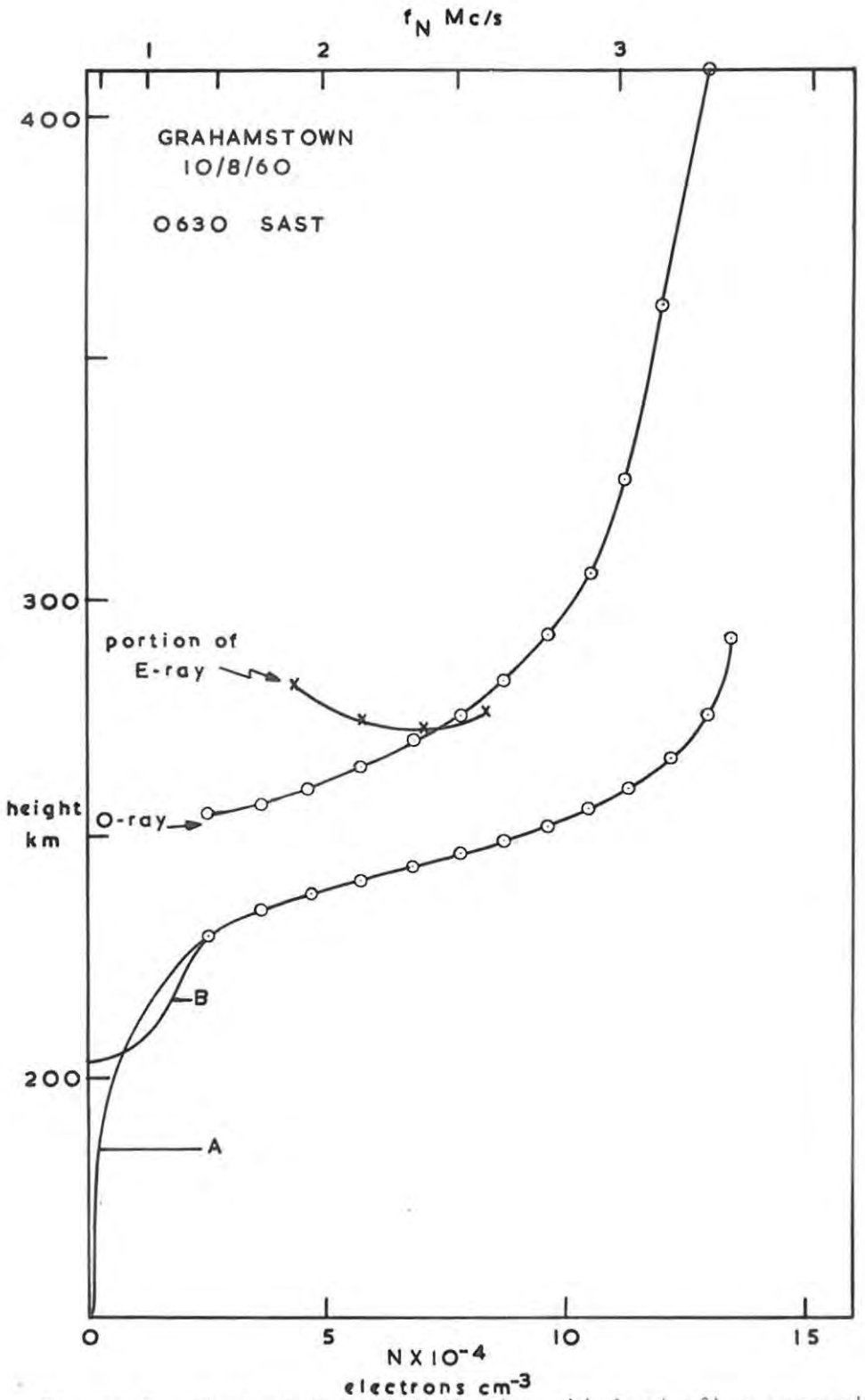

Fig. 3.3 Typical N-h distribution obtained after correction for low-lying ionization.

A - calculations started at 0.5 Mc/s.

B - calculations started at 1.0 Mc/s.

E-trace is visible. The corresponding value of h'_o is then found by interpolation in the measured O-ray heights and the initial height, h_s, is calculated from equations 3.21 or 3.22.

Figure 3.3 shows a typical N-h distribution obtained by this method using both equations 3.2 and 3.27.

The curve below $f_N = 1.43$ has been smoothed to give the same amount of ionization below the height of $f_N = 1.43$ Mc/s as in the block

$$h_s\,(0.5 \text{ or } 1 \text{ Mc/s}) - h\,(1.43 \text{ Mc/s}) .$$

The calculation for the amount of low-lying ionization can be checked by comparing the values of h' for the E-ray at a number of Titheridge E-ray frequencies corresponding to the Titheridge plasma- and O-ray frequencies (equation 3.9) with values of h' calculated for these E-ray frequencies from equation 3.18. μ' for the E-ray can be obtained from table 2 (4 Mc/s distribution) or WALKER (1962) (6 Mc/s distribution). Δh is already known since this has been calculated in the reduction of the h'-f (O-ray) curve to the N-h profile

3.3.5 Layer maximum.

The method used to determine the layer maximum is described by PIGGOTT and RAWER (1961).

It depends on fitting a parabola to the portion of the N-h curve near the meximum of the layer and is readily applicable in our case where the N-h curve is known up to a point very close to the critical frequency, f_c.

Consider two plasma frequencies f_1 and f_2 at two convenient values

of the ratio f_N/f_c viz. f_1/f_c and f_2/f_c. $f_1 > f_2$.

Let the heights of the plasma at the points f_1 and f_2 be h_1 and h_2 respectively.

The layer maximum is then determined from

$$h_c = h_1 + a(h_1 - h_2) \qquad (3.28)$$

where a is a constant found from table 7 (Piggott and Rawer's table S2.5).

TABLE 7.

f_1/f_c	0.97	0.97	0.97	0.97	0.97	0.97	0.96	0.96	0.96	0.96	0.95	0.95	0.95
f_2/f_c	0.90	0.91	0.92	0.93	0.94	0.95	0.90	0.91	0.92	0.93	0.90	0.91	0.92
a	1.26	1.42	1.63	1.95	2.49	3.50	1.79	2.08	2.51	3.20	2.53	3.06	3.96

It is possible to draw a graph of a vs f_2/f_c for constant f_1/f_c and to interpolate for values of a, without introducing any significant err error, for values of f_1/f_c and f_2/f_c not given in the table. In this way it is in many instances possible to use values of h_1 and h_2 which correspond to heights calculated at two Titheridge frequency points f_1 and f_2.

Care must be taken to avoid values of f_1 and f_2 very close to and also very far from the critical frequency. Errors are reduced when f_1/f_c and f_2/f_c are decreased, but the risk that the distribution may depart from that given by the parabola of best fit near the centre of the layer increases as the ratio f_2/f_c decreases and may be appreciable for $f_N < 0.90 f_c$.

It is also important that f_c should be known to better than 1% otherwise h_c could be out by as much as 10% or more of the quarter thickness of the parabola of best fit.

This method was used for determining the height of layer maximum for all the iono_rams scaled by the Titheridge method. (See for example Figure 3.3.)

TABLE 1: μ' at Titheridge frequencies. Ordinary Ray. 4 Mc/s distribution.

f_H = 0.82 Mc/s.

f	0.63	1.08	1.43	1.71	1.95	2.16	2.35	2.51
n	1	2	3	4	5	6	7	8
Y	1.295	0.759	0.573	0.478	0.419	0.379	0.349	0.326
r=1	2.00	1.07	1.03	1.02	1.01	1.01	1.01	1.01
2		2.95	1.20	1.08	1.07	1.06	1.05	1.04
3			3.90	1.35	1.25	1.22	1.20	1.18
4				4.84	1.46	1.35	1.30	1.26
5					5.78	1.59	1.49	1.41
6						6.72	1.73	1.54
7							7.65	1.86
8								8.58

f	2.66	2.79	2.92	3.03	3.14	3.24	3.34	3.43
n	9	10	11	12	13	14	15	16
Y	0.308	0.293	0.280	0.270	0.260	0.252	0.245	0.239
r=1	1.01	1.01	1.00	1.00	1.00	1.00	1.00	1.00
2	1.03	1.03	1.03	1.03	1.03	1.03	1.02	1.02
3	1.17	1.16	1.16	1.16	1.15	1.15	1.15	1.15
4	1.24	1.23	1.22	1.21	1.20	1.19	1.19	1.19
5	1.37	1.36	1.33	1.31	1.30	1.29	1.28	1.27
6	1.45	1.41	1.37	1.34	1.32	1.31	1.30	1.29
7	1.63	1.54	1.48	1.43	1.40	1.38	1.36	1.34
8	2.00	1.27	1.62	1.53	1.49	1.46	1.43	1.41
9	9.50	2.13	1.81	1.66	1.58	1.53	1.49	1.46
10		10.42	2.27	1.87	1.73	1.63	1.58	1.52
11			11.33	2.40	1.93	1.87	1.81	1.75
12				12.24	2.54	2.02	1.91	1.85
13					13.14	2.68	2.09	1.95
14						14.04	2.83	2.18
15							14.93	2.98
16								15.82

Table 1 continued:

f	3.51	3.59	3.67	3.74	3.81	3.87	3.94	4.00
n	17	18	19	20	21	22	23	24
Y	0.233	0.228	0.223	0.219	0.215	0.211	0.208	0.205
r=1	1.00	1.00	1.00	1.00	1.00	1.00	1.00	1.00
2	1.02	1.02	1.02	1.02	1.02	1.01	1.01	1.01
3	1.15	1.14	1.14	1.14	1.14	1.14	1.13	1.13
4	1.19	1.19	1.19	1.18	1.18	1.18	1.18	1.18
5	1.26	1.25	1.24	1.23	1.22	1.22	1.22	1.22
6	1.28	1.27	1.26	1.25	1.24	1.23	1.23	1.23
7	1.33	1.32	1.31	1.30	1.29	1.28	1.27	1.26
8	1.39	1.38	1.36	1.35	1.34	1.33	1.32	1.32
9	1.44	1.42	1.40	1.38	1.37	1.36	1.35	1.34
10	1.48	1.45	1.43	1.41	1.39	1.38	1.37	1.36
11	1.69	1.66	1.63	1.60	1.58	1.56	1.55	1.54
12	1.79	1.74	1.69	1.66	1.64	1.62	1.60	1.59
13	1.89	1.83	1.79	1.72	1.69	1.67	1.65	1.64
14	2.01	1.93	1.87	1.83	1.75	1.73	1.71	1.69
15	2.26	2.05	1.97	1.91	1.85	1.79	1.76	1.74
16	3.14	2.35	2.10	2.00	1.95	1.87	1.82	1.79
17	16.70	3.30	2.44	2.14	2.04	1.99	1.90	1.85
18		17.58	3.47	2.52	2.19	2.08	1.97	1.89
19			18.45	3.64	2.61	2.23	2.12	2.00
20				19.32	3.99	2.70	2.28	2.16
21					20.38	4.23	2.78	2.32
23						21.26	4.46	2.87
24							21.82	4.68
								22.76

TABLE 2: μ' at Titheridge frequencies. Extraordinary ray. 4 Mc/s distribution. f_x - E ray frequency. f_N = plasma frequency.

f_H = 0.82 Mc/s.

f_N	0.632	1.081	1.429	1.713	1.954	2.162	2.346	2.510
f_x	1.149	1.553	1.884	2.159	2.394	2.599	2.780	2.942
Y^x	0.7137	.5280	.4352	.3798	.3425	.3155	.2950	.2787
n	1	2	3	4	5	6	7	8
r=1	3.00	2.63	1.05	1.03	1.02	1.02	1.01	1.01
2		3.64	2.87	1.24	1.17	1.13	1.11	1.08
3			4.21	3.13	1.45	1.31	1.25	1.21
4				4.81	3.41	1.62	1.47	1.37
5					5.43	3.65	1.81	1.61
6						5.93	3.92	1.98
7							6.52	4.19
8								7.10

Table 2 continued.

f_N	2.659	2.795	2.919	3.035	3.142	3.243	3.337	3.427
f^N	3.089	3.224	3.347	3.462	3.567	3.668	3.761	3.850
Y^x	.2655	.2543	.2450	.2369	.2299	.2236	.2180	.2130
n	9	10	11	12	13	14	15	16
r=1	1.01	1.01	1.01	1.01	1.00	1.00	1.00	1.00
2	1.08	1.07	1.06	1.06	1.06	1.05	1.04	1.04
3	1.17	1.10	1.14	1.13	1.12	1.11	1.10	1.09
4	1.31	1.27	1.24	1.21	1.20	1.18	1.17	1.16
5	1.49	1.42	1.36	1.32	1.29	1.26	1.25	1.23
6	1.74	1.60	1.53	1.46	1.40	1.36	1.33	1.30
7	2.15	1.88	1.73	1.61	1.54	1.48	1.44	1.40
8	4.42	2.30	2.03	1.83	1.72	1.62	1.56	1.50
9	7.62	4.68	2.49	2.13	1.95	1.81	1.71	1.63
10		8.13	4.93	2.60	2.26	2.05	1.91	1.79
11			8.68	5.15	2.78	2.40	2.15	1.99
12				9.13	5.42	2.90	2.50	2.28
13					9.71	5.61	3.08	2.61
14						10.11	5.83	3.22
15							10.64	6.04
16								11.02

f_N	3.511	3.591	3.667	3.740	3.809	3.875	3.939	4.000
f^N	3.934	4.013	4.089	4.162	4.230	4.296	4.359	4.419
Y^x	.2084	.2043	.2005	.1970	.1939	.1909	.1881	.1856
n	17	18	19	20	21	22	23	24
r=1	1.00	1.00	1.00	1.00	1.00	1.00	1.00	1.00
2	1.04	1.04	1.03	1.03	1.03	1.03	1.03	1.03
3	1.08	1.08	1.08	1.08	1.07	1.07	1.07	1.06
4	1.15	1.14	1.13	1.13	1.12	1.12	1.11	1.10
5	1.21	1.20	1.19	1.18	1.16	1.16	1.15	1.15
6	1.28	1.26	1.25	1.23	1.22	1.21	1.20	1.19
7	1.36	1.34	1.32	1.30	1.28	1.27	1.25	1.24
8	1.46	1.42	1.40	1.37	1.35	1.33	1.32	1.30
9	1.56	1.52	1.48	1.45	1.42	1.40	1.38	1.36
10	1.69	1.64	1.58	1.55	1.50	1.47	1.45	1.42
11	1.86	1.77	1.70	1.65	1.59	1.56	1.52	1.50
12	2.06	1.95	1.85	1.77	1.70	1.65	1.61	1.57
13	2.33	2.15	2.03	1.92	1.84	1.76	1.71	1.66
14	2.71	2.43	2.25	2.11	1.98	1.90	1.92	1.77
15	3.23	2.83	2.52	2.32	2.15	2.05	1.95	1.88
16	6.78	3.45	2.93	2.62	2.39	2.23	2.10	2.02
17	11.52	6.50	3.55	3.04	2.68	2.46	2.30	2.18
18		11.99	6.73	3.67	3.01	2.77	2.52	2.37
19			12.41	6.89	3.74	3.18	2.82	2.62
20				12.77	7.18	3.88	3.28	2.93
21					13.38	7.38	4.00	3.16
22						13.79	7.56	4.15
23							14.22	7.88
24								14.80

TABLE 3: Simplified β coefficients 4 Mc/s distribution.

Ordinary ray.

f_H = 0.82 Mc/s.

n	1	2	3	4	5	6	7	8
f	0.63	1.08	1.43	1.71	1.95	2.16	2.35	2.51
				0.03	0.12	0.15	0.18	0.27
		0.93	1.75	2.55	3.38	4.19	4.99	5.79
	2.00	2.95	3.90	4.84	5.78	6.72	7.65	8.58

n	9	10	11	12	13	14	15	16
f	2.66	2.79	2.92	3.03	3.14	3.24	3.34	3.43
						0.13	0.15	0.20
	0.36	0.39	0.50	0.60	0.75	0.78	0.87	1.01
	6.58	7.37	8.15	8.93	9.70	10.46	11.21	11.95
	9.50	10.42	11.33	12.24	13.14	14.04	14.93	15.82

n	17	18	19	20	21	22	23	24
f	3.51	3.59	3.62	3.74	3.81	3.87	3.94	4.00
	0.20	0.20	0.25	0.30	0.30	0.30	0.30	0.30
	1.09	1.23	1.35	1.57	1.69	1.94	2.19	2.27
	12.68	13.40	14.11	14.81	15.35	16.15	16.80	17.14
	16.70	17.58	18.45	19.32	20.38	21.26	21.82	22.76

TABLE 4: Simplified β coefficients 6 Mc/s distribution.

Ordinary ray (WALKER, 1962)

f_H = 0.82 Mc/s.

n	1	2	3	4	5	6	7	8
f	0.948	1.621	2.143	2.570	2.930	3.243	3.518	3.765
			0.01	0.04	0.11	0.18	0.26	0.32
		1.33	2.03	2.73	3.43	4.13	4.83	5.53
	2.35	3.18	4.01	4.84	5.67	6.50	7.33	8.16

n	9	10	11	12	13	14	15	16
f	3.988	4.191	4.378	4.562	4.713	4.864	5.006	5.139
								0.36
	0.41	0.53	0.58	0.64	0.70	0.84	1.00	0.66
	6.23	6.93	7.62	8.31	9.00	.69	10.38	11.07
	8.99	9.81	10.63	11.45	12.27	13.09	13.91	14.73

n	17	18	19	20	21	22	23	24
f	5.266	5.386	5.500	5.609	5.713	5.813	5.908	6.00
	0.36	0.41	0.45	0.50	0.56	0.60	0.63	0.65
	0.75	0.80	0.86	1.02	1.16	1.24	1.36	1.49
	11.76	12.44	13.12	13.80	14.48	15.15	15.82	16.49
	15.54	16.35	17.16	17.97	18.77	19.57	20.37	21.17

TABLE 5: μ' at Titheridge frequencies. Ordinary Ray.

6 Mc/s parabolic distribution.

$f_H = 0.82$ Mc/s.

f	1.677	2.352	2.850	3.256	3.600	3.900	4.164	3.399
n	1	2	3	4	5	6	7	8
r=1	2.26	1.10	1.06	1.05	1.04	1.04	1.03	1.03
2		3.40	1.26	1.18	1.15	1.12	1.11	1.09
3			4.37	1.41	1.30	1.24	1.20	1.15
4				5.33	1.56	1.40	1.33	1.28
5					6.18	1.69	1.50	1.41
6						7.13	1.85	1.59
7							7.98	1.96
8								8.98

f	4.609	4.800	4.971	5.126	5.264	5.388	5.499	5.598
n	9	10	11	12	13	14	15	16
r=1	1.02	1.02	1.02	1.02	1.02	1.02	1.02	1.02
2	1.09	1.08	1.06	1.06	1.06	1.06	1.06	1.06
3	1.15	1.15	1.12	1.12	1.11	1.11	1.11	1.10
4	1.24	1.21	1.20	1.17	1.16	1.16	1.16	1.15
5	1.35	1.31	1.28	1.25	1.24	1.21	1.21	1.21
6	1.49	1.42	1.40	1.33	1.31	1.29	1.28	1.26
7	1.70	1.57	1.49	1.45	1.40	1.36	1.35	1.33
8	2.09	1.80	1.66	1.55	1.50	1.46	1.43	1.41
9	10.00	2.23	1.90	1.69	1.65	1.56	1.53	1.49
10		10.97	2.39	2.00	1.82	1.71	1.66	1.60
11			12.08	2.55	2.10	1.88	1.80	1.73
12				13.31	2.74	2.21	2.01	1.89
13					14.63	2.95	2.35	2.11
14						16.03	3.21	2.50
15							17.47	3.54
16								19.23

Table 5 continued.

f	5.684	5.760	5.825	5.879	5.923
n	17	18	19	20	21
r=1	1.02	1.02	1.02	1.02	1.02
2	1.06	1.06	1.06	1.06	1.05
3	1.10	1.10	1.10	1.09	1.09
4	1.15	1.14	1.14	1.14	1.13
5	1.20	1.19	1.18	1.18	1.18
6	1.26	1.25	1.25	1.23	1.22
7	1.32	1.30	1.30	1.29	1.28
8	1.38	1.37	1.36	1.35	1.34
9	1.46	1.45	1.43	1.41	1.40
10	1.53	1.52	1.51	1.50	1.48
11	1.67	1.65	1.60	1.52	1.51
12	1.81	1.75	1.70	1.67	1.65
13	1.98	1.89	1.82	1.79	1.75
14	2.23	2.08	1.98	1.93	1.88
15	2.68	2.37	2.20	2.10	2.04
16	3.97	2.90	2.53	2.35	2.24
17	21.18	4.39	3.19	2.75	2.53
18		23.49	5.35	3.58	3.05
19			26.64	6.29	4.20
20				30.10	8.23
21					34.61

TABLE 6: Simplified β coefficients. Ordinary Ray.

6 Mc/s parabolic distribution.

f_H = 0.82 Mc/s.

f	1.677	2.352	2.850	3.256	3.600	3.900	4.164	4.399
n	1	2	3	4	5	6	7	8
								0.20
				0.09	0.15	0.25	0.30	0.26
		1.14	2.18	2.96	3.77	4.49	5.28	6.07
	2.26	3.40	4.37	5.33	6.18	7.13	7.98	8.98

Table 6 continued.

f	4.609	4.800	4.971	5.126	5.264	5.388	5.499	5.598
n	9	10	11	12	13	14	15	16
	0.23	0.29	0.30	0.39	0.36	0.53	0.41	0.57
	0.26	0.29	0.33	0.39	0.45	0.53	0.60	0.71
	6.89	7.77	8.58	9.53	10.57	11.68	12.82	13.93
	10.00	10.97	12.08	13.31	14.63	16.03	17.47	19.23

f	5.684	5.760	5.825	5.879	5.923
n	17	18	19	20	21
	0.53	0.68	0.87	0.97	1.12
	0.86	1.07	1.23	1.77	2.09
	15.26	16.76	18.14	20.35	21.87
	21.18	23.49	26.64	30.10	34.61

CHAPTER 4.

APPARATUS MODIFICATIONS AND EXPERIMENTAL PROCEDURE.

4.1 The Rhodes ionosonde.

A detailed description of the Rhodes ionosonde and its operation is given by McELHINNY, 1958 and a brief description of the same has also been given in Section 1.2.

The author, however, feels that it is necessary to give a short summary of the lay-out and construction of the apparatus, as it was at the start of the project, so that the modifications which were made can be understood more readily.

The ionosonde, a block diagram of which is given in Figure 1.1, with the exception of the recording oscilloscope, is built on five chassis placed on a rack, one above the other.

The lowest, or first, chassis houses the filament, H.T. and 2KV E.H.T. supplies.

The 500 kc/s frequency calibrator, audio-beat amplifier and detector stage, and part of the programme unit are situated on the next chassis.

Chassis 3 contains the monitor oscilloscope, pulsed 3 kc/s height calibrator, gating stage, video-amplifiers and pulsing unit.

The Variable Frequency Oscillator (V.F.O.) (30 - 50 Mc/s), 30 Mc/s pulsed oscillator, mixer, the receiver and other half of the timing unit are housed on chassis 4.

The first driver stage for the pulse transmitter was built on a vertical sub-chassis on chassis 4 and its output was fed to the transmitter stages on the top chassis (number 5) by means of a clip

connection.

Cross-connections between the various stages were made with suitable coupling leads.

The recording oscilloscope and its power supply were built on separate chassis.

At the start of this project (March, 1960) it became apparent that several modifications and repairs would have to be made to the ionosonde.

These are listed under the headings of the units involved.

4.2 Power supply.

In the interests of personal safety all fuse-holders were moved and rewired so that the fuses were accessible from the front of the ionosonde.

The E.H.T. transformer, which had been burnt out, was replaced by another.

4.3 Frequency Calibrator.

The principle used here is the production of audio beats between the harmonics in the distorted wave shape from a 500 kc/s crystal oscillator and the V.F.O. Thus, for example, audio beats will be produced between the 77^{th} harmonic of the 500 kc/s signal and a V.F.O. signal of 38.5 Mc/s.

These beats are amplified by amplifiers with a band width restricted to about 20 kc/s and then detected. The D.C. output thus developed is applied to the height-marker gating stage. In this way the gating stage will be open only when the harmonics of the

500 kc/s signal and the V.F.O. frequency are within ± 10 kc/s of each other.

It was found that the D.C. output thus produced was insufficient to operate the gating stage.

The gains of the various audio amplifiers were therefore considerably increased by increasing the plate loads of the amplifying tubes.

In order to allow the frequency-markers to appear on the recording oscilloscope long enough for them to be registered on the recording film when the V.F.O. was sweeping through the higher frequencies ($>$8 Mc/s) it was found necessary to increase the band width of these amplifiers. This means that audio-beats will be produced for a greater time interval and that the gating stage would be "open" for a longer period.

An undesirable feature of this modification was the increased width of the height marks at the low-frequency end of the ionogram and thus an increased error in the scaling of these frequencies.

In order to overcome this the coupling condensers between the audio amplifiers were reduced until the low-frequency cut-off of the audio-amplifiers occurred at about 1 kc/s. This 2 kc/s gap (1 kc/s on either side of the zero audio beat position) should therefore appear as a gap in the middle of the frequency marks.

This measure met with limited success, and the gap can be seen in the first set of height marks on figure 7.1, but not in the rest since the time constant of the gating stage was approximately equal

to or greater than the time taken for the V.F.O. to sweep through the frequency marks at frequencies greater than about 2 Mc/s.

4.4 Height calibrator.

The pulsed 3 kc/s oscillator consists of a tuned L-C circuit in the cathode circuit of an oscillator tube.

The oscillator tube is normally conducting but its current is cut off sharply in synchronism with the transmitter pulse.

The inductance discharges into the capacity of the tuned circuit and a damped oscillation of 3 kc/s is produced. The oscillation is amplified, squared and differentiated and then applied to the recording oscilloscope via the gating stage. Height markers appear at regular intervals and also serve as frequency marks since they pass through the gating stage only when audio beats are produced between harmonics of the 500 kc/s crystal and the V.F.O.

It was found that the damped 3 kc/s oscillation died away very quickly, thus resulting in a series of height marks only up to the tenth marker (500 km virtual height) above the ground pulse.

In order to increase the Q of the L-C circuit a new coil with the same inductance as the original (L = 226 m Henries) was wound with a thicker gauge (26 SWG) enamelled wire.

The Q of the circuit was now high enough for the damped oscillation to continue until height marks had appeared across the whole width of the recording oscilloscope's trace.

It was now necessary to recalibrate the 3 kc/s oscillator.

A continuous audio signal was used instead of the pulsed signal to provide height marks. Stationary height marks were visible

whenever the audio signal's frequency was a multiple of the mains frequency or half the mains frequency since the oscilloscope time bases (monitor and recording) are triggered off by the mains input.

The mains frequency during the interval while calibration was being carried out was measured by means of an electronic counter. The average of several determinations was 2,999 cycles per minute.

The frequency of the audio oscillator was slowly changed from 50 to 3000 cps, care being taken to count the multiples of 50 at which stationary height marks appeared. At the 60^{th} multiple i.e. $60 \times \frac{2999}{60}$ or 2999 cps, the oscillator was set so that there was no movement of the height markers.

The distance between successive height marks was determined as accurately as possible by means of measurements made using the expanded sweep and graduated time dial of an EMI WM8 oscilloscope.

The pulsed oscillator's frequency was then adjusted by changing the capacitance in parallel with the coil until the distance between the successive height markers, as measured with the same 'scope, was the same as that for markers produced by the 2999 cps oscillator.

For practical purposes this value of 2999 cps is close enough to 3 kc/s, or more exactly 2.998 kc/s which is the frequency needed for 50 km height marks.

4.5 The variable frequency oscillator.

The only problem here was to decrease the time taken for a complete frequency sweep from 2.1 minutes to about 15 seconds and the interval between successive sweeps from 4.5 minutes to about 1 minute.

PLATE 1

V.F.O. - DRIVE UNIT.

A - Synchronous motor.

B - Reduction gearbox.

C - Programming cams.

D - Three piece axle for V.F.O. condenser.

E - "Clutch" lever.

F - V.F.O. condenser.

G - Oscillator tube.

Plate 1

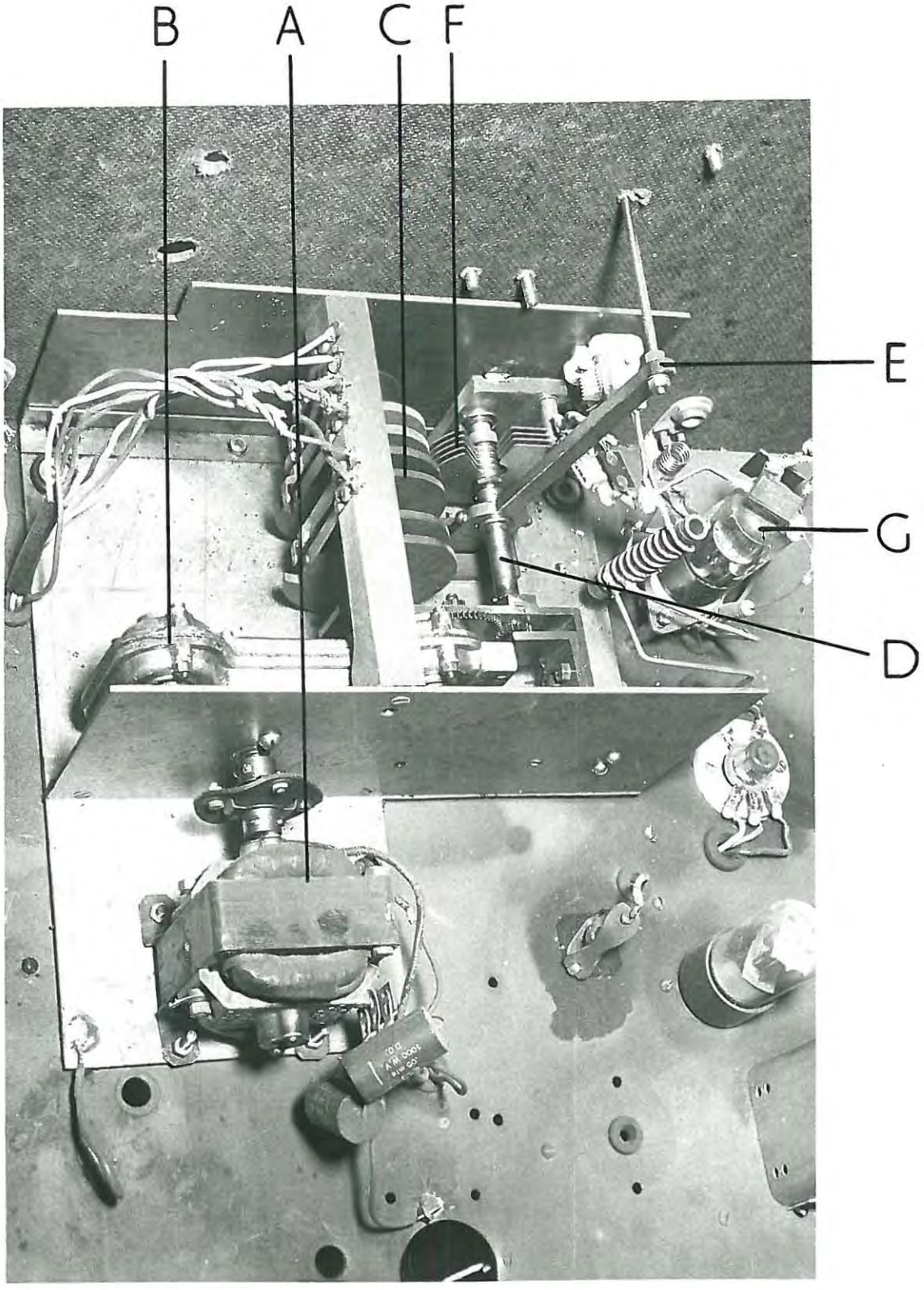

PLATE I

Plate 1 shows how this was accomplished.

A synchronous motor drives a shaft, on which are mounted three sets of cams, at about 1 revolution every 72 seconds via a reduction gearbox.

Two of the cams operate the switches for the HT and EHT supplies and the camera motor. The third enables the motor to switch itself off, if desired, when the cams are in a certain position.

The V.F.O. condenser is mounted on a shaft which makes two revolutions for every one that the cams make.

This V.F.O. drive-shaft is made up of three parts. The first is the short axle on which the rotors of the V.F.O. condenser are mounted. The second is the shaft on which one of the driving gears are mounted. The remaining piece is a hollow cylinder, which can slide over the other two pieces, with a slot at both ends.

The slots in this cylinder engage with pins through the other two pieces. By sliding the cylinder along its axis the slot at one end can be disengaged from the pin, thus allowing the condenser to be rotated by hand for manual operation of the ionosonde.

When the cylinder is slid back the slot and pin are re-engaged. The condenser plates are thus locked in the correct position for automatically repeated sweeps. It is important that the condenser and cams stop and start in the same position if ionograms covering identical frequency intervals are to be obtained.

After rewiring the programme unit the ionosonde could be programmed to sweep automatically at 60, 15 or 4.6 minute intervals.

The motor driving the V.F.O. condenser could also be left running continuously to give ionograms at 72 second intervals.

The time necessary for a complete frequency sweep to be made was about 18 seconds.

4.6 Recording oscilloscope.

Instability, or "jitter", of the oscilloscope trace was found to be due to the fact that the oscilloscope sweep and the main pulse circuit on chassis 3, although both triggered off by the mains input, were not synchronised.

Fortunately phasing controls, by means of which the point on the mains cycle at which the two circuits are triggered off could be varied, were provided.

By suitable adjustment of these controls both circuits can be made to trigger off simultaneously.

The oscilloscope trace was now sufficiently stable and no further modification was necessary.

Because of the shorter time taken for a complete frequency sweep to be made it was necessary to increase the speed at which the film is fed through the camera gate. The camera motor controls were set so that each ionogram would be about three inches long.

As a result of the increased speed at which the film moved the brightness of the oscilloscope trace had to be increased considerably to allow for sufficient exposure of the trace on the film.

This was done by running a high-voltage cable from the 2 kV EHT supply to the recording oscilloscope chassis and connecting the EHT

to the post deflection accelerator contact.

Both the trace intensity and definition (sharpness of focus) were considerably improved by this modification.

4.7 Transmitter.

After careful checking and alignment of all the transmitter stages the power output was still very low. It was therefore decided to rebuild the amplifying stage after the mixer for the 30-50 Mc/s and pulsed 30 Mc/s signals on the top chassis.

The mixer output was fed to this amplifier (the first power stage) via a cathode follower, working into a co-axial cable, on chassis 4.

This amplifier had originally been built on a sub-chassis on chassis 4 and was rebuilt in a screened compartment on chassis 5.

It was found possible to increase the power output of the transmitter at the higher frequencies by using a wirewound resistor in the plate load of this stage. At 15 Mc/s, for instance, the power output was two-and-a-half times that which had been obtained by using a non-inductive load.

4.8 Tuning procedure.

All I.F. stages, both on the transmitter and receiver, were carefully tuned for maximum response to an input signal of the appropriate frequency.

The final tuning of the pulsed 30 Mc/s I.F. stages was done by tuning them for a maximum aerial current as measured by the rf

FIGURE 4.1 A - G

The graph of iso-electronic contours for 10th August, 1960 is presented in seven overlapping diagrams to facilitate binding.

True height is shown on the vertical axis while the horizontal axis shows time in SAST, solar zenith angle and the distance through which Grahamstown had rotated about the earth's axis since the start of the morning's run.

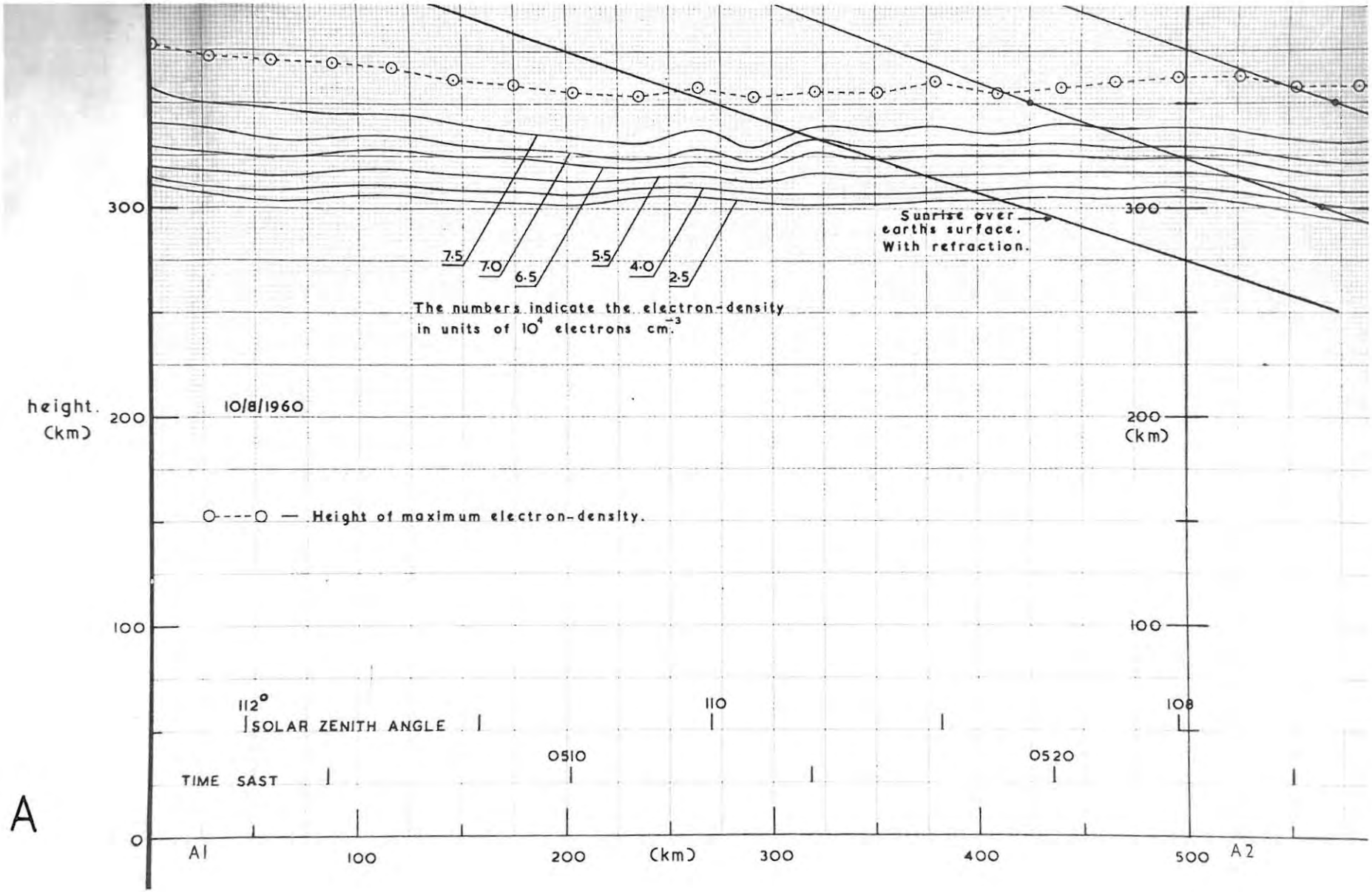
7·5
7·0
6·5
5·5
4·0
2·5
The numbers indicate the electron-density in units of 10^4 electrons cm^{-3}.
Sunrise over earths surface. With refraction.
300
300
height. (km)
200
10/8/1960
200 (km)
O---O — Height of maximum electron-density.
100
100
112°
SOLAR ZENITH ANGLE
110
108
0510
0520
TIME SAST
A
0
A1
100
200
(km)
300
400
500
A2

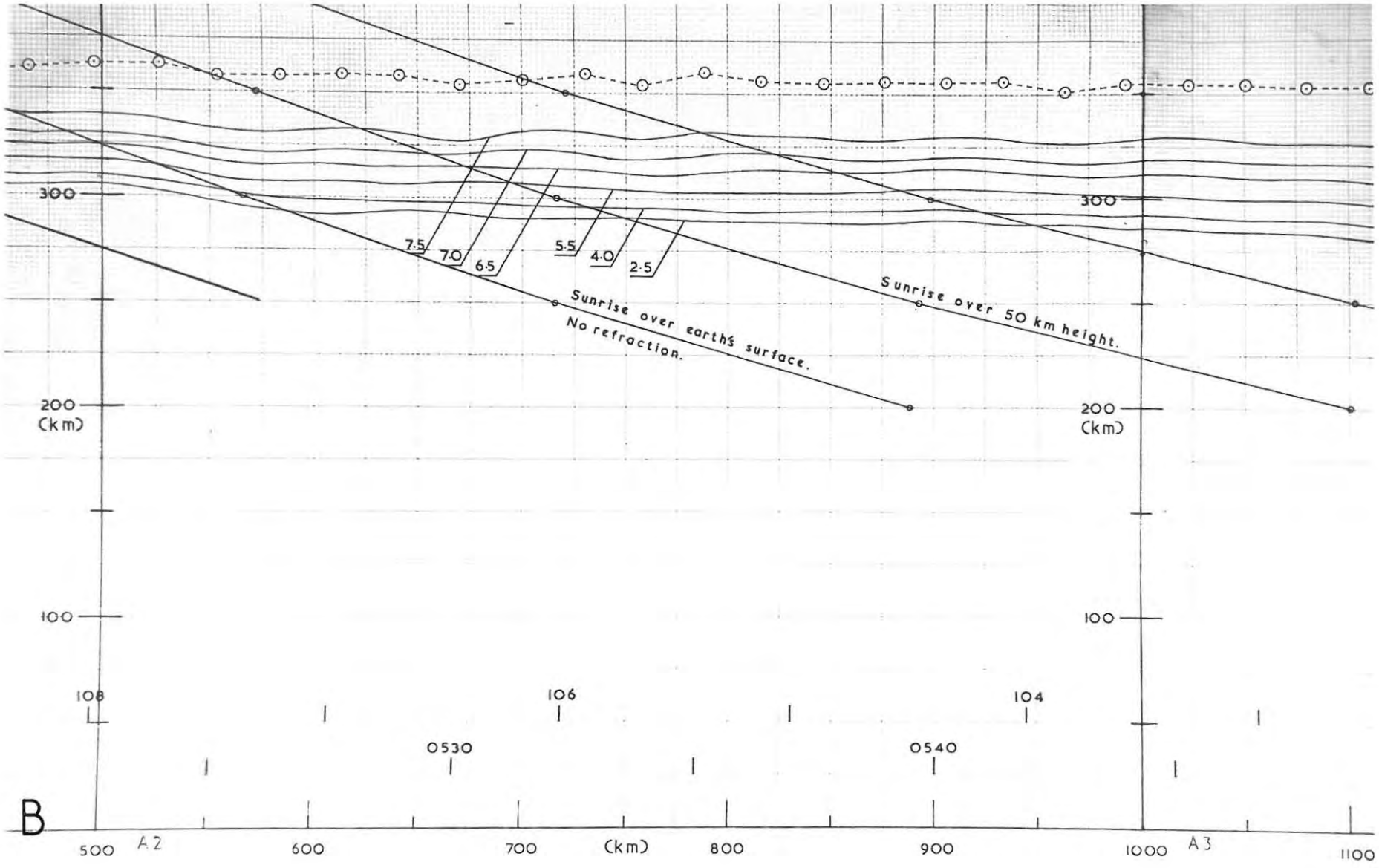
300
200
(km)
100
7·5
7·0
6·5
5·5
4·0
2·5
Sunrise over earth's surface.
No refraction.
Sunrise over 50 km height.
300
200
(km)
100
108
106
104
0530
0540
B
500
A2
600
700
(km)
800
900
1000
A3
1100

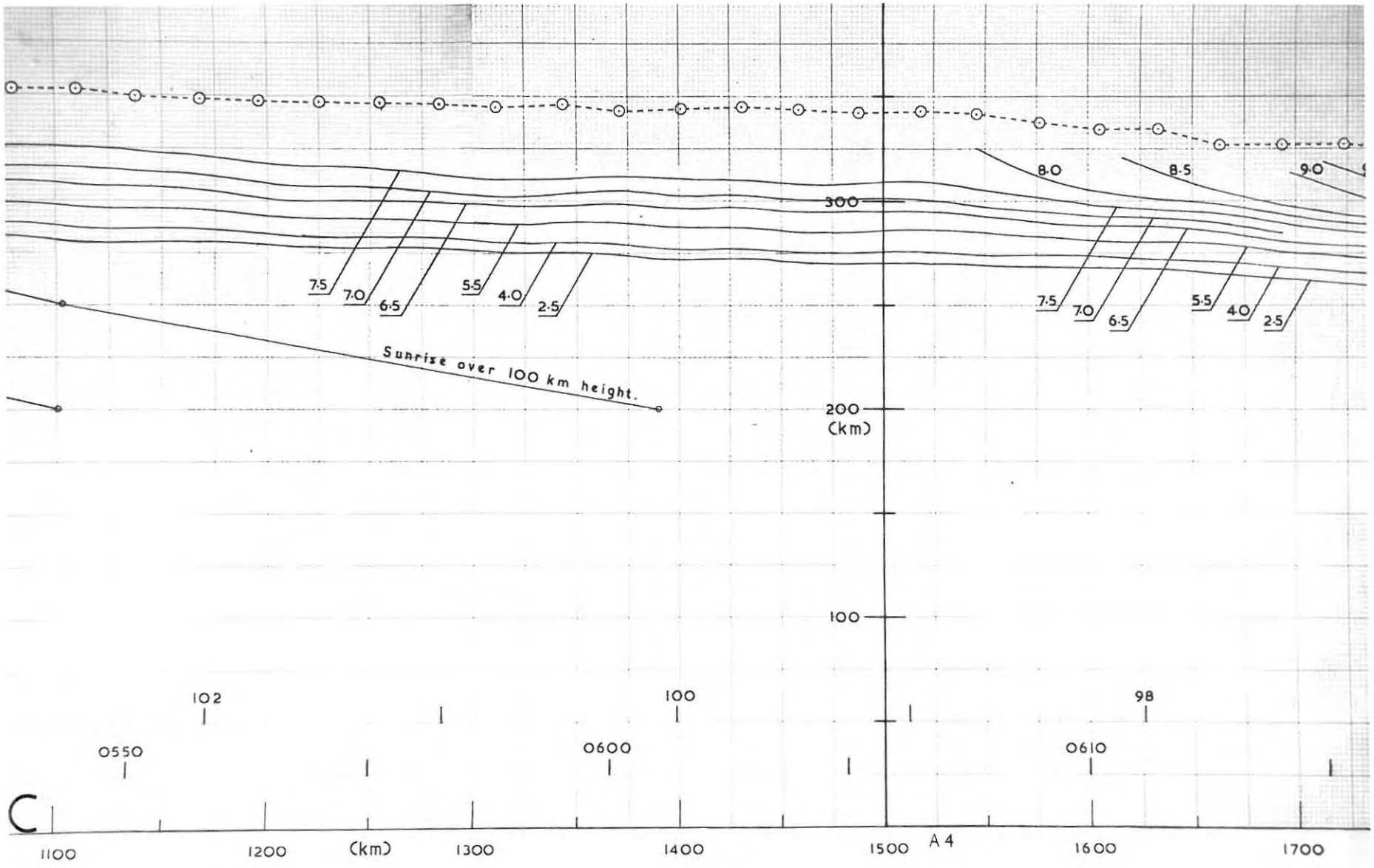
8·0
8·5
9·0
300
7·5
7·0
6·5
5·5
4·0
2·5
7·5
7·0
6·5
5·5
4·0
2·5
Sunrise over 100 km height.
200
(km)
100
102
100
98
0550
0600
0610
C
1100
1200
(km)
1300
1400
1500
A 4
1600
1700

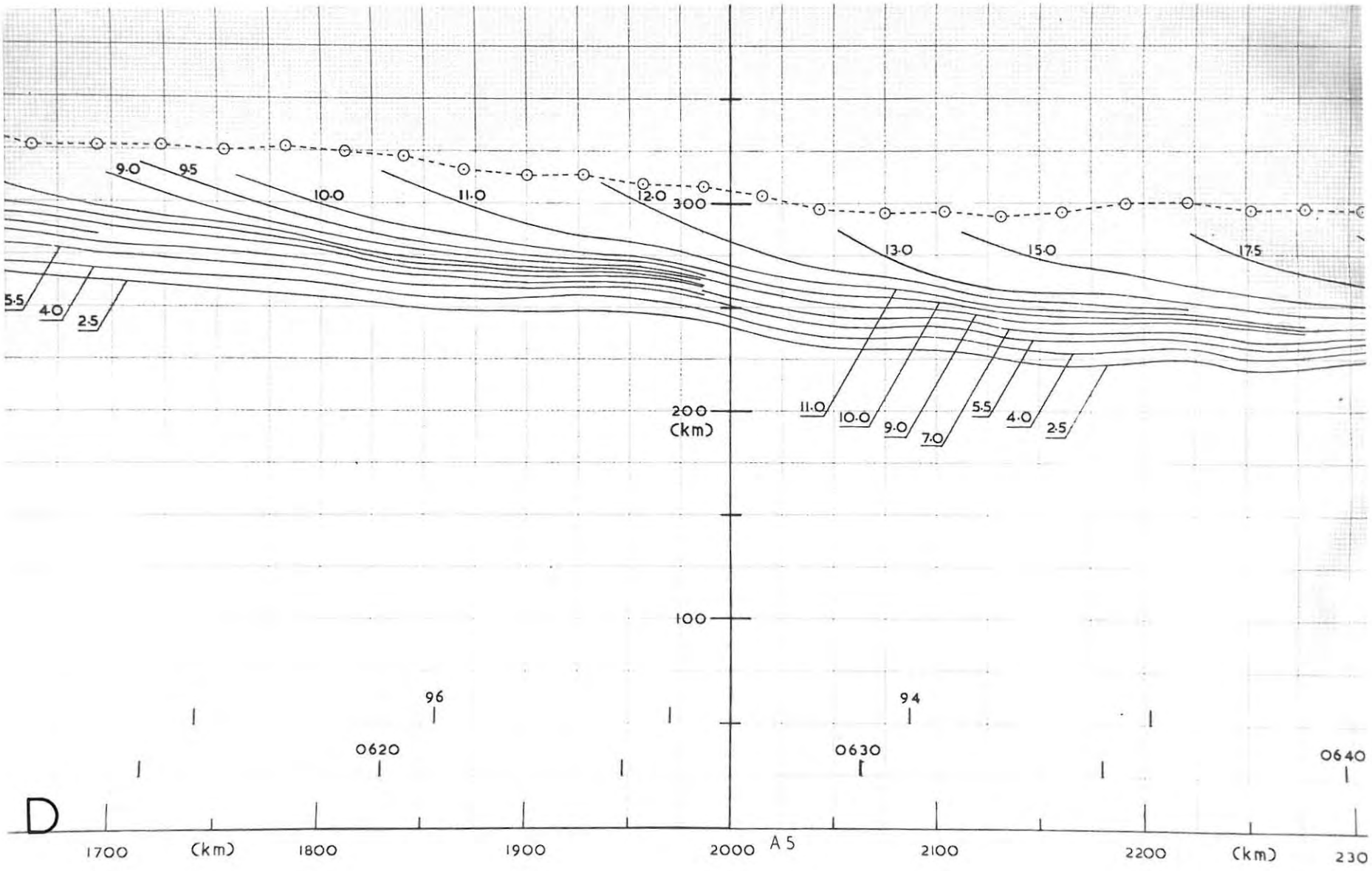
9.0
9.5
10.0
11.0
12.0
300
13.0
15.0
17.5
5.5
4.0
2.5
11.0
10.0
9.0
7.0
5.5
4.0
2.5
200
(km)
100
96
94
0620
0630
0640
D
1700
(km)
1800
1900
2000
A 5
2100
2200
(km)
230

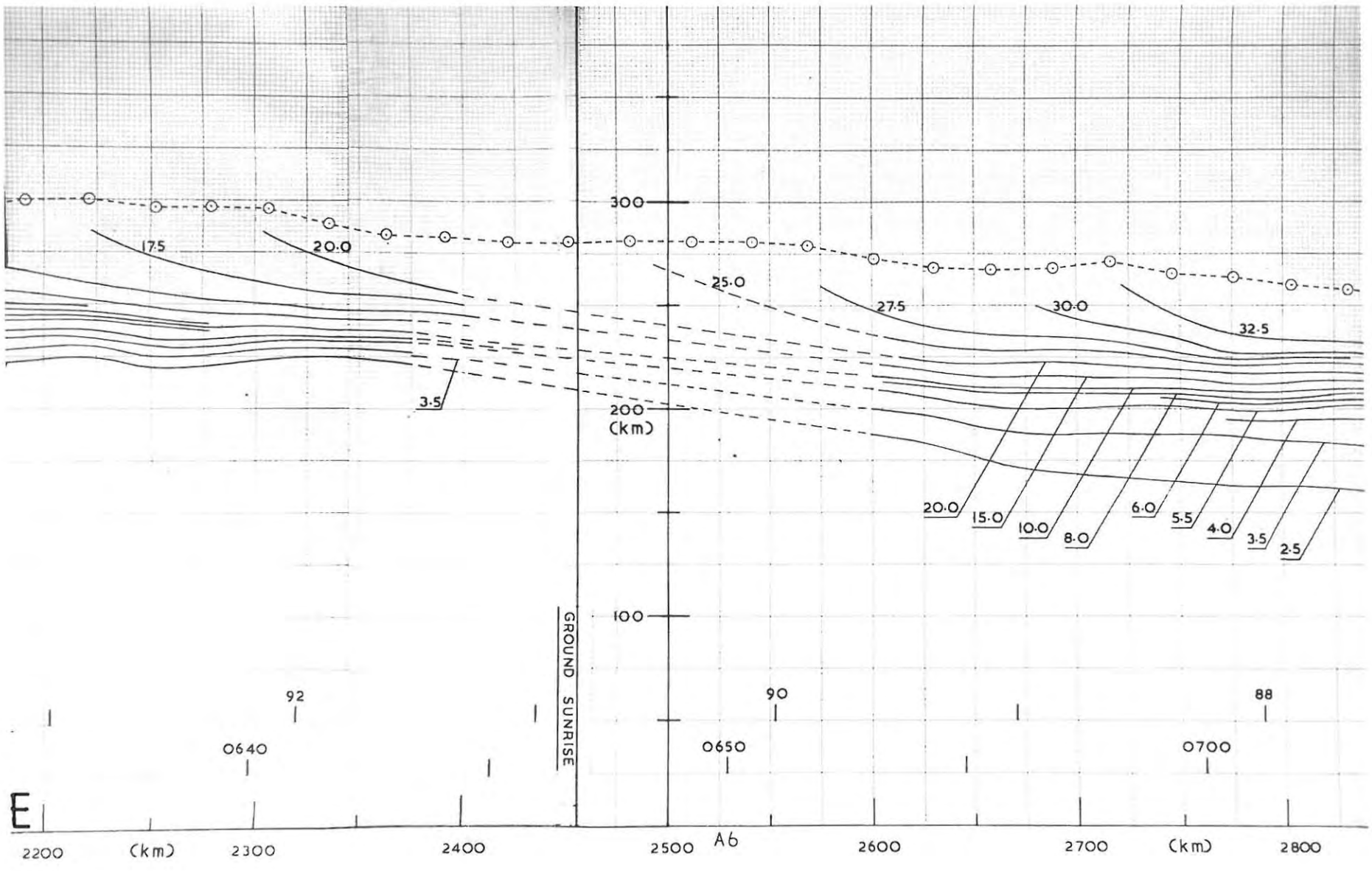
300
200
(km)
100
17·5
20·0
25·0
27·5
30·0
32·5
3·5
20·0
15·0
10·0
8·0
6·0
5·5
4·0
3·5
2·5
GROUND SUNRISE
92
90
88
0640
0650
0700
E
2200
(km)
2300
2400
2500
A6
2600
2700
(km)
2800

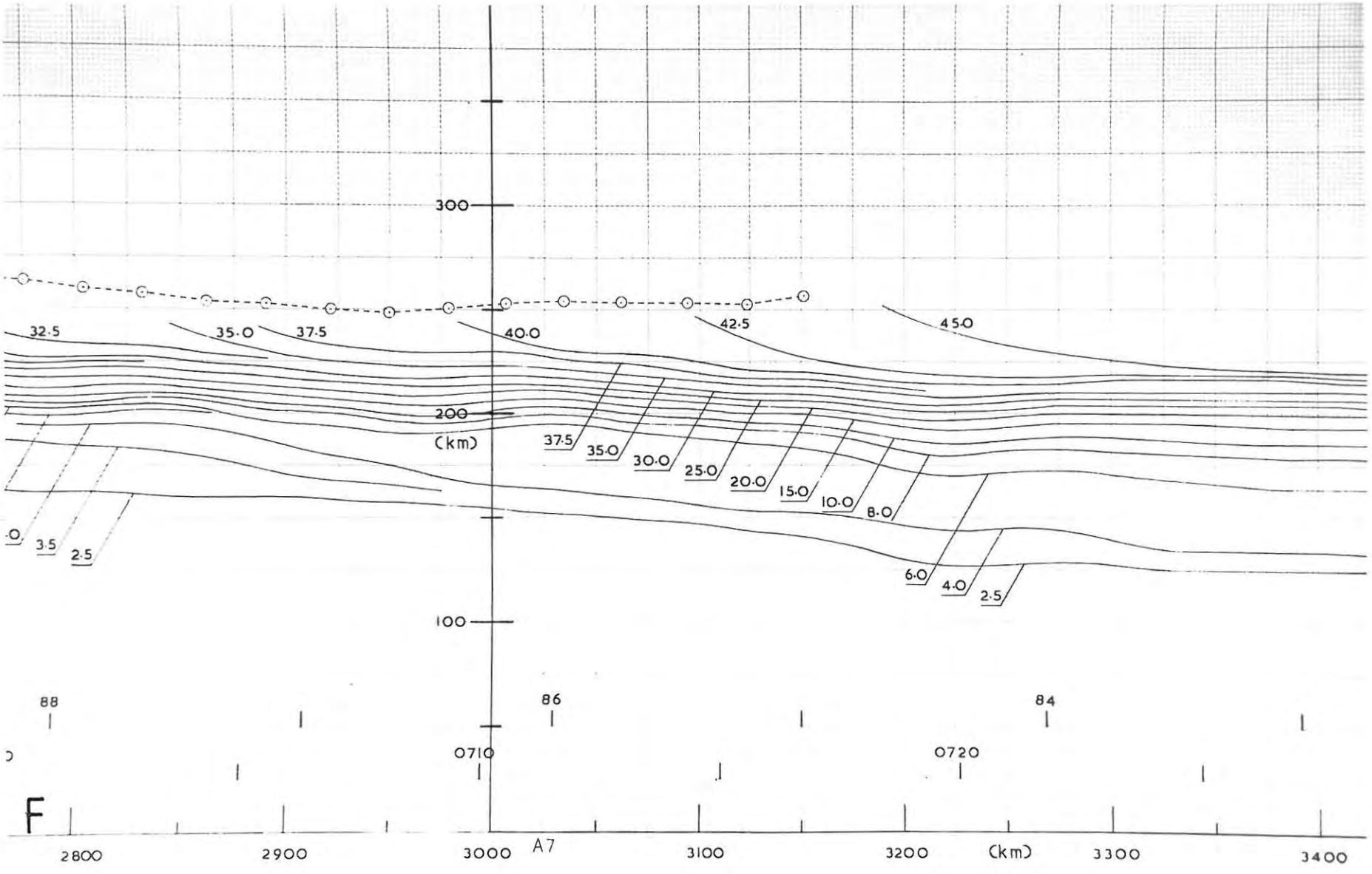
300
200
100
(km)
32·5
35·0
37·5
40·0
42·5
45·0
37·5
35·0
30·0
25·0
20·0
15·0
10·0
8·0
6·0
4·0
2·5
3·5
2·5
88
86
84
0710
0720
F
2800
2900
3000
A7
3100
3200
(km)
3300
3400

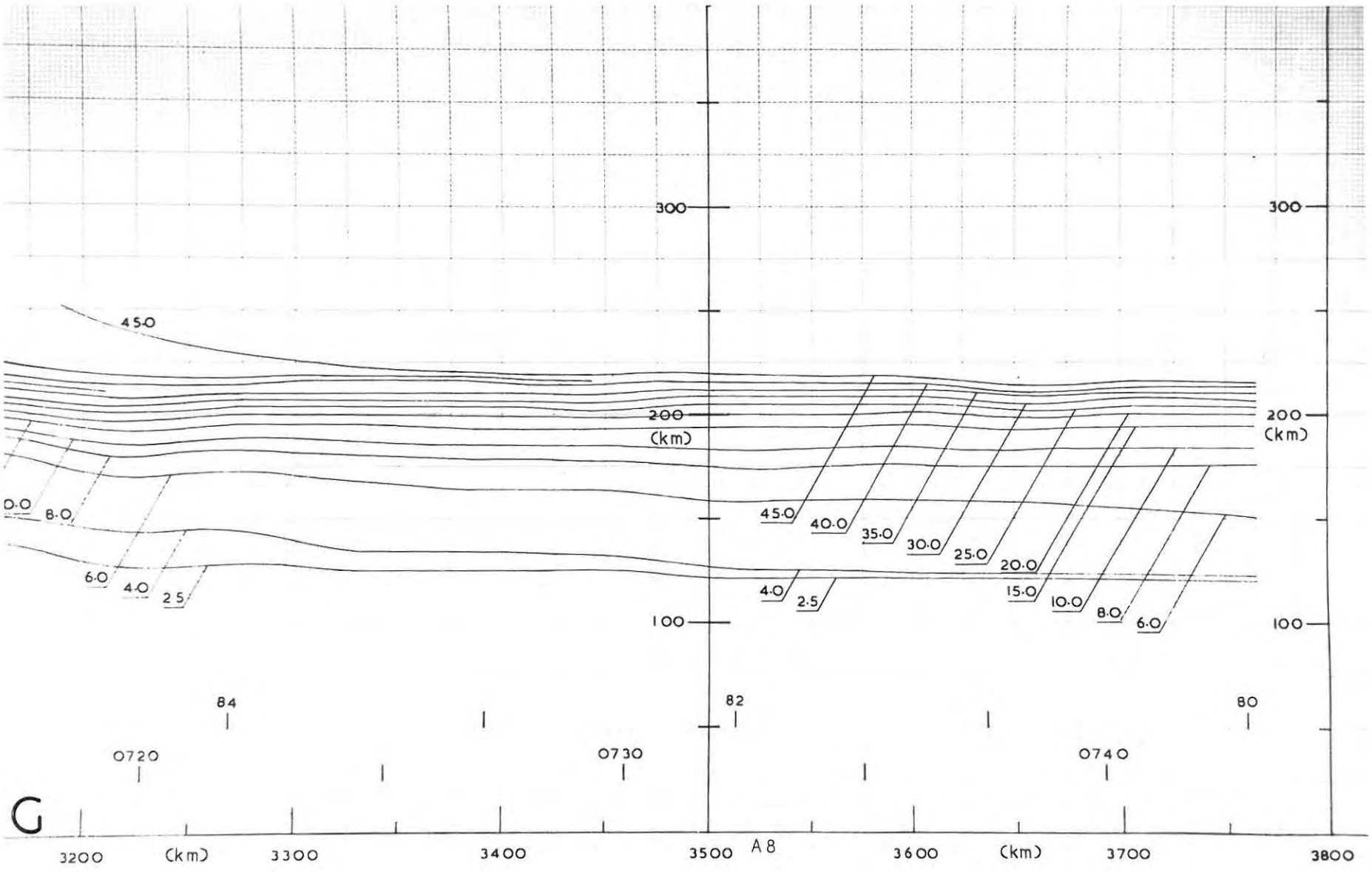
300
200
(km)
100
45·0
40·0
35·0
30·0
25·0
20·0
15·0
10·0
8·0
6·0
4·0
2·5
0·0
8·0
6·0
4·0
2·5
84
82
80
0720
0730
0740
G
3200
(km)
3300
3400
3500
A8
3600
(km)
3700
3800

current milliameter in the antennae circuit.

To tune the receiver the V.F.O. signal was varied until an echo could be observed on the monitor oscilloscope and the I.F. stages were then tuned for maximum echo amplitude.

4.9 Experimental procedure.

Ionograms from several minutes before sunrise at ionospheric heights until the E layer has been formed were taken at 1.25 minute intervals on several arbitrarily selected days during 1960.

One of these sets showed the effects of what was believed to be a large travelling disturbance (see Chapter 5). The ionograms in this set were scaled as accurately as possible by the methods described in Section 3.3.

From the N-h profiles thus obtained two graphs were drawn.

The first is shown in the series A - G which constitutes Fig. 4.1. This is a graph of the variation of the height of equal electron density (iso-electronic) contours with the distance through which Grahamstown had been rotated around the axis of the earth since the start of the set of ionograms.

The graph can thus be taken to represent a map of the ionosphere along the latitude on which Grahamstown lies. The relationship between the vertical and horizontal scales is fixed by the speed at which Grahamstown rotates about the earth's axis and the presentation of the iso-electronic contours is the same as that used by GLEDHILL (1959).

The ionosonde can be positioned anywhere along the horizontal

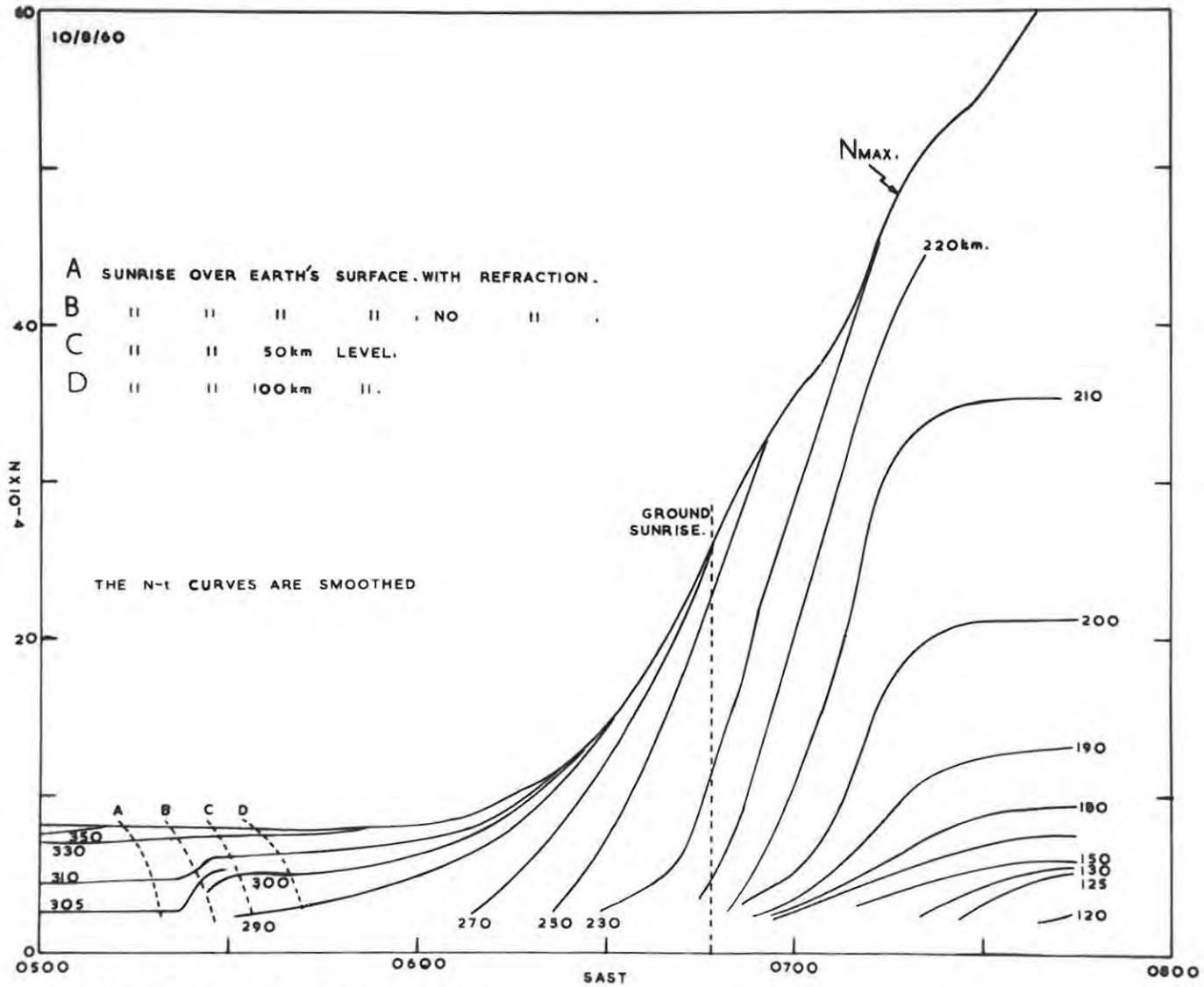

FIG. 4.2 N vs. t at constant h.

scale, which now represents the distance along the earth's surface at the latitude of Grahamstown The state of the ionosphere at points east (in the direction of increasing distance) and west (distance decreasing) can thus be ascertained.

It is assumed that the same ionospheric conditions at the same solar zenith angles are present along the latitude of Grahamstown.

Also shown along the horizontal scale are the time in S.A.S.T. and the solar zenith angle in degrees. The times of sunrise at different heights over various layers are also indicated.

These times of sunrise were calculated from a procedure given by MITRA (1952a). (See Appendix A.)

A portion of the contour map around ground sunrise has been drawn with dotted lines to indicate that the actual contours are uncertain. Correction for low level ionization in this region required scaling of the O- and E- ray Titheridge frequencies on very steep parts of the h'-f curves as a result of low level retardation when the probing frequency is low and the density of the low lying ionization high. The method used to allow for this ionization breaks down under these conditions. An alternate method will have to be devised to overcome this shortcoming before a complete analysis of h'-f curves over sunrise can be made.

The second graph is shown in Figure 5.3 and shows the variation of electron density at constant heights with time.

These graphs will be discussed more fully in the succeeding chapters.

PART II

RESULTS AND DISCUSSION.

Fig 5.1

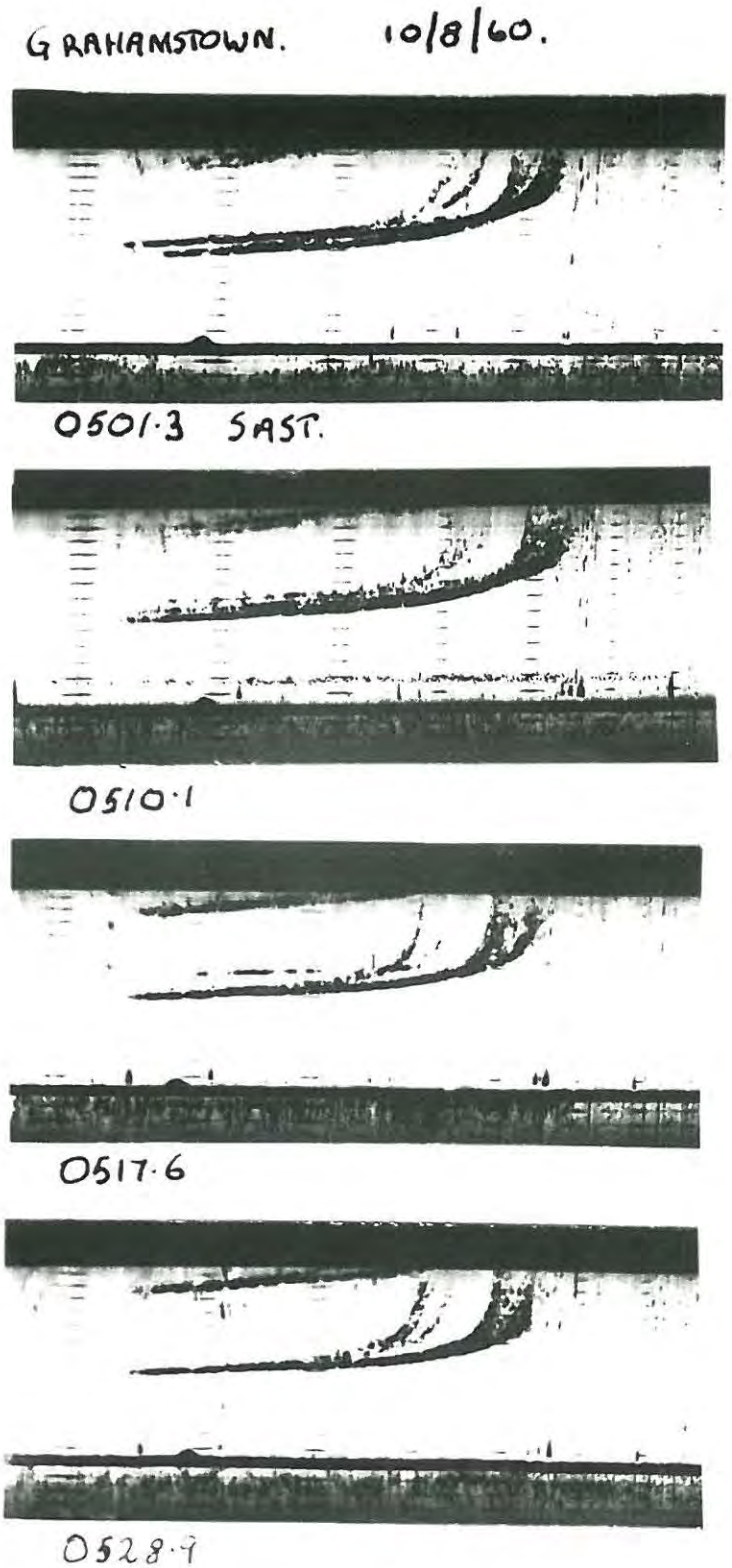

Fig. 5.1 Sequence of ionograms showing behaviour of main and satellite traces observed at Grahamstown.

CHAPTER 5.

HORIZONTAL IRREGULARITIES AND MOVEMENTS.

5.1 Range multiplets.

5.1.1 Introduction.

Figure 5.1 shows a sequence of ionograms obtained on the morning of the 10th August, 1960.

These ionograms show a number of h'-f curves one above the other. The curves above the lowest or "main" trace are referred to as "satellite traces" or "range multiplets" (McNICOL, WEBSTER and BOWMAN, 1956).

Before examining the records obtained more closely it is necessary to consider the various ionospheric conditions which can give rise to these multiplet reflections.

5.1.2 Multiplet reflection mechanisms.

Range multiplets such as those shown in figure 5.1 can be explained by three reflection mechanisms. These are:-

(a) Stratification hypothesis.

In this hypothesis it is assumed that the echoes are returned from layers above the F region. The implication is that the echoes come down nearly vertically and that considerable variation of electron density exists in the F region.

Directional observations by McNICOL, WEBSTER and BOWMAN (1956), however indicate that, for multiplets of large range separation the signals arrive at a considerable angle to the vertical. For multiplets close to the main trace the direction of the multiplet signals cannot be determined accurately, but the hypothesis

breaks down for the following reasons:-

The main h'-f trace suggests a thick layer of uniform consistency and variations in maximum electron density would lead to a considerable spread in critical frequency which is not characteristic of range multiplets (McNICOL and WEBSTER, 1956). Furthermore, it is difficult to see how penetration through the F region can take place. This must be considerable to produce traces which have an intensity comparable with that of the main trace. Considerable group retardation, increasingly marked at higher frequencies, would occur as the signals travel through the F region. This is not the case since the multiplet and main traces do not diverge, but remain separated by an almost constant distance for most of the trace.

(b) E_S scatter.

ECKERSLEY (1937) suggested that spread echoes from the F region could be obtained after reflection of the signals at non-horizontal contours of the E_S layer. The signal is thus reflected off an E_S "cloud", obliquely off the F region and back to the ionosonde either directly or along the original path.

The general features of range multiplets, however, cannot be reconciled to this hypothesis either.

For an oblique reflection the critical frequency of the satellite would be higher than that of the main trace by a factor of sec θ, where θ is the angle of incidence of the signal on the F layer. One would also expect the satellite h'-f trace

to bulge slightly beyond the critical frequency of the main trace before turning up to infinity at the critical frequency. This is the characteristic appearance of oblique incidence h'-f curves.

There is little correlation between the occurrence of satellite traces and the presence of E_S (McNICOL, WEBSTER and BOWMAN, 1956). Furthermore, there is no correlation between satellite traces and geomagnetic disturbances. The currents responsible for these disturbances flow close to the heights of the E_S layer (MITRA, 1952) and might be expected to lead to a scattering of E_S clouds and thus a greater number of satellites.

(c) The F-irregularity hypothesis.

The most likely reflection mechanism seems to be that proposed by GIPPS, GIPPS and VENTON (1948) who concluded that satellites arise from reflections from a portion of the ionosphere where the gradient of ionization is inclined at a considerable angle to the vertical. These regions are displaced horizontally but are at the normal height. BRADLEY and ROSS (1953); BIBL, HARNISCHMACHER and RAWER (1955) and RATCLIFFE (1955) have shown that such non-horizontal gradients frequently exist.

This hypothesis is consistent with general conclusions reached by McNICOL, WEBSTER and BOWMAN (1956) after a study of a large number of satellites. These are:-

(a) Experiments had shown that the relation between the virtual range (R') of a particular frequency of a satellite trace and the virtual

height (h') of the main trace at the same frequency was

$$R' = h' \text{ Sec } \Theta \qquad (5.1)$$

where Θ is the angle between the direction of the satellite signal and the vertical.

This follows by simple gemometry in the F-irregularity hypothesis.

(b) The quantity x defined by

$$x = \sqrt{(R'^2 - h'^2)} \qquad (5.2)$$

varies roughly uniformly with time. x is thus the apparent displacement of the reflection point from the vertical. This follows reasonably if one assumes that the irregularity moves horizontally with a more or less constant velocity.

(c) From observations made at a number of stations it has been concluded that the irregularity is of considerable extent. This can be accounted for by extending the hypothesis to a long ripple or front in the ionosphere with a constant configuration perpendicular to the direction of motion.

(d) The appearance of satellites on multiple hop reflections can also be explained by reflection from non horizontal contours.

5.2 The behaviour of the observed range multiplets.

The range doublet can be seen some 50 km or so (virtual height) above the main trace on the first ionogram, Figure 5.1,a, recorded at 0501.3 S.A.S.T. It has a critical frequency somewhat higher than that of the main trace.

The range of this doublet decreases steadily with time and by 0517.6 (Figure 5.1,c) it has merged with and is indistinguishable from

the main trace except near the critical frequencies.

In the meantime a range triplet has appeared on the records. This can be seen as an intermittent trace in figures 5.1 b and c, some distance above the main and doublet traces. The virtual height of this reflection decreases slightly and then increases again. Its disappearance after about eight minutes is presumably due to ionospheric absorption or a low reflection coefficient since this echo is at no stage as marked as the main and doublet traces, but always appears to be somewhat diffuse and does not appear to have a clear critical frequency.

The range doublet stays merged with the main trace and the records now resemble Figure 5.1,d until 0604 hours.

A careful examination of the records shows that the lowest critical frequency is part of the main trace. The slightly higher critical frequency is discussed in section 6.

Between 0604 and 0611 hours a very faint range doublet is discernable, but the traces are too faint to be scaled with any accuracy by the Titheridge method. Because of the long delay between the appearance of the first range multiplets and those at 0604 it is unlikely that the latter originate from the disturbance recorded on the ionograms shortly after 0500. Both these sets of range multiplets may arise from a series of disturbances resulting from a wave of disturbance propagated through the ionosphere. (TITHERIDGE, 1963)

5.3 The assumed shape.

MUNRO (1953) in his explanation of day-time satellites postulated an inverted trough configuration for the travelling disturbance.

Fig 5.2

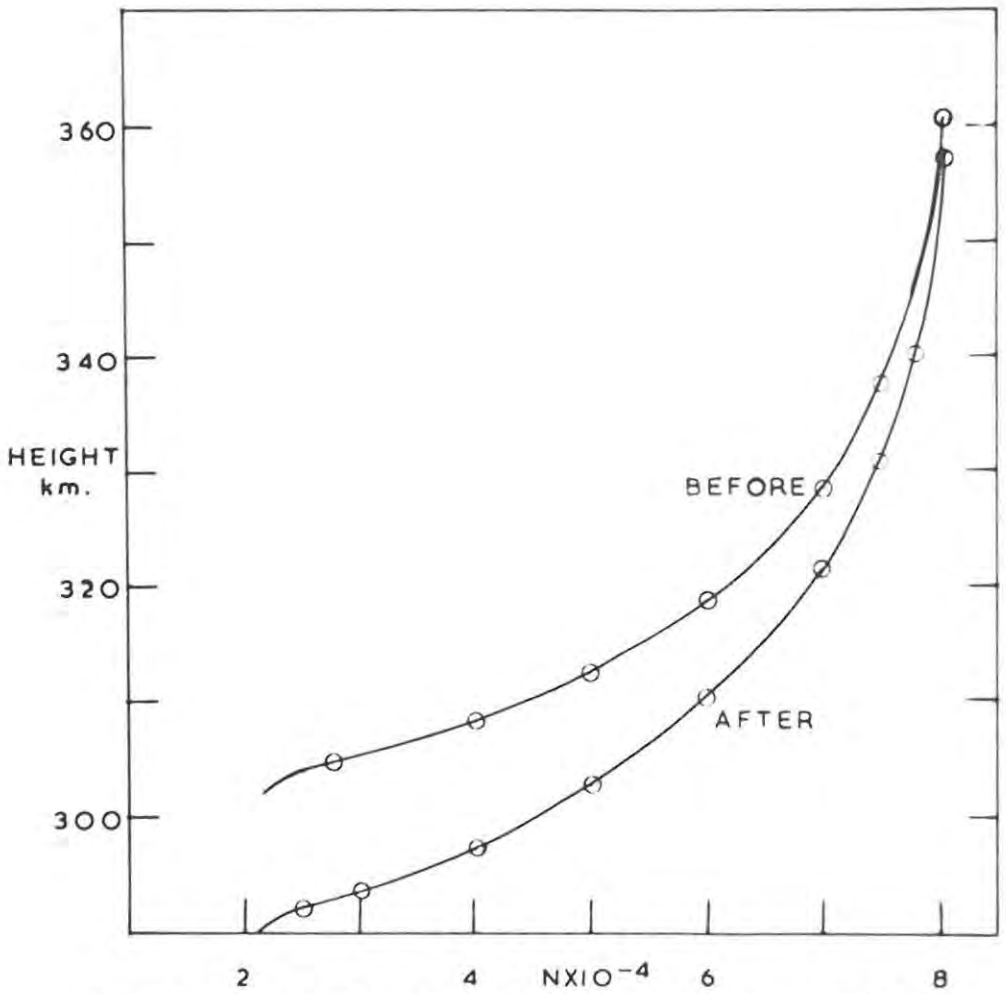

FIG. 5.2. AVERAGE Nh PROFILE BEFORE & AFTER DISTURBANCE.

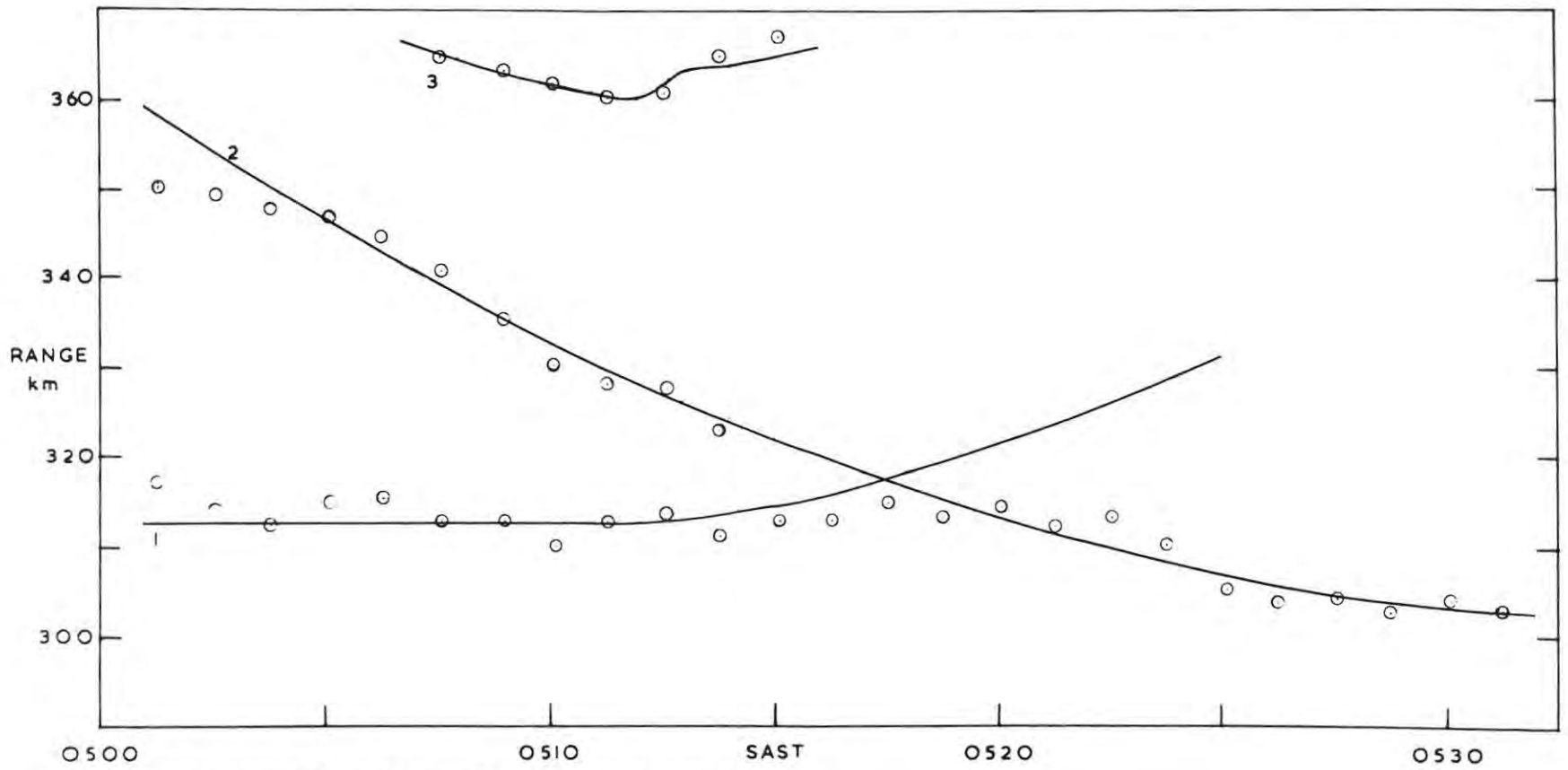

FIG. 5.3. RANGES OF 2 Mc/s REFLECTION LEVELS.

Fig 5.3A

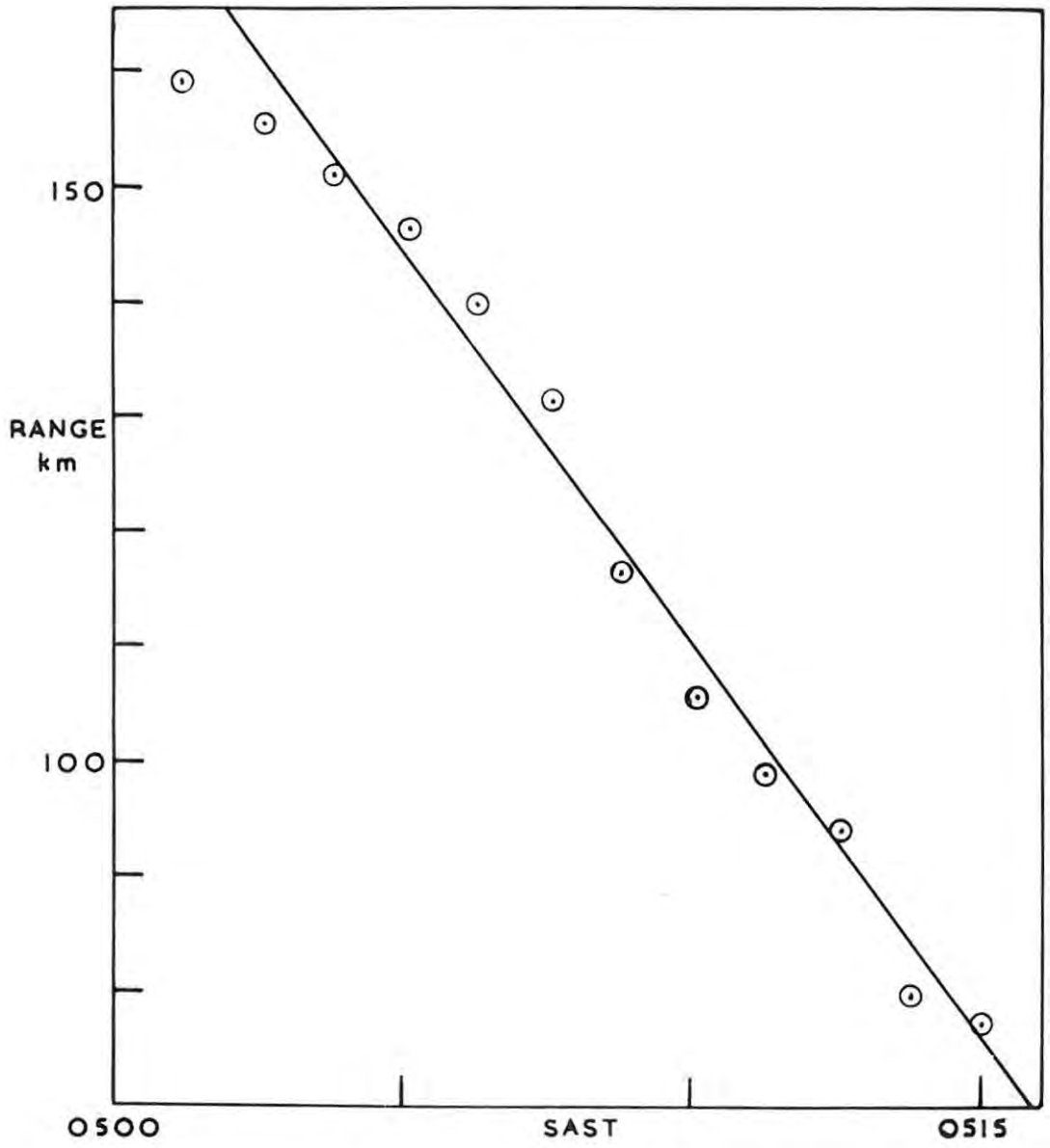

FIG. 5.3.A. RANGE OF 2 Mc/s DOUBLET REFLECTION FROM THE VERTICAL.

It was found that an inverted trough will explain the disturbance described in section 5.2, the main and doublet traces being reflected from the two edges and the triplet from the peak of the trough.

It should be noted that a narrow gap with ionization contours at different heights on both sides can give rise to the main and doublet traces but not the triplet.

5.4 Velocity of the disturbance.

Since the main and satellite traces had been scaled as accurately as possible by the methods described in section 3.3 it was possible to draw an N-h profile for each of the observed traces.

It was found that the average height of any particular electron density was lower after the disturbance than before it, this can be seen from figure 5.2.

The quantity x, defined by equation 5.2 was calculated for the 2 Mc/s doublet reflection point. This frequency was chosen because the range plots for this iso-electronic contour (5×10^4 cm^{-3}) showed the least scatter around a smooth curve drawn through them, and because this frequency is low enough to avoid scaling errors near the critical frequency. The curve drawn corresponds with the full curve 2 on Figure 5.3. Since the actual heights and ranges are known from Titheridge scaling the velocity could be calculated from a graph of x versus time, shown in figure 5.3.A. The velocity at which the disturbance was propagated was found to be 414 km/hour (115 metres/second).

MUNRO (1958) in a study of travelling disturbances in the F region estimated an average velocity of propagation of 120 meters per second for the larger disturbances.

5.5 Cross section of the trough.

It was assumed that the disturbance was a long inverted trough and that the height of any particular electron density is independent of distance along the trough. This is also implicit in the hypothesis of TOMAN (1955). It was further assumed that the main and doublet traces were due to reflections off the edges of the trough, and the triplet from the top of the inverted trough and that the signals were vertically incident on the contours and did not undergo lateral deviation in the lower ionosphere.

The velocity of the disturbance was taken to be 414 km/hour.

Figure 5.3 shows a plot of the experimental values of the range of the 2 Mc/s reflection level from the ionosonde for the main, doublet and triplet traces, against time. These are labelled 1, 2 and 3 respectively.

The approximate height of any particular electron density at the edges of the trough were found from figure 5.2 and the maximum height of the iso-electronic countours could be found from the minimum of curve 3 in figure 5.3.

A large scale map of the cross section of the trough was then constructed as follows:-

(a) The horizontal scale of the map represented the distance "travelled" by the ionosonde relative to the disturbance. On this were marked distances equivalent to the distance "travelled" in one minute at 414 km/hour. Each distance thus marked could also be regarded as a time interval and these were accordingly labelled at one minute

Fig 5.4

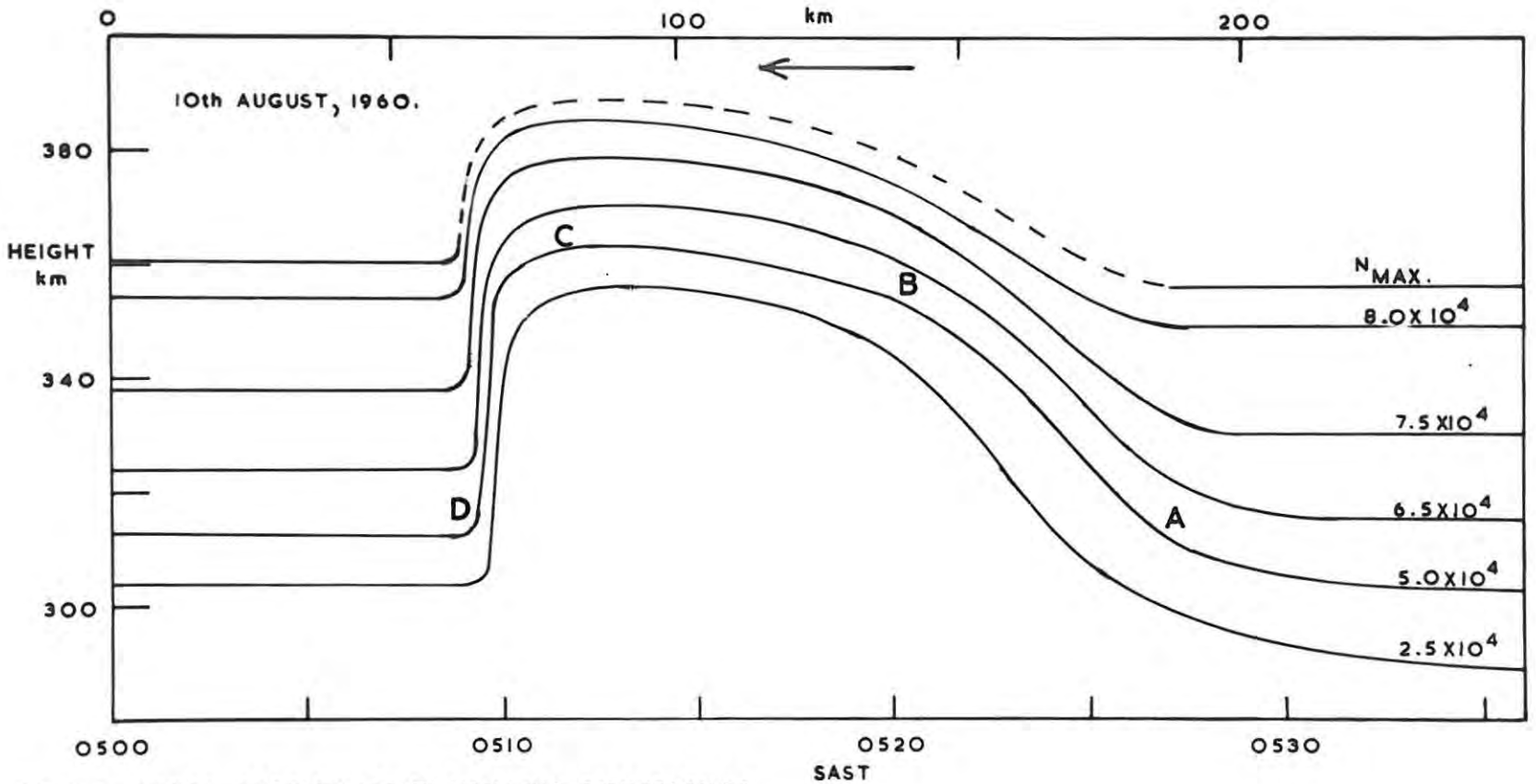

FIG. 5.4. CROSS SECTION OF TRAVELLING DISTURBANCE, SHOWING ISO-ELECTRONIC CONTOURS.

intervals in S.A.S.T. from the start of the set of ionograms. The vertical scale represented the true height.

(b) From smooth curves drawn through the range plots of several levels of constant ionization density the ranges of all three traces were scaled at one minute intervals. These range plots all resembled figure 5.3.

(c) Arcs with radii proportional to these scaled ranges were drawn at the three appropriate heights obtained from figures 5.2 and 5.3 at one minute intervals.

(d) Smooth curves were drawn tangential to these arcs and joined to form a continuous contour.

This process was repeated for a number of contours and only part of the maximum height contour since the triplet trace showed no clear critical frequency, which is necessary for a determination of the height of maximum electron density (see section 3.3.5).

The profile thus obtained for the electron density distribution in the disturbance is shown in figure 5.4. The horizontal scale shows both time and distance and is in fact the same as that used in the construction of the profile. The direction of motion of the irregularity is indicated by an arrow.

From figure 5.4 it is apparent that the trough is between 120 and 150 km wide.

This size lies in the range estimated by TITHERIDGE (1963) for large disturbances observed at Auckland. MUNRO (1950, 1958) obtained evidence for the existence of irregularities with dimensions of several hundred kilometres and a few isolated irregularities as large as 2000 km. have been observed by CHAN and VILLARD (1962), who give many references to previous work.

A range versus time graph was constructed for signals reflected from the edges and top of the inverted trough at the 5×10^4 electrons cm^{-3} (f_N = 2 Mc/s) contour.

The curves thus obtained are shown as full lines in figure 5.3.

Curve 1 was obtained for reflections from the edge D of the trough (see figure 5.4) and curve 2 from the edge A.

Curve 3 arises from reflections in the vicinity of B before the minimum at 0511 hours. After the minimum, however, the reflection point moves rapidly along the arc BC and by 0514 the signals are reflected from the peak of the inverted trough. This rapid change of the point of reflection accounts for the sudden increase in range after 0512 hours.

The asymmetry of curve 3 with respect to curves 1 and 2 is explained by the shape of the trough. If the trough had a semi-circular cross section the minimum of curve 3 would have occurred near where curves1 and 2 crossed and it would have been symmetrical about the minimum.

In figure 5.3 it will be noted that, after the crossing over of curves 1 and 2 there are no experimental range value for curve 1, which has now become the range doublet.

This can be accounted for by a sudden increase in height of the iso-electronic contours at the edge D. The amount of energy reflected back to the ionosonde from the very sharp edged D would then be small and the sensitivity of the receiver could well be too low for it to be recorded.

The weak appearance of the triplet and its absence from the records except for a few minutes around 0511 leads to the conclusion that the upper part of the trough is only weakly reflecting, possibly

due to strong absorption immediately below the reflection level.

Signals reflected from the upper part of the trough in the vicinity of C will not necessarily be focussed on the receiver since the curve could well be much sharper than indicated. It could be compared with a concave mirror of small radius of curvature and small aperture. As can be seen from the accompanying sketch, signals returning to the ionosonde at A can undergo considerable defocussing when the radius of curvature is small compared with the range and will be focussed when the range is approximately equal to the radius of curvature.

Radius of curvature $\ll$ than range.

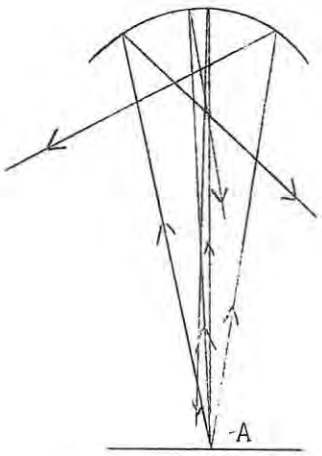

Radius of curvature approximately equal to range.

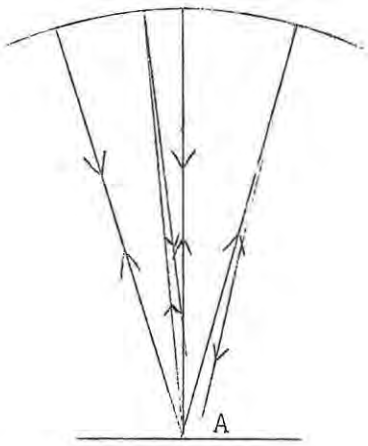

The absence of the triplet does not necessarily imply a gap in the ionosphere. Other records of multiplets exhibit this discrepancy even more markedly (McNICOL and WEBSTER, 1956) and the presence of a distinct triplet seems to be more the exception than the rule.

The iso-electronic contour map (figure 4.1) was drawn before the configuration of the travelling disturbance was worked out. The contours of section A1 and part of A2 were drawn for the main trace. The

disturbance was not indicated because of the crossing of the main and doublet traces. As can be seen from figure 5.3 there is no marked increase in the range of the main trace before the cross-over.

Figure 5.4 therefore replaces A1 and part of A2. It should be noted that the curves in figure 5.4 have been smoothed considerably.

5.6 Critical frequency differences.

A careful examination of the records obtained on the morning of 10th August, 1960 shows that the lower critical frequency is part of the lowest or main trace. The higher critical frequency can be explained by a greater maximum electron density in the trough than in the ionosphere on either side.

This is indicated by a dotted line in figure 5.4.

Further evidence that this may well be the case is the fact that the higher critical frequency trace becomes very much less marked shortly after the disturbance has passed overhead and disappears almost completely a few minutes later.

TITHERIDGE (1963) points out that an increase (or decrease) in the electron density at the centre of the irregularity is roughly proportional to the size of the irregularity. Thus for the largest irregularities the variation in electron density may be as high as 20% of the normal electron density in the ionosphere.

5.7 Origin of disturbances and irregularities.

It has been suggested that large-scale travelling disturbances may be due to an atmospheric wind, possibly associated with a cellular wave (MARTYN, 1950), or alternatively that of an ionization drift induced by an electric field (MARTYN, 1955).

An atmospheric wind would tend to produce a vertical shift of the ionosphere as a whole. An irregularity would tend to diffuse away along geomagnetic field lines if a uniform wind or external field lines if a uniform wind or external field were acting. This is not consistent with the long duration of multiplets (from one to two hours).

In contrast with the expectations of either a wind or a field process values of horizontal speeds deduced from neighbouring stations differ from those obtained when the stations are widely separated.

These features are, however, consistent with the assumption of a propagating atmospheric wave and this is now the most commonly accepted theory (HINES, 1959). The wavelength on this basis would be typically of the order 100 - 200 km and the period of the order 15 - 20 minutes.

Such waves would be strongly affected by gravitational forces and restorative pressure gradients. Waves of this type would be propagated as a perturbation, leaving the layer as a whole essentially unchanged. Such oscillations would also create their own inhomogeneities as they progress and thus avoids the problem of diffusion. The speed from observations by stations with distances of separation comparable to a wavelength would be the phase speed, but that from widely spaced stations would be the group speed; the two would thus not be the same.

The waves could arise from: thermal effects within the atmosphere (PIERCE and MINNO, 1940), interactions between the interplanetary gas and the earth's outer atmosphere (DUNGEY, 1954) and shock waves emitted by the sun (AKASOFU, 1956).

The possibility of a compressional wave which is propagated through

Fig 5.5

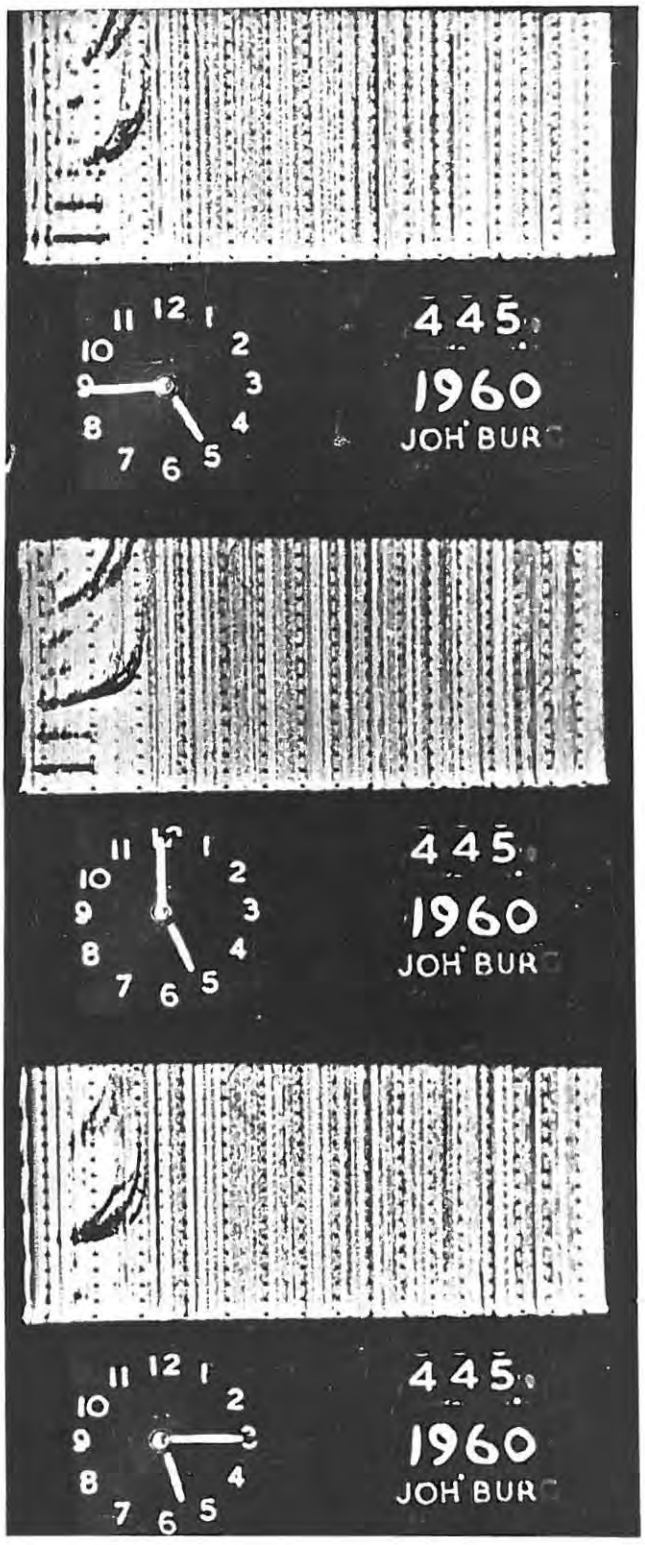

Fig. 5.5 Johannesburg ionograms for the morning of 10th August, 1960, showing the effects of a large-scale travelling disturbance. Frequency mark intervals 1.0 Mc/s starting at 1.0 Mc/s.

the ionosphere has been examined from two view points. Both these involve the concept of resonance, firstly in an electromagnetic field produced by a moving charge (HINES, 1955) and secondly in the oscillation of the electron plasma itself (HINES, 1956). HINES (1959) points out that the theoretical development of the latter was faulty and that it would have to be converted in effect to a study of resonance in the ion plasma before further detailed comparisons with the observations can be made. The orders of magnitude involved in the phenomenon remain essentially the same, and these are pertinent to the observed disturbances.

5.8 Evidence for propagation of disturbance parallel to the sunrise line.

Records obtained at 15 minute intervals on the 10th August, 1960 at Cape Town and Johannesburg were scrutinised carefully for disturbances similar to that already described.

While no disturbances were noticed on the ionograms for Cape Town, what seems to be an oblique reflection appeared at Johannesburg at 0445 S.A.S.T. This was followed at 0500 and 0515 by ionograms resembling the range doublets on Figure 2 of Plate 2 given by McNICOL, WEBSTER and BOWMAN (1956).

The three ionograms from Johannesburg are reproduced in figure 5.5.

The evidence thus tends to suggest that the disturbance was propagated roughly parallel to the sunrise line since Johannesburg and Grahamstown have approximately the same longitude.

It is possible that the effects of the disturbance at Cape Town

may have been obscured by the sunrise effect, or that any noticeable effect may have occurred between soundings.

Because of the long interval between successive soundings at these two stations it is not possible to determine at what time the disturbance passed overhead. For this reason the direction and velocity of the disturbance cannot be determined more accurately. The velocity of 414 km/hour obtained in section 5.4 could thus not be confirmed by observations from stations other than Grahamstown.

5.9 Errors arising from the use of Titheridge coefficients.

The assumption that the Titheridge β coefficients can be used in scaling the oblique traces is not strictly accurate. The values of the coefficients depend on the angle between the direction of propagation and the magnetic field (see equations 3.15 and 3.20).

The errors introduced by this assumption are, however, small and will amount to only a few kilometres unless the rays are deviated very considerably from the vertical (WALKER, 1962). The errors are largest for ray frequencies which are close to the critical frequencies of the layers.

Should a computer become available for analysis of ionospheric data it would be possible to recalculate the ranges of the contours of constant electron density accurately by allowing for the deviation of the rays from the vertical.

The analysis presented here is, as far as can be ascertained, the most detailed investigation of a large-scale irregularity yet published. It is felt that the method outlined in section 5.5 will serve to give a good first approximation of the iso-electronic contours in the vicinity

of a large-scale travelling disturbance until a more accurate analysis can be performed by computer techniques.

Fig 6.1

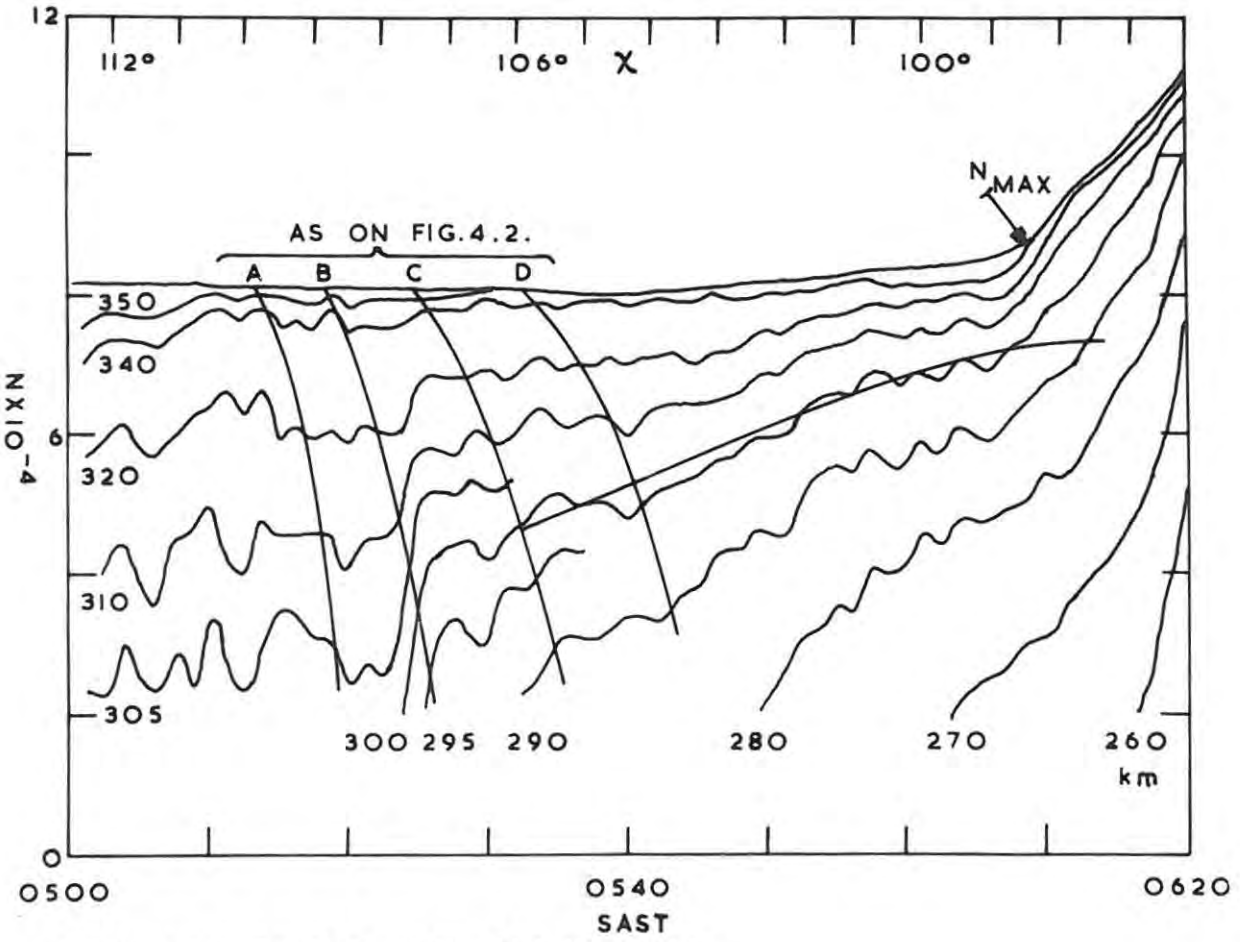

FIG. Nh-t CURVES. 10th AUGUST, 1960.

CHAPTER 6.

ANALYSIS OF Nh-t CURVES.

6.1 Possible presence of negative ions in the F layer.

SETTY (1960) attributed an increase in electron density at constant height between the time of layer sunrise and the main increase resulting from ionization to the detachment of electrons from negative ions. The height of the screening layer calculated from the delay between the times of sunrise at ionospheric levels and the reversal of the observed N(t) curves, is found to agree with that of the Ozone layer.

Spectral investigations have shown that, of the gases present at F layer heights, only atomic and molecular Oxygen can form stable negative ions. The electron affinities of O and O_2 are generally taken to be 2.2 eV and 1 eV respectively (MITRA 1952c).

The processes are thus

$$O^- + h\nu \longrightarrow O + e^-$$

$$O_2^- + h\nu \longrightarrow O_2 + e^-$$

The atomic and molecular oxygen may be in an excited state after the detachment of an electron.

Figure 6.1 shows the Nh-t curves obtained on 10th August, 1960 between 0500 and 0620 hours S.A.S.T.

It is evident from the curves that there is a steady increase in electron density shortly after the time of sunrise at ionospheric levels. The exact time at which this increase begins can unfortunately not be determined accurately because of the effects of the

travelling disturbance already described.

It is certain, however, that this increase began within a few minutes of the time that the sun rose over a 50 km level.

It also appears that the rate of electron production at any particular height increased gradually at first, reached a maximum and then decreased slowly.

The gradual increase in $\frac{dN}{dt}$ can be explained by an increasing flux of solar radiation as the sun rises over a thick layer with no sharply defined boundary.

The decrease in $\frac{dN}{dt}$ is easily explained by a gradual depletion of the number of negative ions available for photodetachment.

6.2 Calculation of reaction cross-sections.

The rate of electron production from negative ions by photodetachment is given by

$$\frac{dN}{dt} = N_- \gamma \beta \qquad (6.1a)$$

where N_- is the density of negative ions,

γ the flux density of solar radiation involved in the reaction

and

β is the photodetachment cross-section.

The derivation of equation 6.1a is given in Appendix A.

The negative ions are depleted at the rate $\frac{dN_-}{dt}$, which is equal to $-\frac{dN}{dt}$.

From this it follows that

$$\frac{dN_-}{dt} = - N_- \gamma \beta \qquad (6.1b)$$

where the symbols have the same meanings as in expression 6.1a.

At this point it should be noted that the literature is somewhat vague on the subject of the units to be assigned to γ and β, and that β is often referred to as the detachment coefficient (see SETTY, 1960).

$\gamma\ \beta$ is most frequently quoted as the photodetachment rate of electrons from negative ions (see BAILEY, 1959; WEBBER, 1962; NICOLET and AIKEN, 1960).

It seems reasonable that the units of γ are the number of quanta available for the photodetachment process entering the earth's atmosphere per sq.cm. per sec, and those of β are sq.cm., since $\gamma\ \beta$ has units of sec^{-1}.

By integration of equation 6.1 it is possible to show that

$$N_- = (N_-)_o\ e^{-\gamma\beta t} \qquad (6.2)$$

where $(N_-)_o$ is the number of negative ions per cm^3 before the start of photodetachment by solar radiation,

γ the number of quanta available for the process in units of $cm^{-2}sec^{-1}$

β the detachment cross-section in cm^2

N_- the number of negative ions per cm^3 left after a time t(in secs) has elapsed since the start of the photodetachment process.

γ is given as 10^{14} and 9×10^{14} for oxygen atoms and molecules with electron affinities of 2.2 eV and 1 eV respectively (MITRA, 1952c).

From equation 6.2 it is possible to calculate β if N_- and $(N_-)_o$ are known.

This method of calculation of the constant β differs somewhat from that used by Setty who assumed that the electrons would be produced

throughout the reaction at a constant rate.

An estimate of $(N_-)_o$ can be obtained from the difference between the asymptotic value of N at constant height which is reached when all the electrons have been detached from the negative ions.

For the purposes of this calculation it is assumed that the sun rises over a sharply defined layer with an outer boundary 50 km above the earth, that the time the sun takes to rise can be neglected and that N at constant height tends to an asymptotic value. $(N_-)_o$ can be obtained from the difference between the asymptotic value of N and N at the time that the sun rises over the 50 km level. One of the resulting assumed Nh-t curves is drawn in figure 6.1 as a smooth curve on the Nh-t curve at 300 km. Time is measured from the point where this curve crosses the 50 km sunrise line.

This process was repeated for all the complete curves from 290 to 340 km on Figure 6.1.

The value of β was then calculated at these heights from equation 6.2 after substitution of values obtained from the smoothed Nh-t curves.

The average results for β obtained were

1.6×10^{-17} cm^2 for O^- and

1.5×10^{-18} cm^2 for O_2^-.

These values are higher than those obtained by Setty by a factor of 10. This difference could possibly be explained by Setty's assumption of a constant rate of electron production for substitution in equation 6.1.

The orders of magnitude of the cross-sections obtained compare

favourably with the results of other workers, both theoretical (BATES and MASSEY, 1943), and experimental (BRANSCOMB et al, 1958 and BURCH et al, 1958).

It should be noted, however, that the relative abundances of O^- and O_2^- are not known, that there is not much difference between the probabilities of reaction for the two photodetachment processes and that only a mean detachment cross-section can be obtained by the method used, because of the energy spectrum of the quanta involved.

The number of negative ions, available for the photodetachment process is not known accurately because the main increase in electron density, by photo-ionization, obscures the asymptotic value of N which would otherwise be reached.

For an order of magnitude estimation of β the time at which the increase in electron density by photodetachment starts need not be known to better than a few minutes. From equation 6.2 it can be shown that the order of magnitude of β remains unchanged even if T, the time in which N_- falls to exp(-1) of $(N_-)_o$, varies by as much as $\pm$ five minutes.

The calculation of β from the Nh-t curves is complicated still further by the possible existence of a dawn wave which travels through the ionosphere parallel to the sunrise line (see section 6.3).

BATES and MASSEY (1943) obtained a theoretical value for the order of magnitude of 10^{-17} cm^2 for the mean photodetachment cross-section of O^- assuming that the light emanates from a black body at 6000^oK.

BRANSCOMB et al (1958) determined the photodetachment cross-section for O^- near the threshold energy for photodetachment and also

Fig 6.2

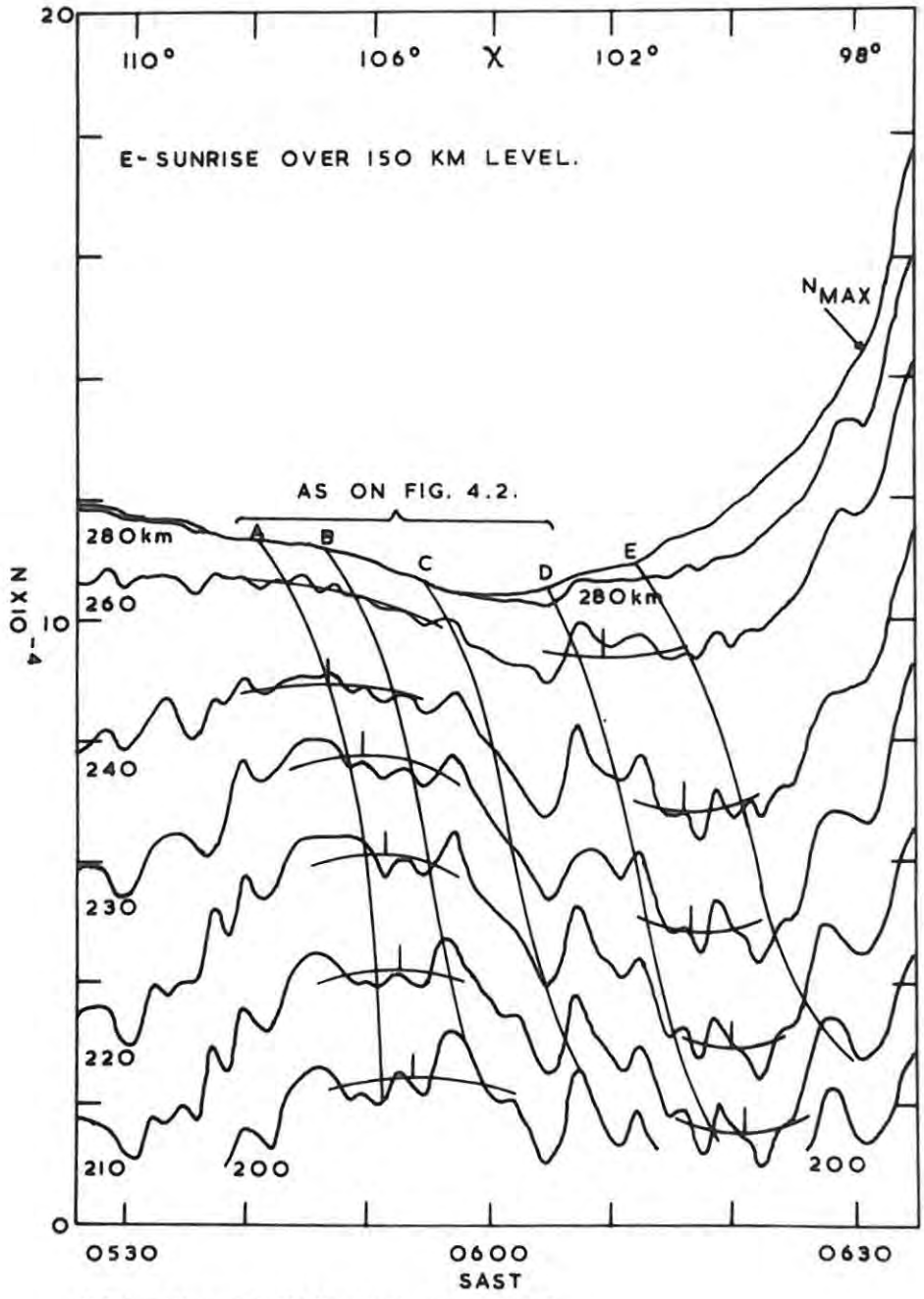

FIG. Nh-t CURVES. 18th MAY, 1960.

found it to be of the order of 10^{-17} cm^2.

The photodetachment cross-section of O_2^- was determined for photons with energies in the range 0.5 to 3.0 eV by BURCH et al (1958), the order of magnitude obtained being 10^{-18} cm^2.

The increase in electron density at constant height which takes place between the times of layer sunrise and the main increase due to photo-ionization could thus possibly be explained by the attachment of electrons to atomic and molecular oxygen and their subsequent detachment by solar radiation.

In order to confirm or refute the existence of negative ions it was decided to scale the ionograms obtained on some other morning and to examine the Nh-t curves for similar results to those discussed.

The sequence of ionograms obtained on the 18th of May, 1960 was selected after rejecting sequences having spread F, travelling disturbances, poorly defined traces, uncertain timing intervals and all records obtained on magnetically disturbed days. The sequence selected was obtained on an International Quiet Day.

The Nh-t curve obtained after scaling these ionograms by the methods described in Section 3.3 are shown in figure 6.2.

It is evident that there is no increase in electron density immediately after layer sunrise, in fact $\frac{dN}{dt}$ is negative. The possible implications of this feature will be discussed in the next section.

Two successful rocket flights with mass spectrometers have yielded results which are difficult to reconcile with the expected behaviour of negative ions (BRANSCOMB, 1957). The results indicated that only

negative ions and no positive ions were present during the day and that only positive ions and no negative ions were present at night. This is the exact reverse of what would be expected although it could be explained by an accumulation of charges of opposite polarity on the rocket. It seems reasonable that negative ions formed during the day would be destroyed by solar radiation and that they could form and exist for a substantial time only at night when no solar radiation was present. In addition a number of unidentified atomic mass numbers were recorded and NO_2^- was found to be the predominant negative ion.

It is at this stage not possible to verify the existence of negative ions at night over Grahamstown and the evidence presented must be regarded as inconclusive until more observations are made.

6.3 Possible existence of a "dawn-wave".

Figure 6.2 gives the impression that the ionosphere as a whole is depressed and then elevated over a period of some 30 or so minutes.

This effect could be due to a very long travelling disturbance with a small amplitude.

Smooth curves drawn through the Nh-t curves show that there is a constant lag of 29 minutes between the maximum and minimum values of N at constant h. Portions of the smooth curves have been drawn in only at the maxima and minima of the curves in figure 6.2 in order not to introduce too many lines on the diagram. The turning points are indicated by short vertical lines.

It is evident from the diagram that the points at which $\frac{dN}{dt} = 0$ lie nearly parallel to the lines depicting the times of sunrise over various layers at different ionospheric heights.

Fig 6.3

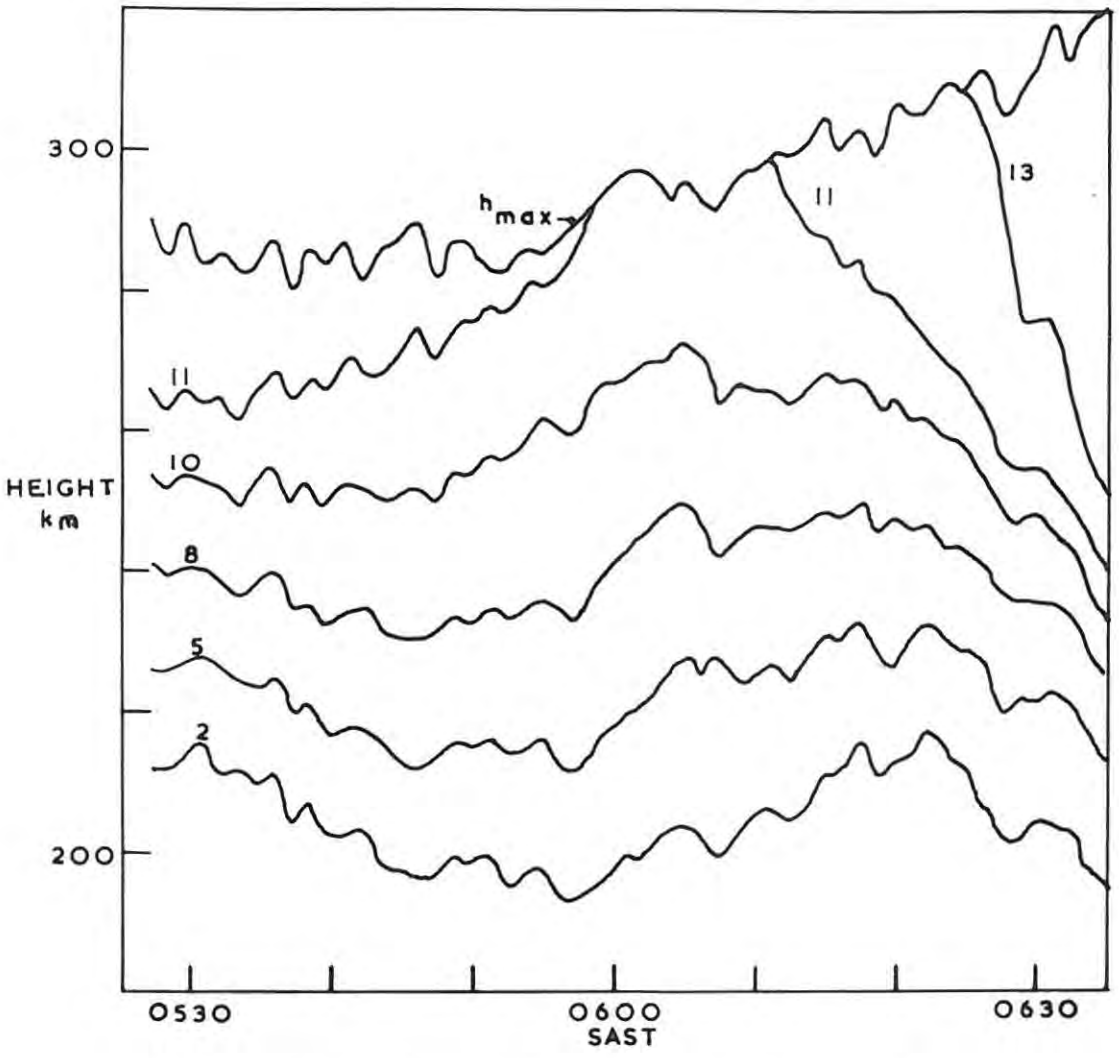

FIG. 6.3. h VS. t FOR CONSTANT N. 18th MAY, 1960.
ELECTRON DENSITY GIVEN IN UNITS OF 10^4 CM^{-3}.

On the basis of this evidence it is possible to postulate the existence of a "dawn-wave" with a small amplitude travelling parallel to the sunrise line in the ionosphere. It should be remembered that the available evidence suggests that the latter condition applies to the disturbance of the 10th August, 1960. (See section 5.6, Chapter 5.)

The amplitude of this particular wave, as found from a graph of h versus t at constant N (shown in figure 6.3) is about 20 km and its wavelength is 1350 km. The calculation of the wavelength is based on the constant lag of 29 minutes between the maxima and minima and the assumption that the wave travels parallel to and at the same speed as the sunrise line.

Because of the small amplitude and long wavelength no range multiplets were observed. The N-h contours do not change rapidly enough to give rise to reflections such as those discussed in Chapter 5.

It is possible that the amplitude of the wave may be large. In this case range multiplets could be observed, but only if the isoelectronic contours are inclined sufficiently to the horizontal to form reflection edges (see section 5.1.2, Chapter 5).

The energy source for this wave is not obvious. It is suggested that this may possibly be the same as that producing large-scale travelling disturbances (section 5), i.e. thermal effects within the atmosphere (PIERCE and MIMNO, 1940), interactions between the interplanetary gas and the earth's outer atmosphere (DUNGEY, 1954) and shock waves emitted by the sun (AKASOFU1956). It is also possible that energy may be transmitted forward beyond the sunrise line, i.e. towards the unilluminated ionosphere, thus giving rise to the observed

phenomenon.

The theory of the "dawn-wave" has not been developed sufficiently to make any predictions as to its behaviour or more definite suggestions concerning its formation.

6.4 Ionospheric ripples.

From figures 4.1, 6.1 and 6.2 it is clear that there are present in the ionosphere a number of ripples. These have a small amplitude of the order of a few kilometres and do not give rise to range multiplets.

In figure 6.1 the "ripples" between 0510 and 0530 are believed to be due to turbulence at the edges of the trough. To verify that these ripples were not due to a faulty scaling technique the records up to 0535 on the 10th of August, 1960 were rescaled. The Nh-t curves and iso-electronic contours derived from the new set of Nh curves remained substantially the same.

Moreover, these small ripples appear to indicate movement of a vertical column in the ionosphere as a whole. They correspond to a distortion of the ionosphere analogous with the distortion of a reflecting surface.

The "ripples" on figures 6.1 and 6.2 with a periodicity of two-and-a-half minutes or so can be regarded as being due to scaling techniques and instrument shortcomings. This aspect will be discussed in section 9.2.

Other "ripples", however, exist and these have a longer periodicity of five to ten minutes. These correspond to small irregularities with amplitudes of a few kilometres and a wavelength of 100 to 200 km.

Evidence of such frontal irregularities, some tens of kilometres long, extending in directions parallel to the sunrise line and travelling, relative to the earth, with this line, have been obtained by BOWMAN (1960), using direction finding receiving equipment and vertical and oblique incidence single frequency pulsed transmissions.

These "ripples" could focus and defocus radio waves and so bring about fading of these signals (BRIGGS and PHILLIPS, 1950; BRIGGS, PHILLIPS and CHINN, 1950).

Fig 7.1

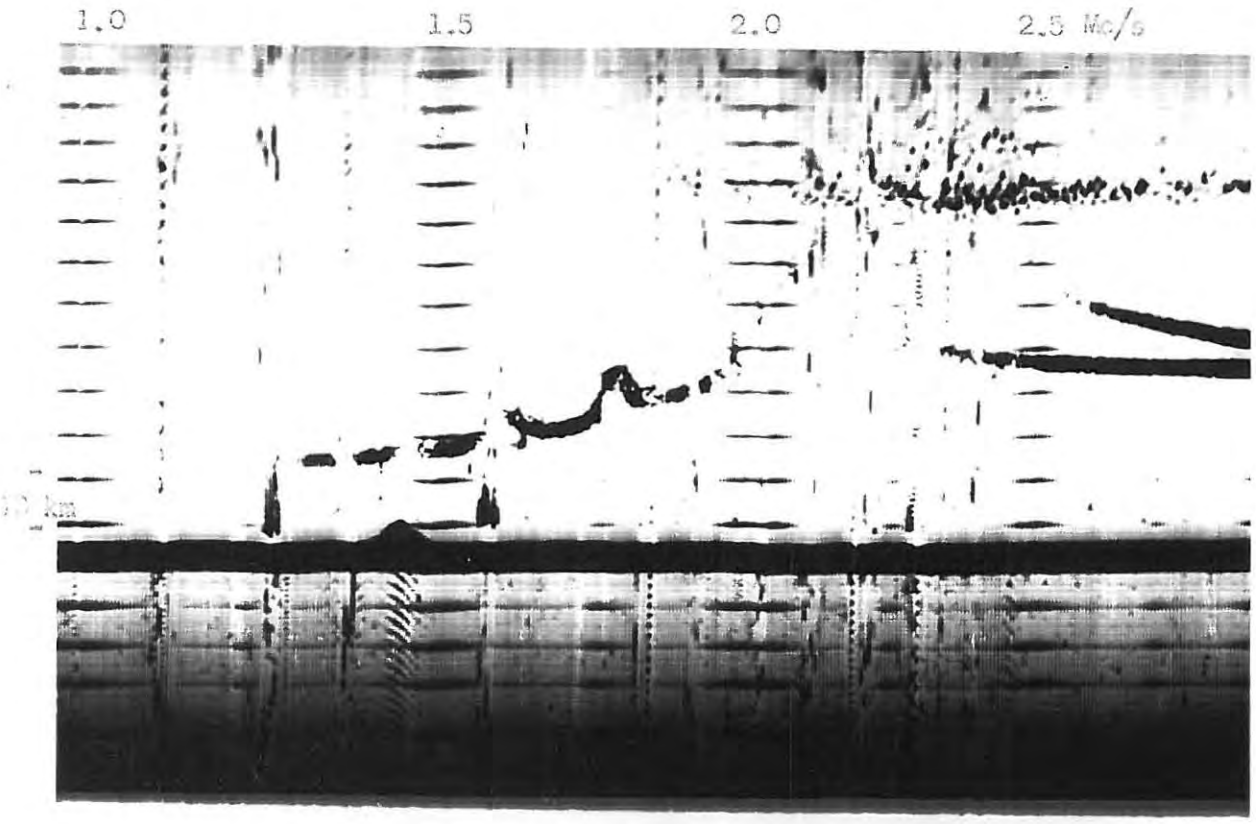

Fig. 7.1 Portion of ionogram obtained at 0723 on 10th August, 1960 showing typical fine structure of newly formed E layer.

Fig 7.2

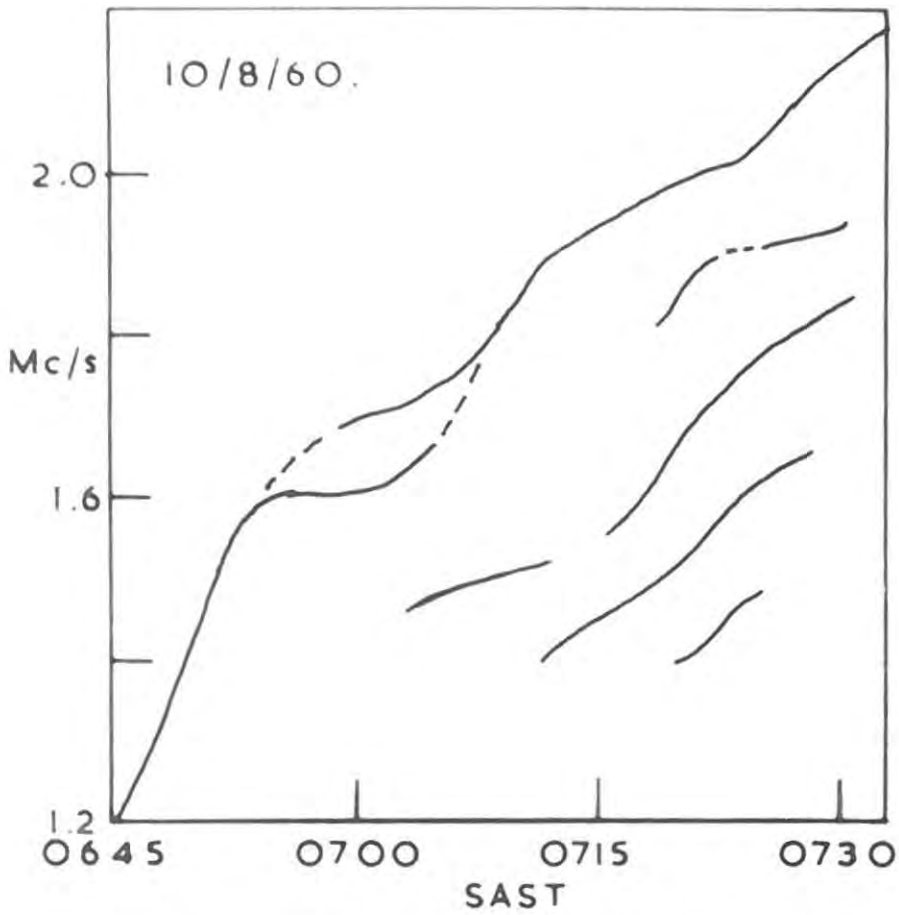

FIG.7.2. VARIATION OF "f_{crit}" OF E-REGION CUSPS WITH TIME.

CHAPTER 7.

THE EARLY MORNING E LAYER.

7.1 Fine structure.

HALLIDAY (1936) made a detailed study of the occurrence of "ledges" and "abnormal E-regions". Some of the complications which often occur in the E region were noted by BEST, FARMER and RATCLIFFE (1938) mainly for the purpose of recognizing with certainty the normal behaviour of this region.

Figure 7.1 shows portion of the ionogram obtained at 0723 on the 10th of August. The first frequency mark is 1.0 Mc/s and frequency marks occur at 0.5 Mc/s intervals. The height markers represent 50 km intervals.

A number of small cusps are visible on the O-trace below 2.0 Mc/s. Two of these, at 1.78 and 1.60 Mc/s, are clearly visible while the third, at 1.44 Mc/s, has been partially obscured on the record by a station. The critical frequency of the layer is doubtful because of absorption in the vicinity of layer maximum.

This type of record is typical of the records obtained during the runs made while the E layer was developing.

The cusps correspond to almost imperceptible kinks in the N-h contours and the shape of the h'f curves greatly overemphasize the shape of the "layers" and it is dangerous to make deductions about the shape of the layer simply from a superficial examination of the h'-f curves.

Figure 7.2 shows a plot of the "critical frequencies" of the cusps against time. Because of absorption in the vicinity of the

Fig. 7.3 Typical examples of quasi-oblique reflections near value of f_0E. Note that the O ray bends back slightly towards low frequency end, away from f_0E. Frequency marks every 0.5 Mc/s starting at 1.0 Mc/s. Height marks represent 50 km. intervals.

Grahamstown 26/9/1960 0559.6 SAST.

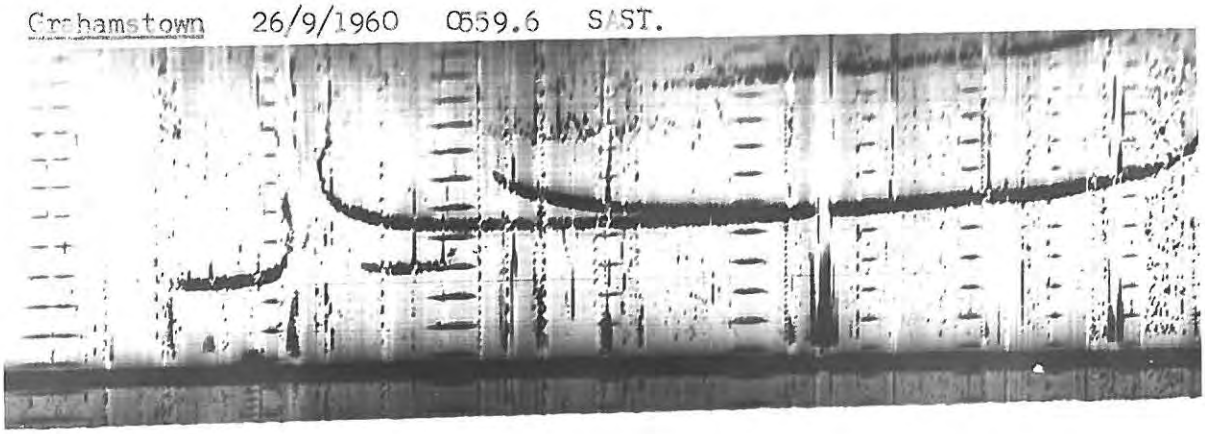

2/10/1960 0556.1 SAST.

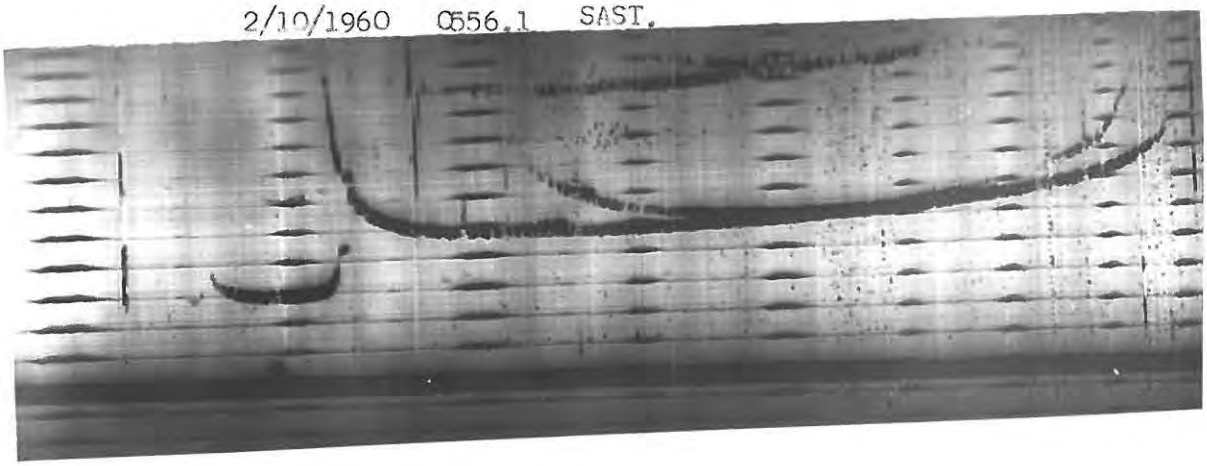

18/5/1960 0703.9 SAST.

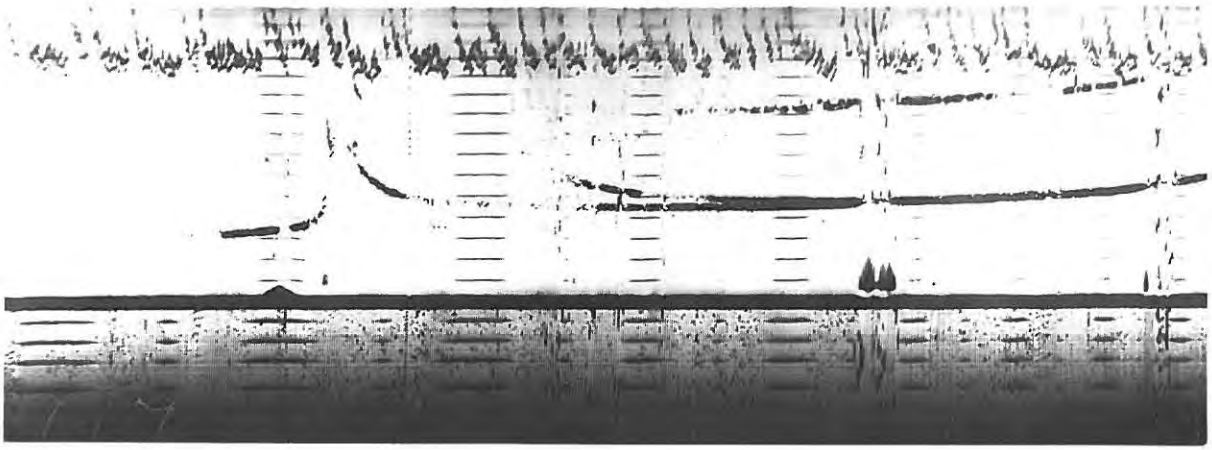

Grahamstown 10/8/1960 0659.2 SAST.

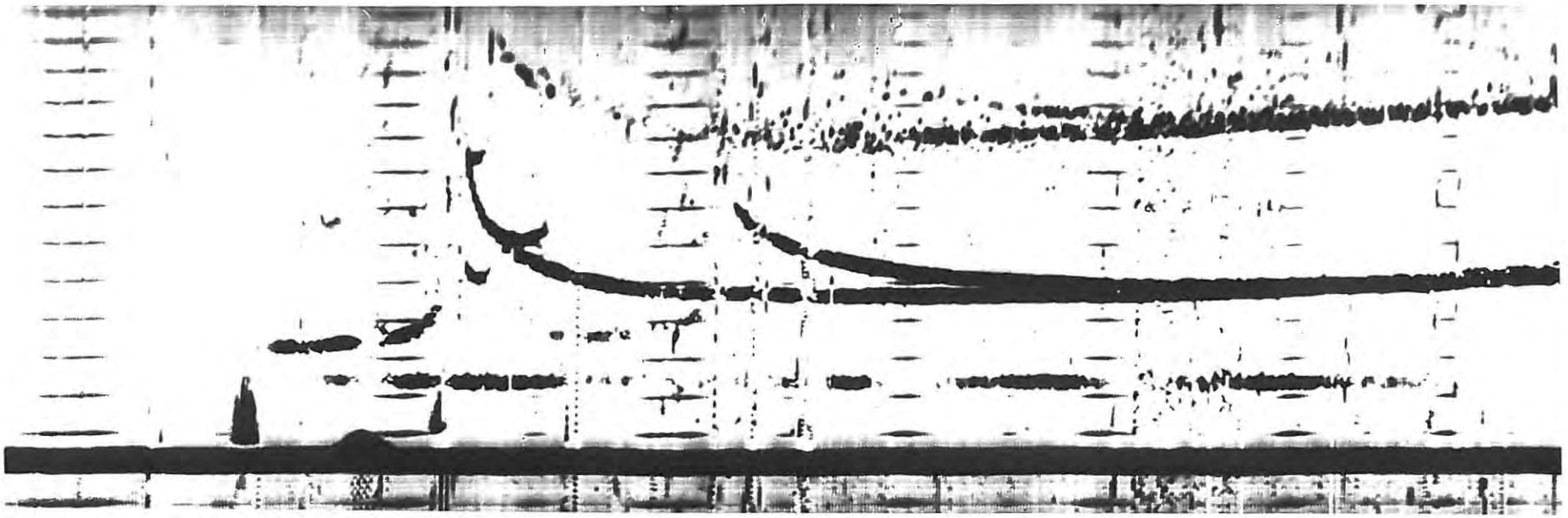

Fig. 7.4 Example of typical complex echo pattern in the vicinity of f_0F_2, usually following quasi-oblique type echoes. Frequency marks at 0.5 Mc/s intervals starting at 1.0 Mc/s. Height marks represent 50 km.

critical frequency at the E layer maximum it has sometimes been necessary to interpolate the curves. Interpolated values are indicated by dashed lines.

This type of "critical frequency" versus time graph is typical of most of the runs obtained during the formation of the E layer.

The fine structure of the E layer has been discussed in some detail by WHALE (1951) and ROBINSON (1959).

Some of the cusps arise from subsidiary regions of various kinds occurring together with the simple E layer, whereas others appear to be due to irregularities or ledges in the normal E layer.

It has been found that the "critical frequencies" which appear regularly are roughly proportional to $(\cos \chi)^{0.25}$, while those which are observable only intermittently do not obey the proportionality law even approximately.

7.2 The "explosive cusp".

Possibly the most interesting feature observed during the formation of the E layer is the appearance of what can best be described as an "explosive cusp" during a number of runs.

Several examples of this type of cusp are shown in Figure 7.3. It is characterised by a slight bending back of the reflected trace towards the low frequency end of the record near the E layer critical frequency, followed by a short gap in which no reflection can be observed, presumably because of absorption, before the lowest reflections from the F region are recorded.

This type of cusp is often followed by records which show a complicated reflection pattern, an example of which is shown in figure 7.4,

Grahamstown 4/9/1960 0628.8 SAST.

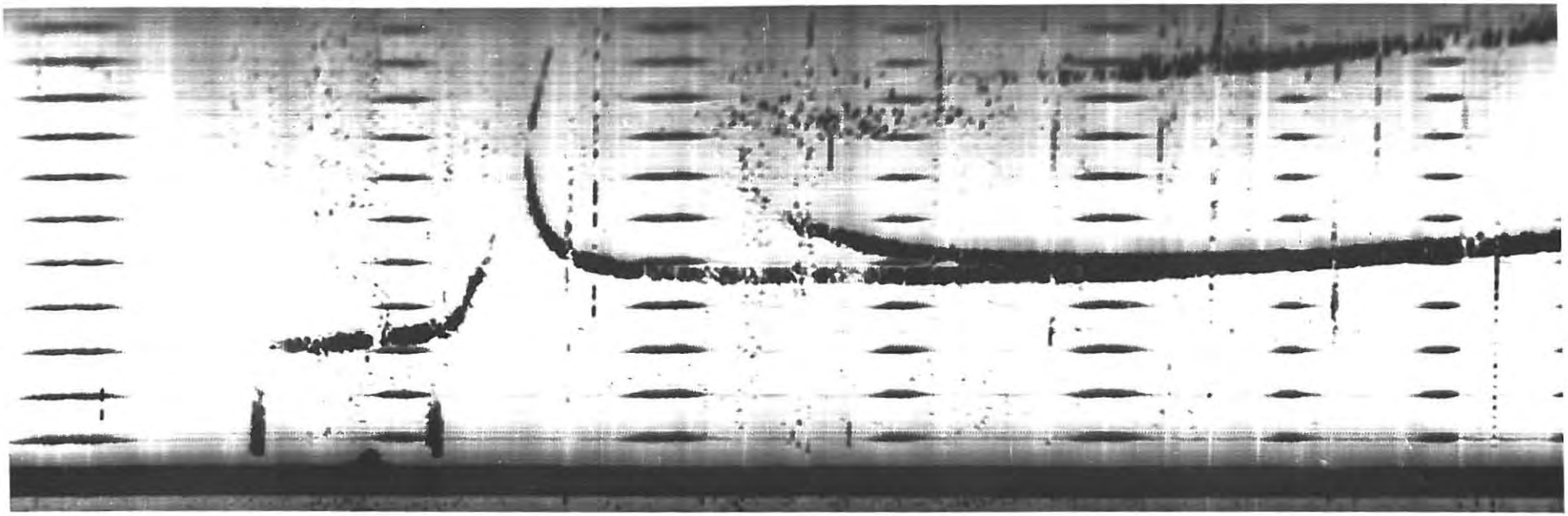

Fig. 7.5 Example of F layer echoes for frequencies slightly greater than f_0E. O ray trace bends away from f_0E towards high frequency end, and somewhat resembles an opened out C. Two ray paths are possible for frequencies just greater than f_0E. Frequency marks every 0.5 Mc/s starting at 1.0 Mc/s. Height marks represent 50 km.

Fig 7.6

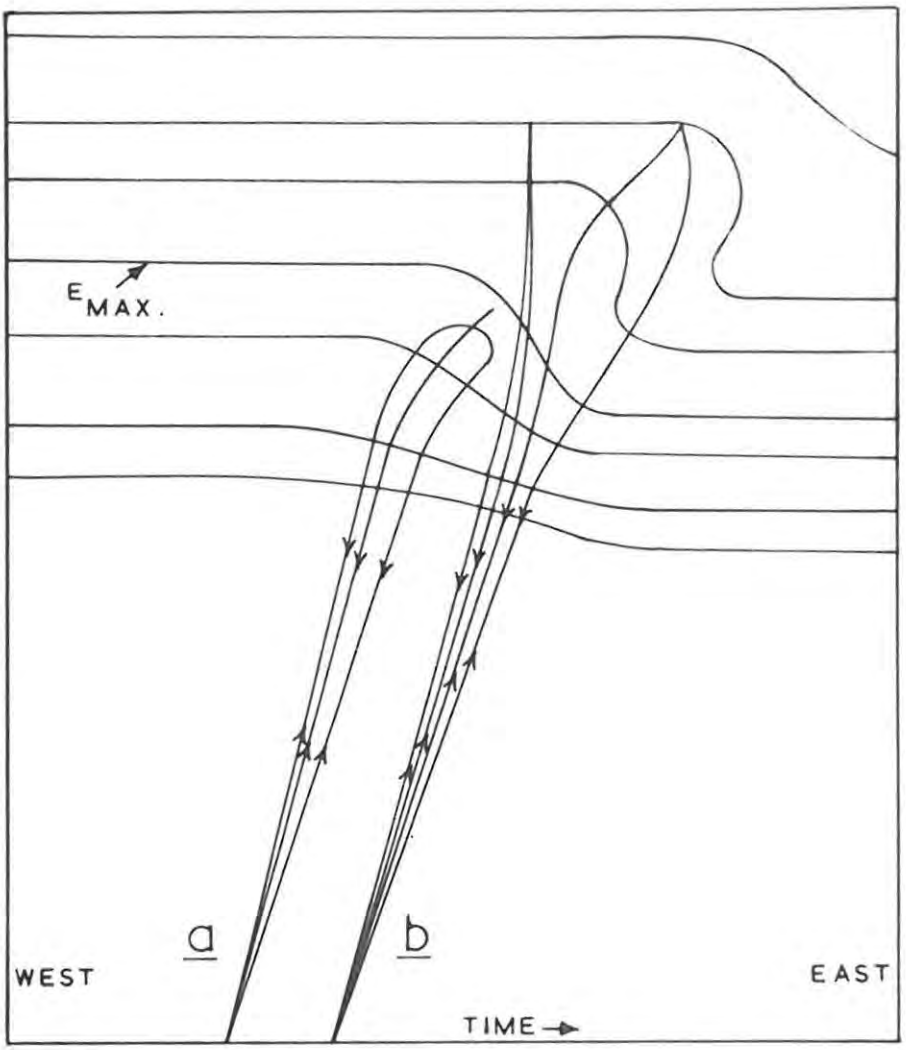

FIG. 7.6 SCHEMATIC REPRESENTATION OF POSSIBLE RAY PATHS WHEN PROBING FREQUENCY IS a SLIGHTLY LESS OR b GREATER THAN f_{crit} OF NEWLY FORMED E-LAYER.

before a new subsidiary layer separates out.

Sometimes records with this type of cusp are followed about five minutes later by an ionogram which displays a bending back of the trace for echoes reflected from the lower region of the F layer towards the high frequency end of the ionogram. The h'f curve for the F layer just after the E layer critical frequency thus resembles a C which has been opened out somewhat. A good example of this is shown in figure 7.5.

Figures 7.3, 4 and 5 have been selected as showing the effects to the best advantage since the quality of many of the other sets of ionograms at this time has been reduced by absorption and radio interference.

As far as can be ascertained the types of reflections described have not been reported anywhere in the available literature.

The "explosive cusp" at the E layer critical frequency can be explained satisfactorily by a downwards bend in the iso-electronic contours just below the E layer maximum. Reflection is from the vicinity of the bend and the radio waves are refracted until at the point of reflection they satisfy the conditions for oblique reflection. The reflected waves return to the ionosonde along a path other than that of the incident waves.

The resulting h'f curve will resemble those obtained in the case of oblique reflection where the pulse transmitter and receiver are separated by some tens of kilometres. It is expected that the effect is small so that the frequency at which the curve turns back is just greater than the critical frequency of the layer.

An exaggerated schematic of the refraction and reflection process is shown in figure 7.6a. Note that the ray path is reversible.

Examination of the records show that this type of reflection occurred when χ was between 87° and somewhat greater than 93° during the winter and summer months respectively. Furthermore such reflection usually appeared on only one, or at most two, records during any particular run indicating that conditions favourable to such quasi-oblique reflections only exist for a few minutes.

The complex echo structure at the E layer critical frequency (figure 7.4) are most probably due to oblique reflections from the inclined iso-electronic surface

The type of h'f curve shown in figure 7.5 can be explained by an extension of the reflection mechanism for the quasi-oblique E reflection. As can be seen from figure 7.5, two ray paths can exist for waves with frequencies just greater than $f_{crit}E$. If the reversible path of 7.6a splits into two separate ray paths at some later time as a result of a small valley between the E layer maximum and the F layer the situation depicted by 7.6b arises. Although there is not much difference between the distances traversed by the two rays, the right hand ray passes through a much thicker portion of the ionosphere where the plasma frequency is just less than the probing frequency. The group retardation is much greater for the right hand ray path than for the left, thus resulting in an h'f curve as shown in figure 7.5.

It would appear that the ray paths described satisfactorily explain the shape of the h'-f curves observed in the vicinity of the E-layer critical frequency.

A more sophisticated treatment will involve the use of ray

tracing techniques such as those discussed by WALKER (1962).

The analysis will, however, have to await the development of computer techniques for this purpose. Because of the considerable deviation of the ray path from the vertical when the wave frequency is nearly equal to the critical frequency, the Titheridge β-coefficients will not be the same as in the case where vertical incidence is assumed. (See section 5.9, Chapter 5.)

If the h'f traces described in section 7.2 arise from refraction by steeply inclined iso-electronic contours or a small valley between layers one would expect similar h'f curves near the F_1 peak, if a valley is formed between the F1 and F2 layers, during an eclipse. As far as can be ascertained these types of curves have not been reported during eclipses. It is possible that the power reflected back to the ionosonde is small and that the receiver is not sufficiently sensitive for the reflected wave to be detected.

CHAPTER 8.

PRODUCTION RATES ON THE MORNING OF 10TH AUGUST, 1960.

8.1 The assumed model.

In order to calculate the production rates from known experimental data it is necessary to assume a model of ionospheric behaviour.

The model used for this purpose is the same as that used by DE JAGER and GLEDHILL (1963) in an investigation of the F1 ledge and is based on that of HIRSH (1959).

de Jager and Gledhill in the model assumed a variation of q given by the modified version of equation 2.1

i.e. $$q = q_o \exp\left[1 - z - e^{-z} \; Ch\,(\chi)\right]$$

and calculated values of N for successive five minute intervals. In our case N is known from N-t curves and we should therefore be able to get q from a reverse application of the procedure used by de Jager and Gledhill.

Following Hirsh, electrons are assumed to be produced by photo-ionization of atomic oxygen, which has a scale height H.

Thus $$O + h\nu \longrightarrow O^+ + e \qquad (8.1)$$

Loss of electrons is now assumed to occur by the two step process of ion-atom interchange between O^+ and a molecule followed by dissociative recombination of the molecule, proposed by BATES and NICOLET (1960), the molecule involved being N_2, O_2 or NO. In order to keep a certain amount of generality the reaction scheme

$$O^+ + XY \longrightarrow OY^+ + X \qquad (8.2)$$

$$OY^+ + e \longrightarrow O' + Y' \qquad (8.3)$$

with rate constants of λ_1 and α respectively, will be considered.

On neglecting the effects of movement the continuity equations corresponding to 8.2 and 8.3 are given by

$$\frac{dn(O^+)}{dt} = q - \lambda_1 . n(O^+) . n(XY) = q - \gamma n(O^+) \qquad (8.4)$$

and $$\frac{dN}{dt} = q - \alpha . n(OY^+) . N \qquad (8.5)$$

where $n(O^+)$, $n(XY)$ and $n(OY^+)$ are the number densities of O^+, XY and OY^+ respectively,

q is the production rate of electrons

$\gamma = \lambda_1 n(XY)$ is the ion-atom interchange rate coefficient which will vary exponentially with height because of the distribution of $n(XY)$, and

α is the effective recombination coefficient.

The condition of charge neutrality requires that

$$N = n(O^+) + n(OY^+) \qquad (8.6)$$

It can be shown that, under the equilibrium conditions

$$\frac{dN}{dt} = \frac{dn}{dt}(O^+) = \frac{dn}{dt}(OY^+) = 0 \qquad (8.7)$$

equations 8.4 and 8.5 lead to the expected results that q is proportional to N at high altitudes and N^2 at low altitudes respectively (HIRSH, 1959; see also section 2.2.3 of Chapter 2).

8.2 The calculation of q.

8.2.1 q in terms of known experimental data.

Equation 8.5 can be rewritten as

$$q = \frac{dN}{dt} + \alpha N\, n(OY^+) \qquad (8.8)$$

Substituting for $n(OY^+)$ from equation 8.6 we have

$$q = \frac{dN}{dt} + \alpha N \left\{ N - n(O^+) \right\} \qquad (8.9)$$

$\frac{dN}{dt}$ and N can be obtained from graphs of N at constant h versus t. The only unknown quantity is $n\ (O^+)$.

In the next section it will be shown how DE JAGER (1963) derived an expression for $n\ (O^+)_n$, the number density of O^+ at the end of an arbitrary time interval, in terms of $n\ (O^+)_{n-1}$, the density at the beginning of the interval, and q_n and q_{n-1}, the production rates at the end and beginning of the same interval respectively.

8.2.2 The expression for $n\ (O^+)_n$.

$n\ (O^+)$ can be obtained by the direct integration of equation 8.4, but this is made difficult by the complicated nature of q.

de Jager overcame this difficulty by means of a step-by-step integration. q was assumed to vary linearly with time during each step, between the values at the beginning and end of that step. If the time interval is small, say five minutes, then the assumed linear variation of q will not differ much from the actual variation during the interval. The change in q is thus given by

$$q = D + B.t \qquad (8.10)$$

during the n^{th} interval with $D = q_{n-1}$, the value of q at the beginning of the interval, so that

$$B = \frac{q_n - q_{n-1}}{T} \qquad (8.11)$$

where T is the time interval in seconds and q_n the value of q at the end of the interval.

Substitution for q in equation 8.4 gives

$$\frac{d\ n\ (O^+)}{dt} = D + Bt - \gamma n\ (O^+) \qquad (8.12)$$

This equation can be written in the form

$$\frac{dy}{dt} = D + B\,t - b\,y \qquad (8.13)$$

where $y = n\,(O^+)$ and $b = \gamma$.

Equation 8.13 is an exact first order, first degree equation and may be solved by multiplying through by an integrating factor $\exp(b\,t)$.

This gives

$$\exp(b\,t) \cdot \frac{dy}{dt} = \exp(b\,t)\,(D + B\,t - b\,y) \qquad (8.14)$$

therefore $$\exp(b\,t)\,dy + \exp(b\,t)\,(bt)\,(by - D - Bt)\,dt = 0 \qquad (8.15)$$

Integration of expression 8.15 gives

$$\exp(bt) \cdot \left(y - \frac{D}{b} - \frac{Bt}{b} + \frac{B}{b^2}\right) = \text{constant} = C \qquad (8.16)$$

On substituting back for b, y and D + Bt we get

$$\exp(\gamma t)\left[n\,(O^+) - \frac{q}{\gamma} + \frac{B}{\gamma^2}\right] = C$$

which gives

$$n\,(O^+) = \frac{q}{\gamma} - \frac{B}{\gamma^2} + C\exp(-\gamma t) \qquad (8.17)$$

for the number density of O^+ at the end of the n^{th} interval.

It is now necessary to fix the integration constant C. Since the value of $n\,(O^+)$ will be calculated for successive five minute steps, C can be found in terms of the number density of O^+ at the beginning of the interval under consideration Let $n\,(O^+)_n$ and $n\,(O^+)_{n-1}$ be the values of $n\,(O^+)$ at the end and beginning of the interval respectively.

We may thus write

at time t = O

$$n\,(O^+)_{n-1} = \frac{q_{n-1}}{\gamma} - \frac{B}{\gamma^2} + C\exp(-\gamma.O)$$

$$= \frac{q_{n-1}}{\gamma} - \frac{B}{\gamma^2} + C.$$

$$\text{therefore } C = n\,(O^+)_{n-1} - \frac{q_{n-1}}{\gamma} + \frac{B}{\gamma^2} \qquad (8.18)$$

At time t = T

$$n\,(O^+)_n = \frac{q_n}{\gamma} - \frac{B}{\gamma^2} + C \exp(-\gamma.T)$$

$$= \frac{q_n}{\gamma} - \frac{B}{\gamma^2} + \exp(-\gamma T)\left\{ n\,(O^+)_{n-1} - \frac{q_{n-1}}{\gamma} + \frac{B}{\gamma} \right\} \qquad (8.19)$$

On substituting for B and collecting terms we obtain

$$n\,(O^+)_n = \frac{q_n}{\gamma}\left\{1 - \frac{1}{\gamma T}(1 - e^{-\gamma T})\right\} + \frac{q_{n-1}}{\gamma}\left\{ \frac{1}{\gamma T}(1 - e^{-\gamma T}) - e^{-\gamma T} \right\}$$

$$+ n\,(O^+)_{n-1}\, e^{-\gamma T} \qquad (8.20)$$

where T is the length of the time interval to be used in the calculation.

Note that equation 8.20 differs from the expression for $n\,(O^+)_n$ given by de Jager. Careful checking of de Jager's theory has shown that only the final expression for $n\,(O^+)_n$ is in error. The mistake is easily explained by a typing error and does not affect the results of DE JAGER (1963) or DE JAGER and GLEDHILL (1963), since a check of some of de Jager's worked examples shows that the correct expression for $n\,(O^+)_n$ was used.

8.2.3 The expression for q_n.

If we now substitute for $n\,(O^+)_n$ from equation 8.20 in equation 8.9, which can be rewritten to give the production rate at the end of the n^{th} interval in terms of $\frac{dN}{dt}$, N and $n\,(O^+)$ at that time as

$$q_n = \frac{dN_n}{dt} + \alpha N_n \left[N_n - n\,(O^+)_n \right] \qquad (8.21)$$

we get

$$q_n \left\{ 1 + \frac{\alpha N_n}{\gamma} \left[1 - \frac{(1 - e^{-\gamma T})}{\gamma T} \right] \right\} = \frac{dN_n}{dt} +$$

$$\alpha N_n \left\{ N_n - \frac{q_{n-1}}{\gamma} \left[\frac{(1 - e^{-\gamma T})}{\gamma T} - e^{-\gamma T} \right] - n\,(O^+)_{n-1}\, e^{-\gamma T} \right\} \qquad (8.22)$$

Equations 8.22 and 8.20 appear formidable but the coefficients of N_n, q_n and q_{n-1} all reduce to constants when constant time intervals are used and the calculation is made for a constant height.

DE JAGER (1963) points out that this model should be well suited for solving the continuity equation near noon when $\frac{dN}{dt}$ and $\frac{dn(ion)}{dt}$ are small and should also serve to give a reasonably accurate solution just after sunrise when the loss term is small compared with the production term.

N_n and $\frac{dN_n}{dt}$ are known from experiment. In section 8.2.7 it will be shown that the values of q_{n-1} and $n\,(O^+)_{n-1}$ need not be known accurately in order to calculate q_n when q_n is small.

It is now necessary to decide on the values to be assigned to γ and α.

8.2.4 The recombination coefficient.

NICOLET and SWIDER (1963) point out that the recombination coefficients of the three processes

$$O_2^+ + e \longrightarrow O + O \qquad (8.22)$$

$$NO^+ + e \longrightarrow N + O, \qquad (8.23)$$

and $$N_2^+ + e \longrightarrow N + N \qquad (8.24)$$

have been determined experimentally but that it is difficult to adopt a correct effective value of α for ionospheric purposes. The temperature dependence of the effective recombination coefficient, α, is also not known.

An analysis of solar eclipse data leads to values of α ranging from 5×10^{-9} to greater than $10^{-7} cm^3 sec^{-1}$ (RATCLIFRE, 1956). TITHERIDGE (1959c) reports values of the order of 2×10^{-8} $cm^3 sec^{-1}$ and WATANABE and HINTEREGGER (1962) quote a value of $\alpha = 3 \times 10^{-8}$ $cm^3 sec^{-1}$ for the E region.

As a more or less representative value α was assumed to be 10^{-8} $cm^3 sec^{-1}$ (KING and LAWDEN, 1962).

8.2.5 The ion atom interchange rate coefficient.

From equation 8.4 it is clear that γ is a function of n (XY). The value of n (XY) is taken to be large enough for any changes in it due to ion-atom interchange to be negligible. n (XY) is therefore a function of height and is assumed to decrease exponentially with height. The molecule (XY) has a scale height of $\frac{H}{k}$, where H is the scale height of the ionizable constituent of the atmosphere, and k the ratio of H and the scale height of (XY).

The number density of XY is thus given by

$$n\,(XY) = n_o\,(XY)\, e^{-\frac{k\,(h - h'_o)}{H}} \qquad (8.25)$$

h'_o is taken to be the same as the reference level h_o of the ionizable constituent.

Substitution for n (XY) in equation 8.4 shows that

$$\gamma = \gamma_o\, e^{-k.z} \qquad (8.26)$$

where z is the normalised height.

NICOLET and SWIDER (1963) in a survey of ionospheric conditions quote values of γ of at least 10^{-4} and 10^{-3} sec^{-1} at 500 and 300 km. respectively. All other results obtained, however, indicate that γ is less than 10^{-3} sec^{-1} at 300 km.

The largest value obtained for day-time conditions near sunspot maximum is 6.8×10^{-4} sec^{-1} at 300 km. (VAN ZANDT et al., 1960). RATCLIFFE et. al. (1956) obtained a lower value of 10^{-4} sec^{-1} for night-time data at this height, while a recent analysis by NISBET and QUINN (1963) leads to even smaller values for night-time data.

The value of Ratcliffe et. al. of 10^{-4} sec^{-1} at 300 km was adopted for the purpose of calculation of γ_o at h_o, but before this can be done it is necessary to decide on values of k and H.

8.2.6 Values of H, k and γ_o.

DUNGEY (1956), MARTYN (1956), DUNCAN (1956) and YONEZAWA (1956) have shown that an α-Chapman distribution (see Section 2.4 of Chapter 2) is to be expected if the processes controlling electron decay in the night F region are diffusion under the action of gravity and a height gradient of electron decay by attachment.

DUNCAN (1958) found that there is a good overall agreement between a Chapman distribution and the observed night-time distribution. At the lower levels of the F region however the observed electron density falls more rapidly than the Chapman function, because of the replacement of the attachment law by the recombination law of electron decay. The results of LONG (1962) also show that, to a first order approximation, night-time N (h) curves correspond to α-Chapman curves.

With this in mind it should be possible to calculate the scale height, H, using the available N-h curves before sunrise and the expression for an α-Chapman electron density distribution viz

$$N = N_m \exp \tfrac{1}{2} \left[1 - z - e^{-z} \right] \qquad (8.27)$$

where z in this case is the normalised height from the height of

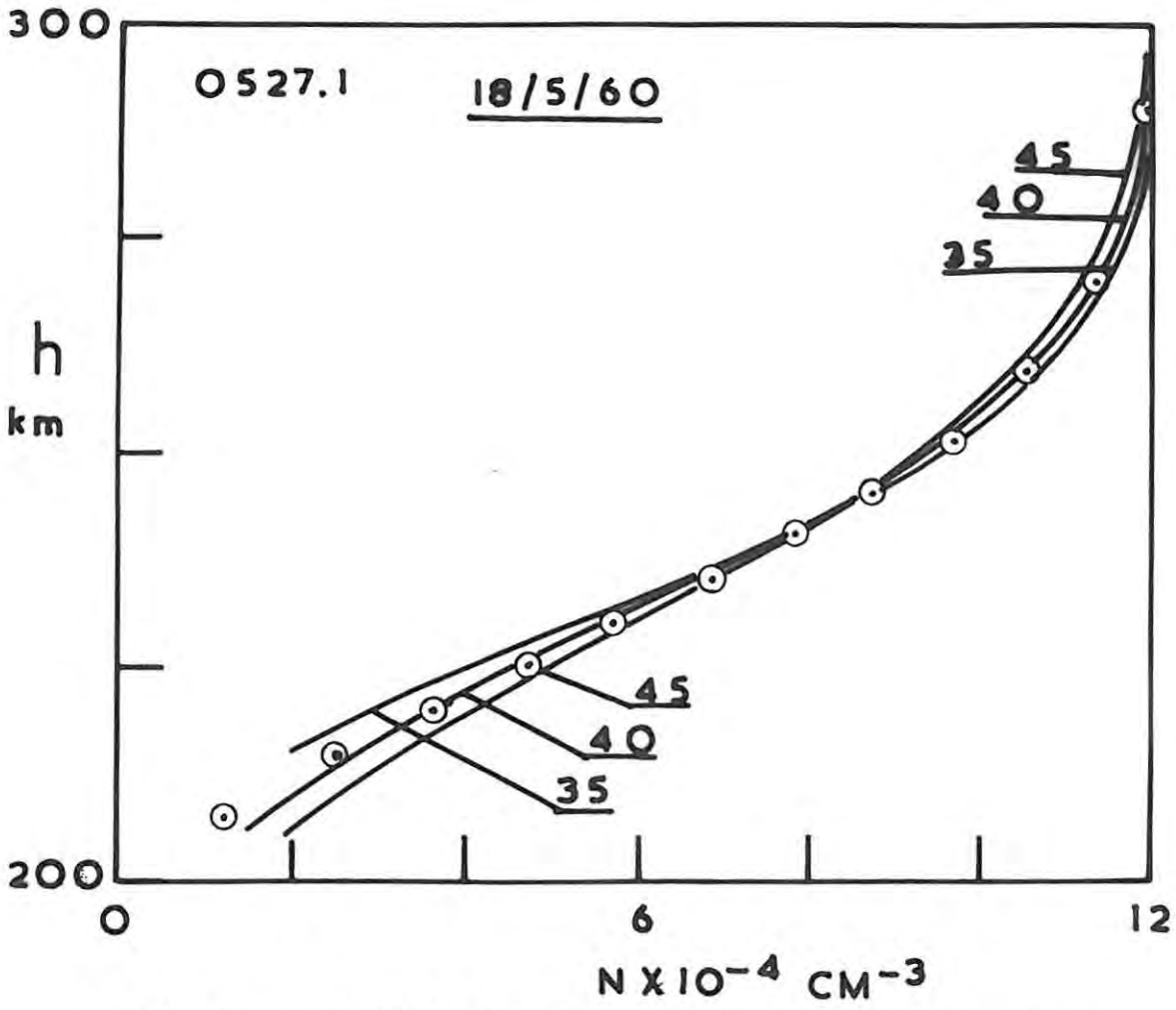

FIG 8.1 CHAPMAN CURVES FOR H EQUAL TO 45, 40 AND 35 KM COMPARED WITH EXPERIMENTAL CURVE.

maximum electron density and is given by $\frac{h - h_m}{H}$.

The N-h curves for the 10th of August, 1960 were not used in view of the presence of the large scale travelling disturbance already discussed. Those for the 18th May, 1960 however were obtained on an International Quiet Day and should therefore yield a reasonable estimate of H.

Figure 8.1 shows the Nh profile obtained at 0527.1 h on the 18th May (circled points) and three Chapman distributions (full lines) calculated from equation 8.27 with values of H equal to 45, 40 and 35 km. respectively. The curve for H = 40 km. appears to provide the best overall fit. Figure 8.1 is typical of the Nh curves obtained shortly after the start of the run on that day.

This value agrees with that obtained by KING-HELE and REES (1962) for 1960 from a study of changes in satellite orbits. It is considerably higher than the value of 30 km. used by DE JAGER and GLEDHILL (1963), but agrees with the estimation of RATCLIFFE et al (1956) of H lying in the range 40 to 45 km.

Following DE JAGER and GLEDHILL (1963) k was taken to be 1.8.

Substitution of these values in equation 8.26 leads to a value of

$$\gamma_o = 3.47 \times 10^{-2} \text{ sec}^{-1} \text{ at } 170 \text{ km.}$$

This value lies in the range estimated by HIRSH (1959) for a value k = 1.8.

8.2.7 Procedure for computation of q_n.

q_n can now be calculated from equations 8.22 and 8.20. The calculation is easily performed with the aid of a desk calculator if it is done in a suitable tabular form.

The procedure is best illustrated with the aid of an example. Table 8 shows the table used in the calculation of q at different times at the 230 km. level. (See pages 96 to 98.)

By way of clarification the following points concerning the table should be noted.

1. Time in S.A.S.T. is recorded in column (1).
2. N_n and $\frac{dN_n}{dt}$ can be obtained from N-t curves such as 4.2 and are recorded in columns (2) and (8).
3. The coefficients of n (O^+) and q_{n-1} in columns (3) and (4) are negative and can be calculated from the expression in equation 8.22.
4. The product $\alpha \times N_n$ is recorded in column (6). The coefficient of αN_n is obtained by the summation of the values in columns (2), (3) and (4) and recorded in column (5).
5. The product of αN_n and its coefficient is obtained by multiplying the values in column (5) and (6). The product, (5) x (6), is entered in column (7).
6. The sum of the two values in (7) and (8) give the right hand side of equation 8.22.
7. The coefficient of q_n can be obtained from the expression in equation 8.22 and is entered in column (10).
8. The value of q_n in column (11) is obtained by dividing the right hand side of equation 8.22, (9), by the coefficient of q_n, (10).

9. $n\,(O^+)_n$ can be calculated from equation 8.20. The coefficients of q_n, q_{n-1} and $n\,(O^+)_{n-1}$ in columns (12), (13) and (14) are obtained from the expressions in equation 8.20. $n\,(O^+)_n$ is the sum of the values in (12), (13) and (14) and is recorded in column (15).

10. The units of the values entered in the various columns are given at the top of each column. Thus for instance the figures in column (2) are in units of 10^4 cm^{-3}, those in (6) are in units of 10^{-4} sec^{-1} and those in (8) in units of 1 cm^{-3} sec^{-1}.

The actual computation proceeds as follows:-

(a) The coefficients of q_n, q_{n-1} and $n\,(O^+)_n$ are calculated from the expressions in equations 8.22 and 8.20 and entered in the relevant columns.

(b) A value of q at the start of computation, is estimated from the continuity equations

$$\frac{dN}{dt} = q - \beta N \qquad (8.28)$$

and $$\frac{dN}{dt} = q - \alpha N^2 \qquad (8.29)$$

at heights greater and less than 180 km. respectively and recorded in column (11).

(c) An intelligent guess is made of a value for $n\,(O^+)$ at the start of computation. This is entered in column 15.

(d) A value of q is now calculated for the end of the first time interval from equation 8.22 and recorded in (11).

TABLE 8. Specimen calculation of q at different times at the 230 km. level.

(1) SAST	(2) N_n	(3) $-n(O^+)_{n-1}$ x 0.4971	(4) $-q_{n-1}$ x 95.45	(5) (2) + (3) + (4)
	10^4 cm^{-3}	-10^4cm^{-3}	-10^4cm^{-3}	10^4 cm^{-3}
0625	1.20			
0630	2.00	0.596	0.168	1.236
0635	3.30	0.625	0.391	2.284
0640	5.30	0.805	0.478	4.017
0645	8.20	1.155	0.825	6.220
0650	14.50	1.866	1.406	11.228
0655	23.34	3.769	3.417	16.154
0700	29.10	6.486	4.647	17.967
0705	35.00	8.745	5.121	21.134
0710	41.80	10.778	6.198	24.824

Table 8 continued.

(6) αN_n	(7) $\alpha N_n \times (5)$	(8) $\frac{dN_n}{dt}$	(9) (7) ÷ (8)	(10) $1 + 1.204 \times 10^{-6} \times N_n$
10^{-4} sec^{-1}	1 cm^{-3} sec^{-1}	1 $cm^{-3} sec^{-1}$	1 cm^{-3} sec^{-1}	1
		17.6		
2.00	2.47	39.44	41.91	1.0241
3.30	7.54	44.55	52.09	1.0397
5.30	21.29	70.66	91.95	1.0638
8.20	51.00	110.8	161.8	1.0987
14.50	162.8	226.7	420.6	1.1746
23.34	377.0	246.7	623.7	1.2810
29.10	522.8	201.7	724.5	1.3503
35.00	739.7	183.3	923.0	1.4214
41.80	1037.6	183.3	1220.9	1.5032

Table 8 continued.

(11) $q_n = \frac{(9)}{(10)}$	(12) q_n x 120.39	(13) q_{n-1} x 95.45	(14) $n(O)_{n-1}$ x 0.4971	(15) $n(O^+)$ (12) + (13) ÷ (14)
1 $cm^{-3}sec^{-1}$	$10^4 cm^{-3}$	$10^4 cm^{-3}$	$10^4 cm^{-3}$	$10^4 cm^{-3}$
17.6				1.20
40.9	0.493	0.168	0.596	1.257
50.1	0.603	0.391	0.625	1.619
86.4	1.041	0.478	0.805	2.324
147.3	1.773	0.825	1.155	3.753
358.0	4.310	1.406	1.866	7.582
486.9	5.862	3.417	3.769	13.048
536.5	6.459	4.647	6.486	17.592
649.3	7.817	5.121	8.745	21.683
812.2	9.777	6.198	10.778	26.753

(e) $n\ (O^+)$ at the end of the interval is calculated from equation 8.20.

(f) It is now assumed that the ratio $n\ (O^+)/N$ is the same at the end and start of the first interval. A better estimation of $n\ (O^+)$ at the start of the interval can now be obtained and a more accurate calculation for q at the end of the first interval can be made.

(g) The calculation can then be continued to give q at five minute intervals.

q_n is relatively insensitive to changes in q_{n-1} and $n\ (O^+)_{n-1}$ when q_n, q_{n-1}, and $n\ (O^+)_{n-1}$ are small, as can be shown by the following example:-

In Table 8, q_{0625} was first taken to be equal to $\frac{dN}{dt}$ at that time and $n\ (O^+)_{0625}$ was assumed equal to N_{0625}. If we now take the extreme case of $q_{0625} = n\ (O^+)_{0625} = 0$ and calculate q_{0630} we obtain a value of 42.1 $cm^{-3}\ sec^{-1}$ as compared with the original value of 40.9 $cm^{-3}\ sec^{-1}$. The new value is only 2.9% greater than the original value of q_{0630}.

If q_{0625} is calculated from equation 8.28 we obtain a value of 45.6 $cm^{-3}\ sec^{-1}$. Using this and $n\ (O^+)_{0625} = N_{0625} = 1.20 \times 10^4\ cm^{-3}$ we find that q_{0630} is equal to 40.4 $cm^{-3}\ sec^{-1}$, which is 1.2% less than our first estimate.

q_{0625} under normal circumstances cannot be greater than q_{0630}, but a value of q_{0630} very close to the original estimate is still obtained.

Fig 8.2

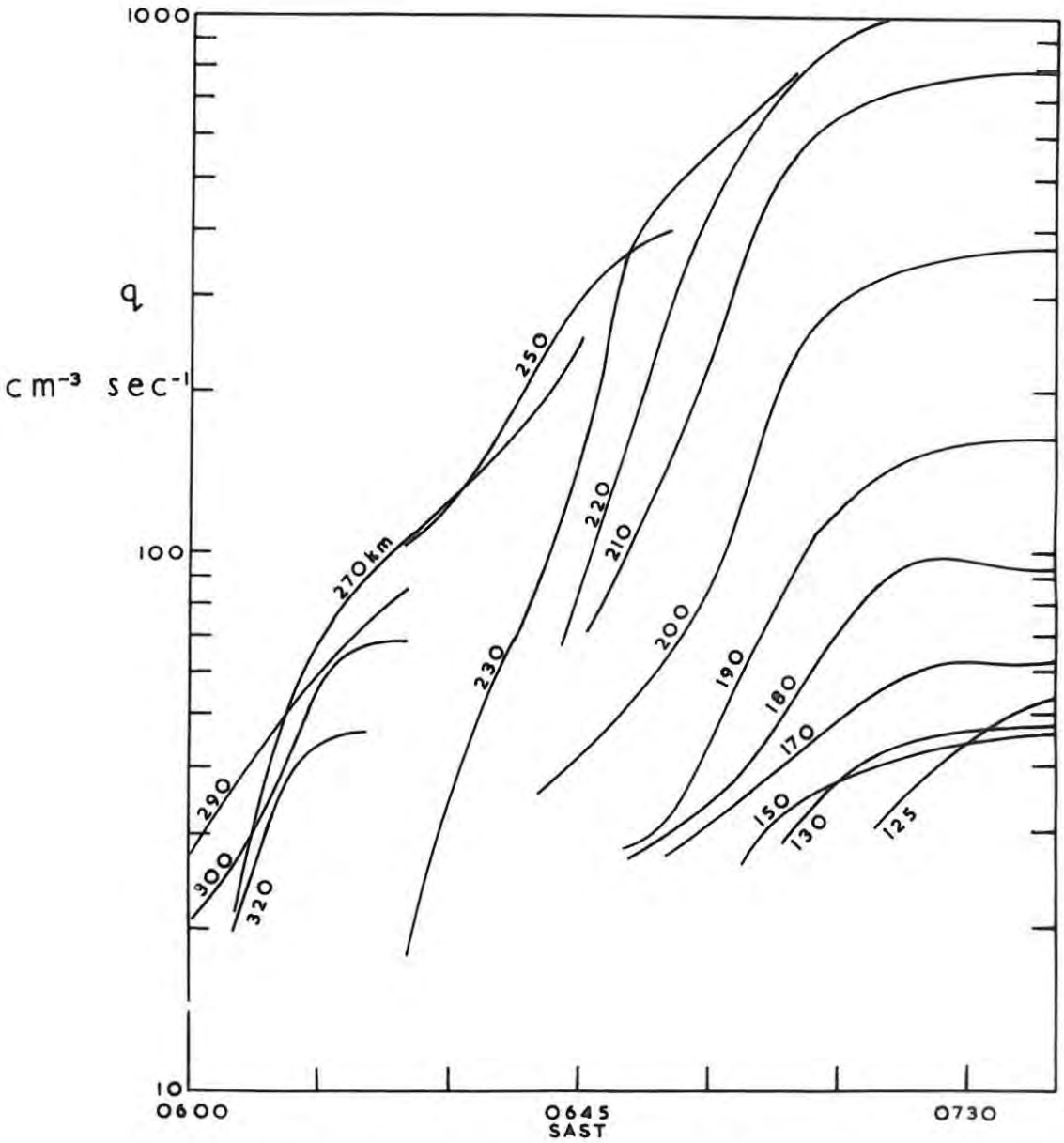

FIG. 8.2 q vs t at constant h.

Fig 8.3

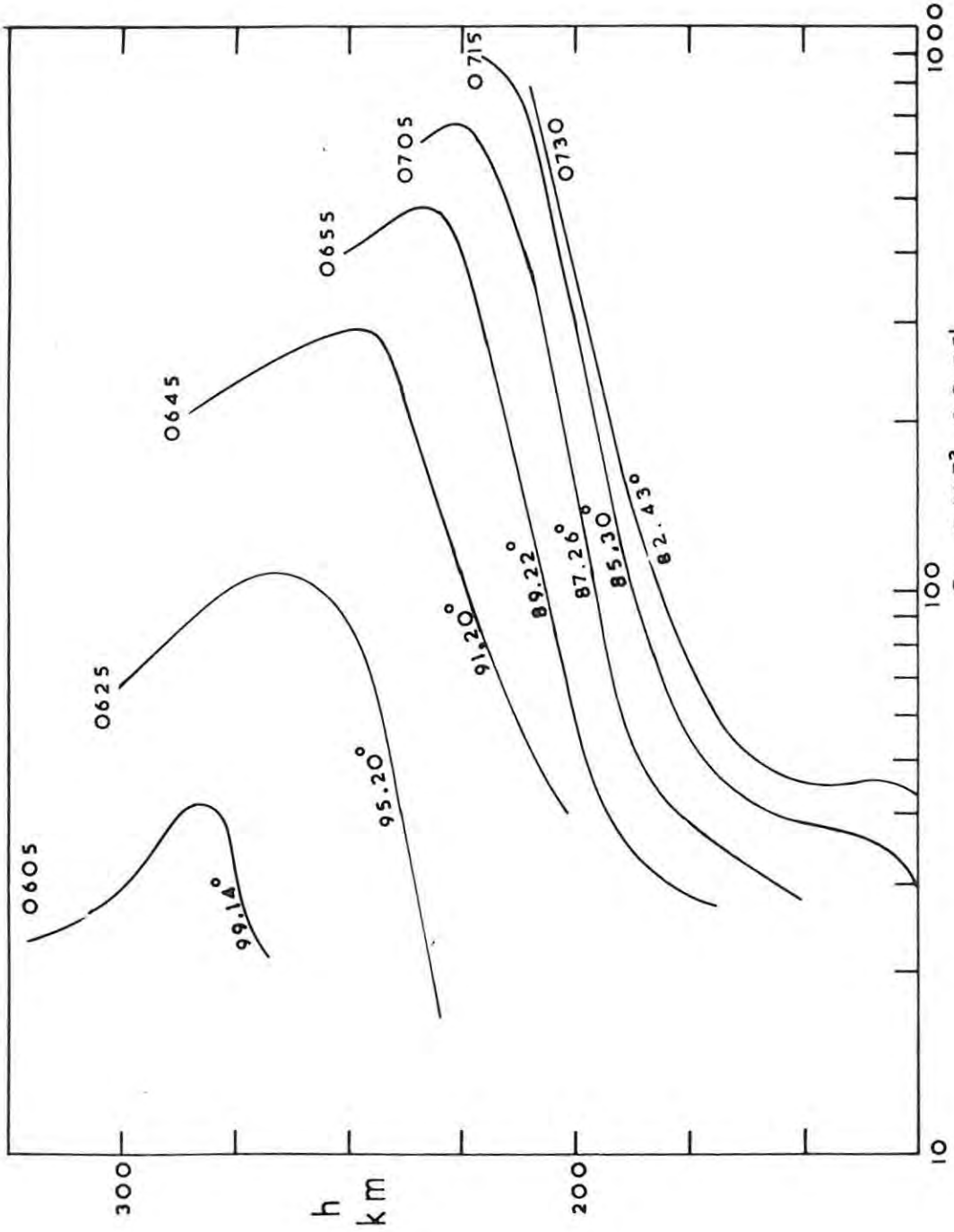

FIG. 8.3 q vs. h for constant χ.

In view of this the calculation of q shown in Table 8 was continued on the basis of the original assumptions for q_{0625} and $n\,(O^+)_{0625}$.

The calculations for q were made for a series of heights from 0600 to 0740 hours for the N-t curves obtained on the 10th August, 1960 (Fig. 4.2).

The data thus obtained are presented graphically in Figure 8.2, which shows the variation of q at constant height with time.

From this data it is also possible to draw curves of production rates at different heights for a fixed solar zenith angle or time. This has been done in Figure 8.3. The solar zenith angles and the times to which they correspond are marked on the curves.

The implications of and the conclusions which may be drawn from the curves will be discussed in section 8.3 of this chapter.

8.2.8 Comparison of q obtained by different methods.

It is at this point convenient to compare values of q obtained by the method described with those which can be derived by the use of equations 8.28 and 8.29. Some of the values at a fixed height and time are presented in Table 9.

Column 1 gives the value of q calculated from equation 8.22 using the method discussed in section 8.2.7, while columns 2 and 3 give q as calculated from the continuity equations

$$q = \frac{dN}{dt} + \beta N \qquad (8.28a)$$

$$q = \frac{dN}{dt} + \alpha N^2 \qquad (8.29a)$$

in which the loss processes are presumed to be attachment and recombination respectively.

TABLE 9. Production rates from different models.

Height	SAST	q from DE JAGER-GLEDHILL model	$q = \frac{dN}{dt} + \beta N$	$q = \frac{dN}{dt} + \alpha N^2$
320	0620	45.1	45.2	
300	0625	67.8	67.6	
290	0625	85.5	89.3	
250	0655	399.0	487.4	998.0
220	0720	972.8	1715.6	1909.7
200	0740	364.3	1909.0	453.0
190	0740	161.2		177.0
180	0740	93.0		96.4
170	0740	62.1		63.4

From Table 9 it is evident that above 300 km. and below 180 km. q may be found with good accuracy from equations 8.28 and 8.29 respectively.

For the intermediate heights, however, it is necessary to use a model which allows a gradual transition from a quadratic loss law at low altitudes (below 180 km.) to a linear loss law at high altitudes (above 300 km).

The DE JAGER and GLEDHILL (1963) model gives the expected results at high and low altitudes and allows a gradual change over from a linear to a quadratic loss law between 300 and 180 km.

Values of q at all heights can be obtained easily by using this model and the method outlined in section 8.2.

8.3 The value of q_o.

It is now possible to calculate a value of q_o, the production rate when the solar zenith angle $\chi = 0$, from the data used to draw the graph of q at constant χ versus t (Figure 8.2) and the Chapman equation for the rate of electron production, q, viz.

$$q = q_o \exp \left[1 - z - e^{-z} \right] Ch(\chi) \qquad (8.30)$$

where z is the height above the level of maximum q when $\chi = 0$ in units of H and $Ch(\chi)$ the Chapman grazing incidence integral (CHAPMAN, 1931b) which is applicable when $\chi > 75^o$.

$Ch(\chi)$ can be obtained from a table given by WILKES (1954). Two quantities are needed for entry in this table. These are:-

(a) The distance x from the centre of the earth to the reference level of 170 km. in terms of H, and

(b) The solar zenith angle χ.

x in this paticular case was 163.7 since H = 40 km. and χ was obtained from the formula

$$\cos \chi = \sin \delta \sin \phi + \cos \delta \cos \phi \cos h \qquad (8.31)$$

where δ is the declination of the sun

ϕ the latitude, and

h the sun's hour angle. (See Appendix A.)

It was necessary to interpolate for a value of $Ch(\chi)$ at the zenith angles shown in Figure 8.2 since the table gives $Ch(\chi)$ for intervals of x = 50 and $\chi = 1^o$.

The values of q_o thus obtained for different zenith angles and heights are presented in Table 10.

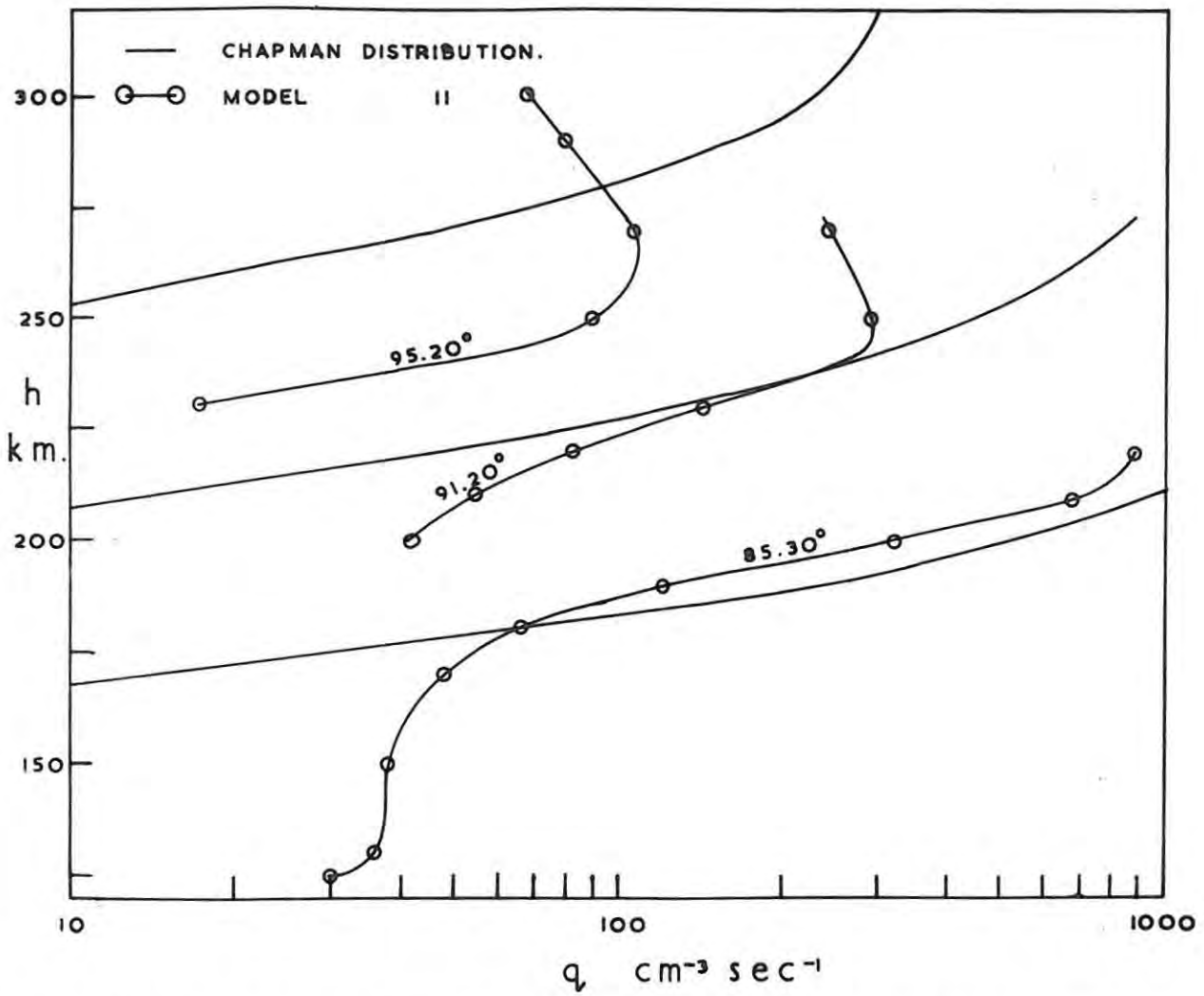

FIG. 8.4. Comparison of Chapman curves with those for q from model.

TABLE 10. Values of q_o from experimental data.

	Height	q_o $cm^{-3}\ sec^{-1} \times 10^{-4}$
$\chi = 95.20^o$	300	0.55
	290	1.00
	270	4.53
	250	52.0
91.20^o	270	0.58
	250	1.24
	230	3.40
89.22^o	250	0.73
	230	1.87
	220	2.07
	210	2.56
87.26^o	230	1.12
	220	1.59
	210	1.86
	200	1.63
	190	2.26
85.30^o	220	1.20
	210	1.37
	200	1.16
	190	1.10
	180	1.98
	170	6.49

If the highest value ($52.0 \times 10^4\ cm^{-3}\ sec^{-1}$) is ignored on the grounds of inconsistency with the general trend an overall average value of $q_o = 1.92 \times 10^4\ cm^{-3}\ sec^{-1}$ is obtained.

The Chapman curves corresponding to this value of q_o and some of the values of χ in Table 10 are shown in Figure 8.4. Only three curves are shown in order not to have too many lines on the diagram.

It is evident from Figure 8.4 that the height of q_{max} decreases more rapidly with increasing χ than is predicted by the Chapman theory, and that the value of q_{max} is also less than the value predicted by Chapman Theory.

The reason for this will be discussed in section 8.4

8.4 Discussion.

The curves shown in Figure 8.3 superficially resemble those given by WATANABE and HINTEREGGER (1962, Figure 8) for theoretical values of q at constant χ versus t. From the curves given by WATANABE and HINTEREGGER however, a value of $q_o = 2.7 \times 10^3$ cm^{-3} sec^{-1} at the F_1 peak can be deduced.

The main differences are (1) the very much higher value of q_o at Grahamstown as estimated from q-t curves for the 10th August and (2) the rapid descent of the height of peak production.

Other notable features are the relatively high production rates at $\chi = 99^o$ and the comparatively short time in which the height of maximum electron density falls to below the height of peak production. This latter point can be inferred from Figure 8.3. As χ increases fewer values are obtained for q at heights greater than q_{max}, until at $\chi = 85.30^o$ the heights of maximum electron density and production rate are the same. At $\chi = 82.43^o$ no value is indicated for q_{max}. This means that the production peak is now above the electron density peak and can no longer be studied by bottom side sounding techniques.

Only two processes can be considered without a more detailed study of q-t curves for several mornings over the sunrise period.

These processes are:- photo-ionization heating of the F region (HUNT and VAN ZANDT, 1961) and diffusion in the early morning F region (GLIDDON and KENDALL, 1960).

Increase of temperature as a result of photo-ionization can be ruled out as the controlling process for the following reasons. An increased temperature would result in an increase of the scale height (section 2.1, equation 2.1). The tendency would be to raise the height of maximum electron density as a result of the upwards expansion of the ionosphere (GLEDHILL and SZENDREI, 1950). χ is, however, increasing with time and the nett result would therefore be to retard the downward movement of the layer maximum. The downward movement of the peak of electron density would therefore lag behind that predicted by Chapman Theory. Furthermore, since the calculation of q depends on the values of N and $\frac{dN}{dt}$, which will in this case be lower than that predicted by the Chapman Theory very low values of q_o would be obtained. All this is contrary to the observed results.

GLIDDON and KENDALL (1960) have shown theoretically by using a simple model ionosphere that the height of maximum electron density decreases rapidly over the sunrise period, as a result of diffusion away from the region of peak production, and that the diurnal variation in N_{max} is a smooth curve with no inflections.

From graphs given by Gliddon and Kendall it is apparent that the height of maximum electron density (h_{max}) decreases by about $1\frac{1}{2}$ scale heights in a very short interval just after sunrise, after which it increases steadily throughout the day.

There appears to be no reason why this theory should not be extended to the layer as a whole, instead of only h_{max}. Diffusion would then take place away from the region of maximum production and tend to lower the F layer as a whole, although the amounts by which the heights of specific electron densities below N_{max} are lowered will decrease from h_{max} to the base of the layer.

As the sun continues to rise the decreasing solar zenith angle means an increasing rate of electron production and a steady decrease in the height of peak production (CHAPMAN 1931a). This will result in an increased ionization gradient with height below the layer maximum, and consequently an increase in the rate of downward diffusion.

If the layer as a whole is lowered N and $\frac{dN}{dt}$ at a given height will be greater than predicted by Chapman Theory. The calculation of q by the method described in section 8. 2 is dependent on the experimental values of N and $\frac{dN}{dt}$. If diffusion is therefore neglected in the calculation of q it is to be expected that considerable error can be made in an estimate of q_o.

It is expected that this process of diffusion will become less noticeable as N and time increase and as the electron density gradient below N_{max} decreases. That this may well be the case is borne out by the behaviour of the q-t curves in Figure 8.2.

The tendency seems to be for the q-t curves to flatten out after a while and for the time at which this happens to increase as the height decreases.

It has unfortunately not been possible to extend the q-t curves beyond 0740 hours because of the poor quality of the ionograms at this time. It is therefore not certain whether q as calculated from experimental values of N and $\frac{dN}{dt}$ remains at a steady value or decreases before increasing to the noon value.

In view of the possibility that the effects of diffusion become less noticeable as N at a given height and time increase, and the electron density gradient below N_{max} decreases it is suggested that q_o for the 10th August will be less than about 0.6×10^4 cm^{-3} sec^{-1}. This is the order of the two minimum values of q_o given in Table 10. The upper limit of q_o can be compared with the maximum value of q at the F_1 peak as calculated from the continuity equation under the equilibrium condition $\frac{dN}{dt} = 0$, i.e.

$$q = \alpha N^2 \qquad (8.32)$$

Using an average noon value of f_oF_1 of 5.0 Mc/s (obtained from the Johannesburg and Cape Town ionograms for the date in question) and $\alpha = 10^{-8}$ cm^3 sec^{-1} a maximum noon value of $q = 961$ cm^{-3} sec^{-1} is obtained. This value is still very much less than the upper limit proposed. This discrepancy could possibly be due to the lowering of the F region by diffusion and thus very much higher values of N and $\frac{dN}{dt}$ at a constant height than would be expected from Chapman Theory, and consequently very high values of q.

Diffusion could thus possibly account for the high values of q_o calculated from data shortly after sunrise and also the shape of the q-t curves, although a much more thorough investigation would be necessary before any definite conclusions could be reached.

From the times at which the N-t curves of Figures 4.2 and 6.1 first show a definite increase in N, the height of a screening layer for a spherical earth can be calculated from the expression given by SETTY (1960) as

$$h = (a + H) \operatorname{Sin} \chi - a \qquad (8.33)$$

where a is the radius of the earth

H is the height at which the increase in ionization is observed

χ the solar zenith angle (See Appendix A)

The average value for the height of the screening layer calculated in this manner is 250 ± 5 km.

This value compares favourably with the heights of the F region maximum to the East of Grahamstown on section F of Figure 4.1 i.e. 245 - 275 km.; implying that ionizing radiation is absorbed in the ionosphere to the east of the sunrise line and only becomes available for photo-ionization at a particular level in the F region overhead when the sun rises over the peak of the F region to the east.

The suggested processes for increase of electron density in the F region just after layer sunrise are therefore:-

1. Photo-ionization of some atmospheric constituent (believed to be O) after the sun rises over the F layer maximum horizon to the east, and diffusion downwards away from the height of layer maximum as a result of the increasing electron density gradient. This has the effect of lowering the layer as a whole, thus resulting in extremely high estimated values of q_o. This process at first

obscures much of the photo-ionization effect at different heights and is expected to become less noticeable as N at any given height increases and as the electron density gradient below N_{max} changes more slowly.

2. After this the increase in N at a given level will be mainly due to photo-ionization.

More data over the sunrise period is, however, necessary before a more detailed examination of the possible effects of diffusion and, to a lesser extent, photo-ionization heating can be made.

8.5 The loss coefficients, α and γ and k.

In a recent survey of ionospheric conditions NICOLET and SWIDER (1963) have indicated that considerable uncertainty exists concerning the values of the loss coefficients α and γ. An idea of the spread in currently accepted values can be gained from the discussions in sections 8.2.3, 4 and 5 concerning the choice of representative values for the recombination (α) and ion-atom interchange (γ) coefficients to be used in the calculation of q.

As a result of the uncertainty concerning these coefficients it is not possible to calculate absolute values of q. Relative values of q are, however, obtained, and must be treated as such.

The ratio of the scale heights k is in effect a measure of the amount of diffusive separation present in the F region between the ionizable constituent and the gas (XY) involved in the ion-atom interchange process. (See sections 2.2.3 and 8.1) If the gases are completely mixed k will be unity. When the gases are separated

by diffusion each will be distributed with its own scale height. In an isothermal atmosphere k will be given by

$$k = \frac{H_i}{H_\gamma} = \frac{m_\gamma g}{k_1 T} \cdot \frac{k_1 T}{m_i g} = \frac{m_\gamma}{m_i} \qquad (8.34)$$

where m denotes the mean molecular weight, subscript i the ionizable constituent (believed to be atomic oxygen) and subscript γ the XY molecules. All the other symbols have the usual meanings except k_1 which is the Boltzmann constant.

If XY is O_2 k will be 2, but if XY is N_2 k will be 1.75.

The choice of k = 1.8 is the same as that used by DE JAGER (1963) and DE JAGER and GLEDHILL (1963).

RATCLIFFE (1959a) considers the values of k between 1.1 and 1.5, but in his arguments is mainly concerned with the behaviour of the F_2 region. HIRSH (1959), investigating F_1 ledge effects, showed that large values of k accentuate the F_1 ledge and thus makes its behaviour more discernible. The value of k = 1.8 will thus lead to a distinct ledge while still allowing for a considerable degree of diffusive separation of the gases. Should the substance (XY) be O_2 the amount of diffusion taking place will be underestimated. On the other hand, if the substance is N_2 the diffusion will be overestimated.

CHAPTER 9.

SUGGESTIONS FOR FURTHER RESEARCH.

9.1 Equipment.

The accuracy with which virtual heights could be scaled was limited by the relatively low definition of the recording oscilloscope trace and the fact that the start of the ground pulse did not coincide with the start of the series of virtual height calibration pulses. The overall scaling accuracy amounted to $\pm$ 2 km., although in some instances the error was as low as $\pm$ 1 km. The need for greater scaling accuracy is commented upon in section 9.2.

It is expected that the new ionosonde at present being constructed by the Rhodes University Physics Department will satisfactorily resolve this problem. Use has been made of crystal controlled frequency calibration synchronised with the pulse repetition frequency and a flat-faced recording oscilloscope tube with a relatively high definition phosphor. Scaling accuracies of $\pm$ 0.5 km. should be attainable, while the flat phosphor surface means that the trace will not be defocussed near the edges when it is recorded on the film.

Some system for automatically dating the ionograms with the time (in hours and minutes SAST) and the date (day and month) is recommended. Scratching of numbers on each ionogram is not entirely satisfactory because of possible omission of numbers.

The use of wide-band antennae with vertical directivity is strongly recommended for both transmitting and receiving systems. It was found that the quality of ionograms after about 0830 SAST

was poor because of non-deviative absorption of the lower frequencies. The proposed antenna system would radiate more power towards the ionosphere directly overhead and will result in good echo patterns over the entire frequency range of the ionosonde.

9.2 Scaling practices.

In section 3.3.4 the method of allowing for ionization below the night-time F region was described. The method depends on the difference between the O- and E-ray virtual heights at corresponding plasma frequencies and the minimum O-ray virtual height (Equation 3.26) for the calculation of the reference height, h_s. Calculation of real heights at Titheridge points is then started from h_s which is the real height of an arbitrarily selected plasma frequency below the minimum recorded frequency.

Large scaling errors will have the effect of introducing apparent fluctuation in the value of h_s, for the same plasma frequencies, in successive N-h curves. This in turn will introduce real height fluctuations which are best described as "scaling" ripples. Such ripples will have a periodicity comparable with twice the interval between two successive ionograms. Examples of these ripples can be seen on Figures 6.1, 6.2 and 6.3 and to a lesser extent on Figure 4.1, where they appear less marked because of the large horizontal scale used.

Unless the "scaling" ripples can be eliminated the presence of ripples with an amplitude of a few kilometres will be obscured.

In addition to this there is the variation in the Titheridge

β coefficients with the angle between the direction of propagation and the magnetic field. This has been commented upon in section 5.9.

β-coefficients are only available up to 2 Mc/s. For any investigation of the diurnal variation of electron densities or production rates at constant heights it will be necessary to use coefficients covering the range 1 - 15 Mc/s or more. Because of the relatively high number of Titheridge scaling points involved several frequency distributions should be available so that the observer can select scaling points to give a sufficiently accurate coverage of an ionogram without involving time consuming and tiring scaling of a large number of virtual heights for each ionogram.

The suggestions for further research all involve the reduction of large numbers of ionograms to Nh-t curves. Depending on the ionogram 5 - 15 minutes will be taken up in scaling off the virtual heights at Titheridge points and another 10 - 15 minutes in the Titheridge reduction of the h'-f curves to electron density profiles. Should a computer become available at some future date it will be possible to punch the scaled virtual heights directly onto data cards. These cards can then be fed into the computer, suitably programmed, to give the required Nh-t curves. This will present a considerable saving of time and, possibly more important, reduction of nervous strain on the observer. In addition a computer would also facilitate the correction of ionogram reduction techniques to allow for variations of the angle between direction of propagation and the geomagnetic field.

9.3 General.

Four main lines of research are indicated by the results obtained so far. These are (1) a study of the possible effects of diffusion in the early morning ionosphere, (2) an investigation of the early morning E region, with emphasis on the effects discussed in section 7.2, (3) an investigation into the presence of negative ions in the ionospheric F region and (4) a closer study of travelling disturbances including the proposed "dawn-wave" (section 6.3).

Of these different projects the study of diffusion effects and of the "dawn-wave" could easily be included in the Rhodes University ionosphere sounding programme for the I.G.S.Y. Records obtained at five-minute intervals over the sunrise period should give sufficient information for a study of these two phenomena. A five-minute interval sounding programme throughout the day is recommended for Regular World Days in the I.G.S.Y. Instruction manual for the ionosphere. It is suggested that this five-minute sounding programme should be extended to include Regular Geophysical Days. Such a sounding programme would result in complete coverage of at least one day per week.

Ionograms from certain selected days could be scaled as accurately as possible by the Titheridge method. Production rates could be calculated at five-minute intervals using the method described in section 8.2

It should then be possible to form estimates of the effects of diffusion and temperature increases and the "dawn-wave", which may be very closely related to the other two processes.

For a study of the production processes in the early morning E layer a sounding programme yielding 2, or possibly 4, ionograms per

minute is suggested. This intense sampling of ionospheric conditions is necessary because of the relatively short time during which cusp patterns such as those described in section 7.2 are believed to be observable. Considerable ray tracing, possibly using computer techniques and Titheridge scaling at a large number of frequency points may then be necessary to explain the observed data satisfactorily. Unfortunately no indication can be given at this time as to when, with relation to the formation of the E-layer, this intense sounding programme should start.

NICOLET and SCHIDER (1953) believe that "- even for night-time conditions, negative ions are important only in the D-region, and it is difficult to find adequate processes to introduce negative ions in the E layer". This opinion presumably holds also the F layer. SETTY (1960), however, feels that certain observed electron density increases in the F region after sunrise can only be satisfactorily explained by photodetachment of electrons from negative ions.

In the photodetachment process for O^- the oxygen atom may be left in an excited state. This can in turn return to the ground state by the process:-

$$O'\ (^1S) \longrightarrow O'\ (^1D) + h\nu\ (\lambda\ 5577\ \text{Å})$$

$$O'\ (^1D) \longrightarrow O\ (^3P) + h\nu\ (\lambda\ 6300, 6363 \text{ and } 6392\ \text{Å})$$

(BRANSCOMB et. al, 1956, wavelengths from MITRA, 1952d).

These emitted wavelengths are frequently observed (MITRA, 1952e).

In order to prove or refute the existence of negative ions in the early morning F region it would therefore be necessary to operate

an airglow photometer concurrently with the ionosonde, preferably when the delay between layer sunrise over the earth's surface and over the F layer maximum is greatest i.e. during summer. A sounding programme with five-minute intervals would suffice although a shorter interval would be preferable in order to obtain more data for the Nh curves. The occurrence or absence of the above spectral lines during intervals when increases of electron density in the F region, believed to be due to photodetachment processes (SETTY, 1960; see also section 6.1), are observed, will prove or disprove whether a sufficient number density of negative ions exists in the F region for the effects of the photodetachment processes to be observable as marked electron density increases.

According to McNICOL et. al (1956) range doublets occur most frequently between two hours after sunset and an hour or two before sunrise.

A detailed study of such doublets arising from large-scale travelling disturbances (see Chapter 5) would involve the complete analysis of ionograms at intervals of one minute or less from three stations a few hundred kilometres apart to give velocity and direction of propagation. Alternately a one station system comprising an ionosonde and single frequence pulse transmitter and directional receiver could be used. Velocity could be estimated from the ionosonde data. Since the disturbances are believed to extend along a considerable horizontal front and to travel in a direction perpendicular to this front, a rough determination of its direction of propagation could be obtained.

From data thus obtained an attempt could be made to correlate the observed results with the theory of propagation of disturbances and possible production mechanisms.

For the study of ionospheric ripples ionograms obtained at intervals of 30 seconds or so could be reduced to N-h curves using the strictest possible application of the Titheridge scaling method, or any other, to avoid fluctuations in N-h curves caused by scaling techniques. This would, however, form part of the study of horizontal irregularities and movements.

Investigations along the suggested lines, in some cases possibly with the aid of a computer to facilitate ray tracing, ionogram reduction, correction of β coefficients and μ' etc., should contribute much to a knowledge of the processes occurring in the F layer and in early stages of production of the E layer.

SUMMARY.

1. The pulsed sounding technique used to study ionospheric behaviour is briefly described.

2. A short survey is made of the behaviour of the layers in the different ionospheric regions.

3. A general survey is made of the theory of layer formation and radio wave propagation in ionized media.

4. The method used to obtain N-h profiles from ionograms is discussed.

5. The Rhodes ionosonde and the modifications made to it are described. This is followed by a description of experimental procedure.

6. A large-scale travelling disturbance is analysed as fully as the available techniques allow. Some evidence is presented to show that the disturbance is of considerable extent, parallel to the sunrise line and may be propagated in a direction perperdicular to this line.

7. The possible existence of negative ions in the F region is discussed and the reaction cross-sections of O^- and O_2^- for photodetachment of electrons are calculated and compared with results of other workers.

8. The possible existence of a "dawn-wave", travelling parallel to the sunrise line, is proposed.

9. The presence of small ripples in the ionosphere is discussed.

10. A brief description is given of the fine structure of the early morning E layer. Some unusual reflections are described and possible reflection mechanisms discussed.

11. A method for obtaining production rates from experimental data is described.

12. Exceptionally high values of the production rate when the solar zenith angle is zero are explained in terms of diffusion in the early morning. This has the effect of lowering the ionosphere as a whole shortly after sunrise and values of N and $\frac{dN}{dt}$ are higher than predicted by Chapman Theory. As a direct result the computed values of q, and consequently q_o, will be higher than predicted by Chapman Theory.

13. Suggestions are made for further research and improvements of experimental techniques.

APPENDIX A.

CALCULATION OF TIMES OF SUNRISE.

(MITRA, 1952a)

At different levels.

The shadow of the earth in space may, for the calculation of times of sunrise, be considered to be of cylindrical shape. The height H at which the cylinder cuts the zenith is given by

$$H = a\left[\frac{1}{\cos \Theta} - 1\right] \qquad (A.1)$$

where a is the earth radius and Θ the angle of depression of the sun below the horizon.

The hour angle h of the sun when it rises at a height H may be obtained from

$$\text{Cos } Z = \text{Sin } \phi \text{ Sin } \delta + \text{Cos } \phi \text{ Cos } \delta \text{ Cos } h \qquad (A.2)$$

where Z = the solar zenith distance

δ = its declination

ϕ = the latitude of the place of observation.

δ can be obtained from The Astronomical Ephemeris.

Z is in fact equal to $90^{\circ} + \Theta$.

To this zenith angle must be added 34' to allow for horizontal refraction and 16' for semi-diameter. The true zenith angle of the sun when it rises at a height h is therefore given by

$$Z = 90^{\circ} + \Theta + 50' \qquad (A.3)$$

At actual noon the apparent time is 12^h and the mean time $12^h + \epsilon$, where ϵ is the equation of time. From this it follows that the time t of sunrise at a height h is given by

$$t = 12^h + \epsilon - h \qquad (A.4)$$

It should be remembered that at actual noon the time will be 1200 hours SAST plus a correction of several minutes depending on the longitude of the place of observation, since SAST is based on latitude $30^{o}W$ of Greenwich.

Sunrise over horizons at different heights above the earth.

In order to calculate the time at which sunrise occurs at a fixed height, H, after passing at grazing incidence over a particular atmospheric level a height x above the earth's surface it is only necessary to increase the earth's effective radius by an amount x and to decrease H by the same amount. Equation A.1 now becomes

$$(H - x) = (a + x)\left[\frac{1}{\text{Cos } \Theta} - 1\right] \qquad (A.5)$$

and the calculation proceeds as before.

Allowance need be made for refraction only when the atmosphere through which the radiation passes is relatively dense.

APPENDIX B.

Rate of Phot-detachment of Electrons from negative ions by Solar Radiation.

In section 6.2 the rate of electron production from negative ions by photo-detachment is given as

$$\frac{dN}{dt} = N_- \gamma\beta \qquad (6.1a)$$

Equation 6.1a may be deduced as follows (MITRA, 1952):-

The number of quanta of energy $h\nu$ in the frequency range $\nu \rightarrow \nu + d\nu$ entering into unit area of the earth's atmosphere is given by

$$n_\nu \, d\nu = \frac{2\pi}{c^2} \left[\frac{R}{d}\right]^2 \frac{\nu^2}{e^{h\nu/kT_s} - 1} \, d\nu \qquad (B.1)$$

where R = radius of the sun

d = earth-sun distance

T_s = temperature of the sun

c = velocity of light

h = Planck's constant

k = Boltzmann's constant

Since, for the conditions under consideration $1 \ll \exp h\nu/k T_s$ the expression reduces to

$$n_\nu \, d\nu = \psi^2 \frac{2\pi\nu^2}{c^2} \exp(-h\nu/k T_s) \, d\nu, \qquad (B.2)$$

where ψ is the angle subtended by the sun's readius at the earth.

Now the rate of photodetachment, i.e., the number of electrons detached from negative ions by the impact of radiation per unit

volume per second is given by

$$\frac{dN}{dt} = N_- \int_{\nu_o}^{\infty} Q_a (\nu) \; n_\nu \; d\nu \qquad (B.3)$$

where $Q_a (\nu)$ = cross-section for light absorption of frequency ν .

ν_o = light frequency for the minimum energy of detachment.

N_- = number of negative ions per cm^3.

Substituting in the expression of $\frac{dN}{dt}$ the value of n_ν and using Milne's relation that

$$\frac{Q_a}{Q_e} = \frac{m^2 v^2 c^2}{2 (h\nu)^2} \qquad \text{(MITRA, 1952 page 303)} \qquad (B.4)$$

where Q_e is the cross-section of recombination accompanied by light emission and m and v the mass and velocity of the ejected electron respectively, we have

$$\frac{dN}{dt} = \frac{\pi m^2 N_- \nu^2}{h^2} \int_{v_o}^{\infty} Q_e (\nu) \; v^2 \exp (- h\nu/k \; T_s) \; d\nu \qquad (B.5)$$

Now changing the variable from ν to v with the help of the relation,

$$\tfrac{1}{2} m v^2 = h (\nu - \nu_o) \qquad (B.6)$$

and remembering that when ν is small

$$Q_e (v) \propto \frac{1}{v} \; [1] \quad \text{i.e.} \quad Q_e (v) = Q_{eo} / v \qquad (B.7)$$

where Q_{eo} is a constant, we have

$$\frac{dN}{dt} = \frac{\pi m^3 N_- \nu^2}{h^3} \; Q_{eo} \exp (- h\nu_o/k \; T_s) \int_0^{\infty} v^2 \exp \left[\frac{- m v^2}{2 k \; T_s} \right] d v \qquad (B.8)$$

The product of $Q_e (v)$ and v is the coefficient of detachment β for electrons with velocity v. We therefore have from the expression

$Q_e(v) = Q_{eo}$ that

$$\beta = Q_{eo}. \qquad (3.9)$$

Substituting for Q_{eo} in the expression of $\frac{dN}{dt}$ and integrating we have

$$\frac{dN}{dt} = N_- \psi^2 \frac{(2\pi m)^{3/2}}{4h^3} k^{3/2} T_s^{3/2} \beta \exp(-h\nu_o/k T_s) \qquad (B.10)$$

If we put

$$\gamma = \psi^2 \frac{(2\pi m)^{3/2}}{4h^3} k^{3/2} T_s^{3/2} \exp(-h\nu_o/k T_s) \qquad (B.11)$$

which is the flux density of solar radiation involved in the reaction, we get

$$\frac{dN}{dt} = N_- \gamma \beta. \qquad (B.12)$$

REFERENCES.

AKASOFU, S.	1956	Sci. Reps. of Tohoku University, Japan, S.5. Geophys., November, 8, p24.
APPLETON, E.V.	1927	U.R.S.I. Proc. Washington Assembly.
APPLETON, E.V.	1932	Jour. Inst. Electr. Engrs., 71, p642.
APPLETON, E.V.	1954	J.A.T.P., 5, p348.
APPLETON, E.V. and BARNETT, M.A.F.	1925	Proc. Roy. Soc. A., 109, p621.
BAILEY, D.K.	1959	Proc. I.R.E., 47, p255.
BALFOUR-STEWART	1878	Encyclopaedia Brittanica 9th ed. 16, p181.
BATES, D.R.	1956	Solar Eclipses and the Ionosphere, Pergamon Press, London, p184.
BATES, D.R. and MASSEY, H.S.W.	1946	Proc. Roy. Soc. A. 187, p.261.
BATES, D.R. and MASSEY, H.S.W.	1947	Proc. Roy. Soc. A. 192, p1.
BATES, D.R. and NICOLET, M.	1960	J.A.T.P., 18, p65.
BATES, D.R. and MASSEY, H.S.W.	1943	Phil. Trans. Roy. Soc., 239, p269.
BELLCHAMBERS, W.H. and PIGGOTT, W.R.	1958	Nature, 182, p1596.
BEST, J.E., RATCLIFFE, J.A., and WILKES, M.W.	1936	Proc. Roy. Soc. A., 156, p614.
BEST, J.E., FARMER, F.T. and RATCLIFFE, J.A.	1938	Proc. Roy. Soc. A., 164, p96
BIBL, K., HARNISCHMACHER, E. and RAWER, K.	1955	The Physics of the Ionosphere (Physical Society; London), p113.
BOOKER, H.G.	1936	Proc. Roy. Soc. A., 155, p253.
BOOKER, H.G.	1938	Phil. Trans. Roy. Soc. A., 237, p411
BOWMAN, G.G.	1960	Austral. J. Phys., 13, p52.

BRADBURY, N.E.	1938	Terr. Mag. 43, p55.
BRADLEY, E.N. and ROSS, W.	1953	Proc. Roy. Soc. A., 207, p251.
BRANSCOMB, L.M.	1957	Electronics and Electron Physics, IX, p89.
BRANSCOMB, L.M., BURCH, D.S., SMITH, S.J. and GELTMAN, S.	1958	Phys. Rev., 111, p504.
BREIT, G. and TUVE, M.	1926	Phys. Rev., 28, p554.
BRIGGS, B.H. and PHILLIPS, G.J.	1959	Proc. Phys. Soc., 63, p907.
BRIGGS, B.H., PHILLIPS, G.J. and SHINN, D.H.	1950	Proc. Phys. Soc., 63, p106.
BUDDEN, K.G.	1961	Radio Waves in the Ionosphere (Cambridge)
BURCH, D.S., SMITH, S.J., and BRANSCOMB, L.M.	1958	Phys. Rev., 112, p171.
CHALMERS, J. A.	1962	J.A.T.P., 24, p219.
CHAN, K.L. and VILLARD, O.G.	1962	J. Geophys. Res., 67, p973.
CHAPMAN, S.	1931a	Proc. Roy. Soc., 43, p26.
CHAPMAN, S.	1931b	Proc. Roy. Soc., 43, p484.
DE JAGER, G.	1963	M.Sc. Thesis, Rhodes University.
DE JAGER, G. and GLEDHILL, J.A.	1963	J.A.T.P., 25, p403.
DUNCAN, R.A.	1956	Austral. J. Phys., 9, p436.
DUNCAN, R.A.	1958	J. Geophys. Res., 63, p491.
DUNGEY, J.W.	1954	Electrodynamics of the Outer Atmosphere. Ionospheric Res. Lab., Pennsylvania State Univ., State College, Pa., Sci. Rep., No. 69, September 1954.

DUNGEY, J.W.	1956	J.A.T.P., 9, p90.
ECCLES, W.H.	1912	Proc. Roy. Soc. A., 87, p79.
ECKERSLEY, T.L.	1937	Nature, 140, p846.
FERRARO, V.C.A.	1946	Terr. Mag., 51, p427.
FERRARO, V.C.A. and BZDOGAN, I.	1958	J.A.T.P., 12, p140
GAUSS, C.F.	1839	General Theory of Terrestrial Magnetism. Published in English translation in Scientific Memoirs (Ed. by R. Taylor), Vol. 2, p184, (London 1841).
GIPPS, G. de V., GIPPS, D.I. and VENTON, H.R.	1948	J. Coun. Sci. Industr. Res. Aust., 21, p215.
GLEDHILL, J.A.	1959	J.A.T.P., 16, p360.
GLEDHILL, J.A. and SZENDREI, M.E.	1960	Proc. Phys. Soc. B., 63, p427.
GLEDHILL, J.A. and WALKER, A.D.M.	1960	J.A.T.P., 18, p61.
GLIDDON, J.E.C. and KENDALL, P.C.	1960	J. Geophys. Res., 65, p2279.
HALLIDAY, E.C.	1936	Proc. Phys. Soc., 48, p421.
HARTREE, D.R.	1931	Proc. Camb. Phil. Soc., 25, p143.
HEAVISIDE, O.	1902	Encyclopaedia Britannica (10th Ed.), Vol. 33, p213.
HINES, C.O.	1955	J.A.T.P., 7, p14.
HINES, C.O.	1956	J.A.T.P., 9, p56.
HINES, C.O.	1959	Proc. I.R.E., 47, p176.
HIRSH, A.J.	1959	J.A.T.P., 17, p86.
HUNT, D.C. and VAN ZANDT, T.E.	1961	J. Geophys. Res., 66, p1673.
KAISER, T.R.	1962	J.A.T.P., 24, p864.

KELCO, J.M.	1952	J. Geophys. Res., 57, p357.
KENNELLY, A.E.	1902	Elect. World N.Y., 39, p473.
KING, G.A.M. and LANDEN, M.D.	1962	J.A.T.P., 24, p565.
KING-HELE, D.G. and REES, J.M.	1962	Proc. Roy. Soc. A., 270, p562.
LONG, A.R.	1962	J. Geophys. Res., 67, p989.
MANNING, L.A.	1949	Proc. I.R.E., 37, p599.
MARIANI, F.	1959	J.A.T.P., 16, p160.
MARTYN, D.F.	1947	Proc. Roy. Soc. (London) A., 189, p241.
MARTYN, D.F.	1950	Proc. Roy. Soc. A., 201, p216.
MARTYN, D.F.	1955	The Physics of the Ionosphere (The Physical Society, London), p161
MARTYN, D.F.	1955	Phys. Soc. Rept. Ionosphere Conf., p254.
MARTYN, D.F.	1956	Aust. J. Phys., 9, p161.
MC ELHINNY, M.W.	1958	Ph.D. Thesis, Rhodes University.
MC NICOL, R.W.E. and WEBSTER, H.C.	1956	Aust. J. Phys., 9, p272.
MC NICOL, R.W.E., WEBSTER, H.C. and BOWMAN, G.G.	1956	Aust. J. Phys., 9, p247.
MITRA, S.K.	1952a	p597
	1952b	p387
	1952c	p307
	1952d	p506
	1952e	p507

The Upper Atmosphere, Asiatic Society, Calcutta, (Second Edition).

MUNRO, G.H.	1950	Proc. Roy. Soc. London A., 202, p208.
MUNRO, G.H.	1953	Proc. Roy. Soc. A., 219, p447.

MUNRO, G.H.	1958	Aust. J. Phys., 11, p91.
NICOLET, M.	1951	J.A.T.P., 1, p141.
NICOLET, M. and AIKEN, A.C.	1960	J. Geophys. Res., 65, p1469.
NICOLET, M. and SWIDER, W. Jr.	1963	Planet. and Space Sci., 11, p1459.
NISBET, J.S. and QUINN, T.P.	1963	J. Geophys. Res., 68, p1031.
PHYSICS DEPARTMENT, RHODES UNIVERSITY.	1962 1963	Bulletins of ionosphere characteristics for SANAE base, Antarctica. Observers: D.C. Baker, 1962. D.G. Torr, 1963.
PIERCE, J.A. and MILNO, H.R.	1940	Phys. Rev., 57, p95.
PIGGOTT, W.R. and RAWE, K.	1961	URSI Handbook of Ionogram Interpretation and Reduction (Elsevier) Supplement S2.8, p142.
RATCLIFFE, J.A.	1951	J. Geophys. Res., 56, p487.
RATCLIFFE, J.A.	1955	The Physics of the Ionosphere (Physical Society; London).
RATCLIFFE, J.A.	1956	Solar eclipses and the ionosphere (Eds. W.J.G. Beynon and G.M. Brown), Pergamon Press.
RATCLIFFE, J.A.	1959a	Yearbook of the Phys. Soc.
RATCLIFFE, J.A.	1959b	The Magneto-Ionic Theory and its applications to the Ionosphere (Cambridge), Chapters 2 and 3.
RATCLIFFE, J.A., SCHERLING, E.R., SETTY, C.S.G.K. and THOMAS, J.O.	1956	Phil. Trans. Roy. Soc. A., 248, p621.
RATCLIFFE, J.A. and WEEKES, K.	1960	Physics of the Upper Atmosphere Edited by J.A. Ratcliffe (Academic Press; London). p 377.
RISHBETH, and SETTY, C.S.G.K.	1961	J.A.T.P., 20, p263.

ROBINSON, B.J.	1959	Repts. Progr. in Phys., 22, p241.
SETTY, C.S.G.K.	1960	J.A.T.P., 19, p88.
SHINN, D.H. and WHALE, H.A.	1952	J.A.T.P., 2, p85.
THOMAS, J.O.	1959	Proc. I.R.E., 47, p162.
THOMSON, W.	1860	Papers on Electrostatics and Magnetism, p217, (Macmillan; London, 1884).
TITHERIDGE, J.E.	1959a	J.A.T.P., 17, p96.
TITHERIDGE, J.E.	1959b	J.A.T.P., 17, p110.
TITHERIDGE, J.E.	1959c	J.A.T.P., 17, p126.
TITHERIDGE, J.E.	1961	J.A.T.P., 20, p209.
TITHERIDGE, J.E.	1963	J. Geophys. Res. 68, p3399.
TOMAN, K.	1955	J. Geophys. Res., 69, p57.
VAN ZANDT, T.E., NORTON, R.B. and STONEHOCKER, G.H.	1960	J. Geophys. Res. 65, p2003.
WADLEY, T.L.	1949	J.I.E.E. Pt.III, 96, p483.
WALKER, A.D.M.	1962	M.Sc. Thesis, Rhodes University.
WATANABE, K. and HINTEREGGER, H.E.	1962	J. Geophys. Res., 67, p999
WEBBER, W.	1962	J. Geophys. Res., 67, p5091.
WHALE, H.A.	1951	J.A.T.P., 1, p233.
WILKES, M.V.	1954	Proc. Phys. Soc., 67, p304.
YONEZAWA, T.	1956	J. Rad. Res. Lab. Japan, 3, p1.
YONEZAWA, T., TAKAHASHI, H. and ARIMA, Y.	1959	J. Rad. Res. Lab., Japan, 6, p21.